Epigenetic-mediated apoptosis in aggressive B-cell lymphomas

Inaugural-Dissertation

to obtain the academic degree

Doctor rerum naturalium (Dr. rer. nat.)

submitted to the Department of Biology, Chemistry and Pharmacy

of Freie Universität Berlin

by

Chidimma Agatha Akpa

2019

This dissertation was prepared

at the

Medical University, Berlin

Institute of Pathology

Department of Experimental Hematopathology

under the supervision of

Prof. Dr. Michael Hummel

from January 2016 till November 2019

1st Reviewer: Prof. Dr. Michael Hummel

2nd Reviewer: Prof. Dr. Rupert Mutzel

Date of defense: 16.03.2020

Directory

Summary

Lymphomas are a complex group of cancers arising from mature lymphoid cells. Despite advances in the treatment and management of this disease, it remains a health challenge as response to treatment and survival outcomes differ in various lymphoma subtypes. The exact causes driving lymphomagenesis remain unknown, and although several risk factors have been identified, the complexity of this disorder indicates that different molecular mechanisms drive the disease. One primary event evident in this disease is the presence of epigenetic alterations.

Epigenetic alterations could arise due to changes in the pattern of deoxyribonucleic acid (DNA) methylation or histone modifications. Enhancer of zeste homolog 2 (EZH2) modifies histone and mediates gene silencing by selectively catalyzing lysine 27 trimethylation on histone H3 (H3K27me3). Consequently, genes responsible for tumor suppression and differentiation are repressed, cells undergo uncontrolled proliferation, and this leads to tumor formation. *EZH2* has been mentioned to be a driver oncogene that plays an important role in tumor initiation and progression, especially when overexpressed or when gain-of function mutations occur in this gene. These hotspot gain-of-function mutations (Tyr646, Ala682 and Ala692) that result in increased EZH2 activity, are associated with increased H3K27me3 in several cancer types including lymphomas. Therefore, EZH2 inhibition could be an alternative strategy for lymphoma therapy.

We treated aggressive B-cell lymphoma cell lines with 3-Deazaneplanocin A (DZNep), an epigenetic drug that inhibits EZH2 indirectly and promotes apoptosis in various tumor entities including lymphomas. We aimed to investigate the apoptotic efficacy of DZNep in these lymphoma cell lines, to understand the mechanisms of resistance to DZNep and to determine predictive biomarkers that could be of importance for EZH2 inhibition with DZNep.

Using a combination of molecular and cell biological techniques such as flow cytometry, Western blot, Sanger sequencing, fluorescence in situ hybridization (FISH) and real-time reverse transcriptase polymerase chain reaction (RT-PCR), we showed that DZNep possesses a strong apoptotic and anti-proliferative effect on B-cell lymphoma cell lines. This effect was independent of the lymphoma type, the presence of *EZH2* gain-of-function mutations or the presence of known prognostic lymphoma biomarkers such as translocations of *MYC*, *BCL2* and *BCL6*. To investigate the molecular mechanism behind resistance to DZNep, we generated a DZNep-resistant clone from a B-cell lymphoma cell line that was initially sensitive to DZNep. This clone was used as a model to elucidate this mechanism. Upon molecular characterization,

comparison of this clone with the parent cell line of origin revealed differences in the karyotype, copy number alterations, proliferation rate and response to DZNep. Clonality studies of the rearranged immunoglobulin genes however, demonstrated that the resistant clone and the parent cell line were clonally identical.

Whole exome sequencing performed on this clone in relation to its corresponding control revealed among others, a genomic amplification of the *AHCY* gene - a direct target of DZNep. Methods such as copy number variation assays, FISH, gene expression assays and immunohistochemistry were used to validate this massive *AHCY* gain at the DNA, chromosomal, transcriptional and translational levels respectively. Functional validation of *AHCY* showed that in a DZNep-sensitive osteosarcoma cell line, AHCY overexpression was associated with resistance to DZNep. Unfortunately, reproduction of AHCY function in lymphoma cell lines was not successful due to technical reasons. Further evaluation of the whole exome sequencing data from DZNep-resistant cell lines demonstrated in one of the cell lines, a mutation in the *AHCY* gene. This mutation was predicted from online databases to have a likely damaging effect on the protein.

This study thus presents alterations in the *AHCY* gene as a potential mechanism of resistance to DZNep. It also reveals that molecular mechanisms of acquired resistance are quite distinct from those of intrinsic resistance to DZNep, which themselves, may further differ from one DZNep-resistant lymphoma entity to the next. AHCY could therefore, be a promising biomarker to evaluate prior to the initiation of therapy with DZNep.

Zusammenfassung

Lymphome repräsentieren eine heterogene Gruppe von hämatologischen Neoplasien, die aus reifen lymphatischen Zellen hervorgehen. Trotz der Fortschritte bei der Diagnostik und der Behandlung dieser Krankheit bleiben Lymphome eine therapeutische Herausforderung, da der Therapieerfolg bei den verschiedenen Lymphom-Subtypen sehr unterschiedlich ist. Die genauen Ursachen für die Pathogenese der Lymphome sind weitgehend unbekannt, und obwohl verschiedene Risikofaktoren identifiziert wurden, kann davon ausgegangen werden, dass verschiedene molekulare Mechanismen hierfür verantwortlich sind. Ein wichtiger Mechanismus scheinen jedoch epigenetische Veränderungen zu sein.

Epigenetischen Modifikationen können Änderungen im Methylierungsmuster innerhalb der Desoxyribonukleinsäure (DNA) oder Histon umfassen. Enhancer of zeste homolog 2 (EZH2) modifiziert Histone und katalysiert die Gen-Stummschaltung durch selektive Trimethylierung von Lysin an Position 27 von Histon H3 (H3K27me3). Als Folge dessen, werden Tumorsuppressor- und Differenzierungsgene unterdrückt, so dass die Zellen einer unkontrollierten Zellproliferation unterliegen, welche letztlich zur Tumorbildung führt. Als Onkogen spielt *EZH2* - insbesondere wenn EZH2 überexprimiert wird oder wenn in diesem Gen funktionssteigernde Mutationen auftreten - eine wichtige Rolle bei der Tumorinitiierung und -progression. So führen *EZH2* Mutationen an Position Tyr646, Ala682 oder Ala692 zu einer erhöhten EZH2-Aktivität und somit zu einer Erhöhung der Trimethylierung von H3K27 bei verschiedenen Krebsarten, einschließlich Lymphomen. Deshalb könnte die Hemmung der EZH2-Aktivität eine alternative Strategie für eine Lymphomtherapie darstellen.

3-Deazaneplanocin A (DZNep) ist ein indirekter EZH2-Inhibitor, der bei verschiedenen Tumorentitäten, unter anderen auch aggressiven Lymphomtypen, Apoptose auslöst. Wir haben es uns zum Ziel gesetzt die apoptotische Wirksamkeit von DZNep in aggressiven B-Zell-Lymphomen besser zu verstehen und die molekularen Mechanismen einer potentiellen Resistenz gegen DZNep aufzuklären. Darüber hinaus wollten wir prädiktive Biomarker ermitteln, die für den therapeutischen Einsatz, einer EZH2 Hemmung durch DZNep, von Bedeutung sein könnten.

Unter Verwendung verschiedener molekularer, biochemischer und zellbiologischer Techniken wie Durchflusszytometrie, Western Blot, Sanger-Sequenzierung, Fluoreszenz-in-situ-Hybridisierung (FISH) und Echtzeit-Reverse-Transkriptase-Polymerase-Kettenreaktion konnten wir zeigen, dass DZNep eine starke apoptotische und antiproliferative Wirkung auf

einen Teil der B-Zell-Lymphom-Zelllinien besitzt. Diese Effekte waren unabhängig vom Lymphomtyp, dem Vorhandensein von *EZH2*-Mutationen oder dem Vorhandensein bekannter prognostischer Lymphom-Biomarker wie *MYC*-, *BCL2*- oder *BCL6*-Translokationen. Um den molekularen Mechanismus zu untersuchen, der einer Resistenz gegen DZNep zugrunde liegt, haben wir aus einer zuvor DZNep-sensitiven B-Zell-Lymphom-Zelllinie einen DZNep-resistenten Klon erzeugt, der nunmehr eine erworbene Resistenz gegen DZNep besitzt. Mit Hilfe dieses Klons sollen Ursachen, die zur Entwicklung des Resistenzmechanismus führen, besser verstanden werden. Bei der molekularen Charakterisierung zeigten sich zwischen dem generierten DZNep-resistenten Klon mit der Ursprungslinie (der Elternzelllinie) Unterschiede in Bezug auf Karyotyp, Genkopienanzahl, Proliferationsrate und der generellen Reaktion auf DZNep. Durch eine Klonalitätsuntersuchung der umgelagerten Immunglobulin-Gene konnten wir bestätigen, dass der DZNep-resistente Klon und die Elternzelllinie klonal identisch sind.

Durch eine vollständige Exomsequenzierung des DZNep-resistenten Klon und seiner korrespondierenden Kontrolle, identifizierten wir im resistenten Klon eine genomische Amplifikation des *AHCY*-Gens. Durch verschiedene Methoden wie der Kopienzahlvariationstests, FISH, Genexpressionsanalyse und Immunhistochemie konnten wir diesen massiven *AHCY*-Gewinn auf DNA-, Chromosomen-, Transkriptions- und Translationsebene erfolgreich validieren. Wir konnten auch zeigen, dass in einer DZNep-sensitiven Osteosarkom-Zelllinie die induzierte Überexpression von AHCY mit einer gesteigerten Resistenz gegen DZNep assoziiert ist. Die funktionelle Validierung einer AHCY-Amplifikation in Lymphomzelllinien war aus technischen Gründen nicht erfolgreich. Aus Exomsequenzierungsdaten von DZNep-resistenten Zelllinien zeigten darüber hinaus in einer der resistenten Zelllinien eine Mutation im *AHCY*-Gen. Aus Online-Datenbanken wurde vorausgesagt, dass diese Mutation einen wahrscheinlich störenden Effekt auf die Proteinfunktion hat.

Diese Arbeit zeigt, dass Veränderungen im *AHCY*-Gen einen möglichen Resistenzmechanismus gegen DZNep-Behandlung darstellen kann. Es zeigt darüber hinaus, dass sich die molekularen Mechanismen einer erworbenen DZNep-Resistenz deutlich von denen der intrinsischen Resistenz gegen DZNep unterscheiden können. Dennoch, könnte der genomische und proteomische Zustand von AHCY ein potenzieller Biomarker sein, der vor Beginn einer DZNep-Therapie evaluiert werden sollte.

CHAPTER ONE

BACKGROUND

Cancers are a group of disorders that remain a major challenge of modern medicine until date. Although there has been series of advancements in our understanding of its biology, pathogenesis, diagnosis, management and treatment, they still present a serious health burden. In spite of available treatment options such as radiotherapy, immunotherapy, chemotherapy, hormone therapy and surgical procedures, many cancers have no cure. There are different types of cancers with different molecular mechanisms and treatment options. Many cancer entities for instance, lymphomas, still have a lot unknown about their etiology, pathogenesis, prevention and treatment.

1.1 Lymphomas

Lymphomas are a heterogeneous group of cancers, which originate from mature lymphoid cells. Despite progress in our knowledge of the management and therapeutic approaches for this group of disorders, this disease remains complex, with varying survival outcomes and treatment responses for the different lymphoma types (1). Lymphomas are grouped into two major categories; Hodgkin lymphoma (HL) and non-Hodgkin lymphoma (NHL). The world health organization (WHO) further classifies lymphomas into over 80 different subtypes based on various criteria such as the histopathological, immunophenotypical, molecular and clinical pattern of this disease (2-5). HLs are characterized by the presence of large monoclonal and multinucleated B-cells called Reed-Sternberg cells (RSC) (6-11). They make up about 12% of all lymphomas and have high cure rates following early diagnosis and treatment (7, 12). Other lymphoma types without Reed-Sternberg cells present, are classified as NHLs. NHLs are more common than HLs, and patients with this disease have an overall 5-year survival of about 50 - 60% (13). The NHL are further subdivided into B-cell lymphoma (BCL; approximately 85% of cases) and T-cell lymphoma (TCL; approximately 15% of cases). Both lymphoma types may follow either an aggressive (fast growing) or indolent (slow-growing) clinical course, with the prognosis and treatment success in each case depending on the type and stage of the disease. For the scope of this work, we would address two major B-cell lymphomas with an aggressive clinical course, Burkitt lymphoma (BL) and diffuse large B-cell lymphoma (DLBCL).

1.1.1 Burkitt lymphoma (BL)

BL is the most common form of NHL occurring in children and adolescents, with up to 30% of cases diagnosed in adults over the age of 60 (14, 15). There are three types of BL: sporadic BL, endemic BL and immunodeficiency-associated BL. Sporadic BL occurs worldwide, accounting

for 1-2% of NHL in adults, and about 30-50% of childhood lymphomas in the United States and Western Europe (4, 16, 17). Endemic BL occurs mainly in children of equatorial Africa and South America, with peak incidence at 4-7 years of age (16). The incidence in endemic regions correlates with the geographical distribution of endemic malaria, thus, its designation as endemic BL (16). Immunodeficiency-associated BL is mainly associated with individuals with human immunodeficiency virus (HIV) infection, those with congenital immunodeficiency, and allograft recipients (17-19). BLs proliferate rapidly and are characterized by deregulation of the *MYC* gene caused by a chromosomal translocation between chromosome 8 (*MYC*) and chromosome 14 (immunoglobulin heavy chain gene) in the majority of patients (15, 20). Although the presence of a *MYC* translocation is characteristic of BLs, this aberration is also present in a small proportion (5% to 15%) of DLBCL (21-23). In most cases, BL patients - especially of young age - have a favorable clinical outcome upon intensive treatment with immunochemotherapeutic combinations including Rituximab (20).

1.1.2 Diffuse large B-cell lymphoma (DLBCL)

DLBCLs are the most common type of NHLs worldwide (24). They constitute the largest group of aggressive B-cell tumors, and based on their gene expression profile, they can be subdivided into germinal center B-cell (GCB) DLBCL, activated B-cell (ABC) DLBCL, and primary mediastinal B-cell lymphoma (PMBL) (25-27). The GCB-type DLBCLs have a gene expression profile peculiar to germinal center B-cells, while the ABC-type DLBCLs express genes usually induced during activation of peripheral blood cells in vitro (25). PMBLs present gene signatures similar to that of RSCs of HL (26, 28).

Whole exome and ribonucleic acid (RNA) sequencing has revealed that the mutational landscape in DLBCL is relatively complex and heterogeneous, with several genes and pathways deregulated in different patient groups (29-32). In GCB DLBCLs, one of these genomic aberrations involve translocation of the *BCL2* gene, a phenomenon detected in about 30 - 45% of patients (33-35). This translocation, resulting in the juxtaposition of the *BCL2* gene and the immunoglobulin heavy (IGH) chain locus t(14;18), leads to irregular functioning of the apoptosis regulator BCL2 (33, 36). In ABC DLBCLs, nuclear factor kappa-light-chain-enhancer of activated B cells (*NFkB*) pathway activation and high levels of NFkB expression is characteristic, and its signaling is required for cell survival and proliferation (21, 37, 38). The most common chemotherapeutic agent used against DLBCL is the classical (C)yclophosphamide, (H)ydroxydaunorubicin, (O)ncovin, (P)rednisone (CHOP), or in combination with the monoclonal CD20 antibody (R)ituximab (R-CHOP). Stem cell

transplantation, radiation therapy as well as immunotherapy can be included in the treatment regimen for DLBCLs depending on the type and recurrence. Distinguishing the molecular DLBCL types appears to be clinically relevant. For instance, upon treatment with R-CHOP, patients with GCB DLBCL seem to have better survival outcome than patients with ABC DLBCL (27, 33, 39). Moreover, the overall 5-year survival of PMBL patients following chemotherapy is about 64% in comparison to GBC DLBCL (59%) and ABC DLBCL (30%) (28).

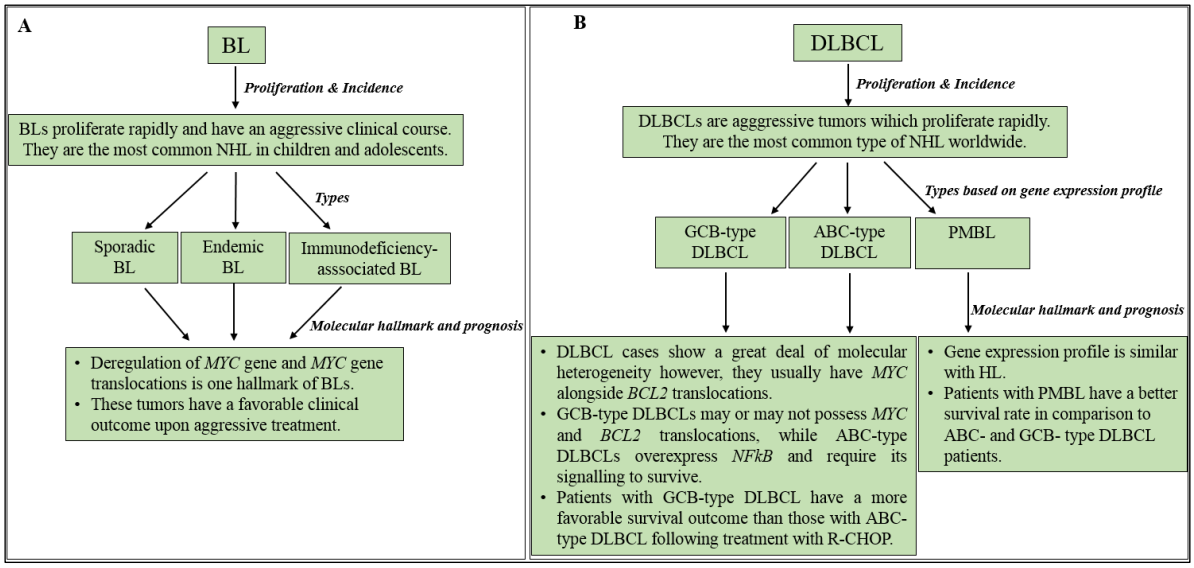

Figure 1: Summary of the characteristics of BLs and DLBCLs.

Although the survival rate of DLBCL patients treated with the standard R-CHOP regimen is around 50-70%, about 30% of relapse cases still occur and up to 30-50% of patients are not cured by this treatment (24, 40, 41). This necessitates the development of further targeted therapeutic options for patients - based on individual biomarkers - to address this heterogeneity.

1.2 Epigenetics and lymphoma

A principal mechanism in cancers - including lymphomas - is the presence of epigenetic alterations, which arise via deregulation of epigenetic switches and result in aberrant gene expression (42-44). These alterations modify the proliferation and differentiation programs of cells, resulting in tumor formation. Epigenetics deals with heritable variations in the DNA structure (which do not involve changes in the DNA sequence) that result in a change of gene expression patterns within organisms (45, 46). As an embryo develops, and during cell renewal/differentiation in adult cells, epigenetic control directs the outcome of different cell lineages (46-48). Epigenetic modifications may comprise histone modifications or alterations in the DNA methylation pattern (49-51).

Histones are basic cellular constituents composed of the core histones H2A, H2B, H3 and H4 and the linker histone H1 (52-54). Histones arrange and package DNA into nucleosome units - the fundamental unit of chromatin. The nucleosome consists of DNA wound around two copies of each core histone, forming a central region and an exposed N-terminal tail extending out from its core (55). These histone tails play an important role via their interaction with a variety of proteins (56). Although nucleosomal packaging restricts the access of many regulatory proteins to the DNA, covalent post-translational modifications of the histone tails by acetylation, ubiquitination, phosphorylation and methylation, could alter gene expression (56-61). Access of transcription factors to DNA and thus, gene transcription depends on the type and location of the histone tail modification. For example, methylation of lysine residues on histone tails can lead to gene activation or repression depending on the position of the lysine. Furthermore, different effects on the transcriptional status can be achieved depending on whether the lysine residue is mono-, di- or trimethylated (55). In contrast, acetylation of lysine residues on histones usually correlates with an active chromatin (62-65).

Epigenetic alterations however, play a role in the development, pathogenesis and progression of tumors (66, 67). When there is an imbalance in epigenetic mechanisms regulating non-coding RNAs, DNA methylation, and post-translational histone tail modifications (68), tumor-suppressor genes may become repressed. This, alongside with genomic alterations in enzymes regulating the cell cycle, and abnormal expression patterns of proteins playing a role in DNA repair and replication leads to tumor initiation and progression (69, 70). This further underscores the need for epigenetic-targeted therapy for the treatment of tumors.

In the fight against lymphoma, epigenetic-based therapy is gaining attention as an alternative treatment option for patients (68, 71-73). Several epigenetic drugs have shown great preclinical potential for the treatment of lymphomas when used independently or as combination therapy (68). There are also clinical trials with various epigenetic therapeutics against lymphomas of B-cell origin (ClinicalTrials.gov identifier: NCT02951156; NCT02846935; NCT01120834; NCT00005639; NCT02951156). Some epigenetic drugs for instance, Vorinostat and Belinostat have been approved, and are now utilized in clinics for treatment of cutaneous T-cell lymphoma (68, 74) and refractory peripheral T-cell lymphoma patients (75) respectively.

A unique set of proteins that modify chromatin structure, thereby, influencing the expression of genes are known as the Polycomb group proteins (PGPs).

1.2.1 Polycomb group proteins (PGPs)

The PGPs were first discovered in the fruit fly *Drosophila melanogaster*, and are known to silence homeotic (*Hox*) genes during embryonic development by regulating the structure of chromatin (76-79). These proteins, which are evolutionarily conserved in plants and animals, are involved in establishing and maintaining gene repression and cell proliferation (76, 80). In mammals, the PGPs also function in X-chromosome inactivation, cell proliferation, tumorigenesis and hematopoiesis (76, 77, 81, 82). Mammalian PGPs consist of two different protein complexes - polycomb repressive complex 1 (PRC1) and polycomb repressive complex 2 (PRC2), which target different genes involved in tumor suppression (83).

PRC1 consists of the polycomb group RING fingers (PCGFs) whose functional roles have been highlighted (82, 84, 85). Although it is unclear how PRC1 mediates gene silencing (86), it is proposed that it compacts chromatin by catalyzing the monoubiquitylation of H2A at position lysine 119 (82, 87-91). In some cases, chromatin compaction by PRC1 occurs independent of enzyme activity (92).

PRC2 comprises EZH1 or EZH2, embryonic ectoderm development (EED), suppressor of zeste 12 (SUZ12) and retinoblastoma-binding protein p46 (RbAp46) (86, 87). PRC2 is a histone methyltransferase, which mediates gene silencing by selectively catalyzing the di- and trimethylation of lysine at position 27 of histone H3 (H3K27me2/3) (82, 87, 93-95). H3K27me3 is a repressive histone mark that plays a role in regulating the expression of genes influencing cell proliferation and differentiation (96). Some additional proteins, such as adipocyte enhancer-binding protein 2 (AEBP2), polycomb-like (PCL) family protein, and Jumonji /AT-rich interaction domain containing 2 (JARID2) sometimes associate with PRC2 complex to modulate and enhance its activity (87, 97-99).

Although H3K27me3 acts as a mark for recruitment of PRC1 to create a more stable transcriptionally repressed state (92, 100-104), the mechanism of PRC2 recruitment to target genes is unclear (87). Recently, two models have been proposed, a PRC2:PRC1-dependent pathway and a PRC2:PRC1-independent pathway (105). PRC1 is recruited prior to PRC2 in the PRC2:PRC1-dependent model, while both PRC1 and PRC2 are recruited randomly or simultaneously to their targets in the described PRC2:PRC1-independent model (105). Both polycomb group complexes can induce the silencing of genes in synergy or independent of each other (106-108). The PGPs have been proposed as druggable targets for tumor therapy, and alterations in the PCR2 core component, EZH2, is suggested to have major prognostic implications for several cancers including lymphomas (109-111).

1.2.2 Enhancer of zeste homolog 1/2 (EZH1 / EZH2)

EZH1 is a variant of EZH2, and it forms a different PRC2 complex with weak H3K27me3 activity (108). EZH1 is poorly characterized in comparison to EZH2 and there are conflicting data about its function where in some cases, it contributes to transcriptional activation while in other instances, it leads to gene silencing (86, 108). EZH1 mediates a closed chromatin state via a mechanism which does not rely on the methyltransferase cofactor s-adenosylmethionine (SAM) (108, 112). EZH2 on the other hand, is a member of the (S)uppressor of variegation, (E)nhancer-of-zeste and (T)rithorax (SET) domain family that transfers methyl groups from SAM to lysine residues on histones, in a reaction resulting in a methylated lysine residue and S-adenosylhomocysteine (SAH) (113). EZH1 is expressed ubiquitously in non-proliferative adult cells while EZH2 expression is tightly linked with proliferation of transformed and non-transformed human cells (112, 114). In differentiated cells however, EZH2 is downregulated (115).

EZH2, whose gene is located on chromosome 7q36.1, is the main PRC2 component important for catalyzing histone lysine methyltransferase reactions (112, 116, 117). Additional evidence suggests that in cancer, EZH2 may act in a manner independent of PRC2 and histone methylation (97, 118, 119). EZH2 plays an important role in tumor initiation, progression, metastasis and drug resistance (31, 120, 121). Moreover, strong EZH2 expression has been linked with neoplastic transformation and aggressiveness of different cancer types (122-126). Furthermore, gain-of-function mutations including Tyr646, Ala682 and Ala692 are known for this gene, which lead to increased H3K27me3 (86, 97, 119, 127-129). Tyr646 indicates the replacement of the amino acid tyrosine at codon 646 (previously Tyr641). Ala682 means exchange of alanine at codon 682 (previously Ala677) and Ala692 implies the replacement of alanine at codon 692 (previously Ala687). In cancer therefore, EZH2 can serve as a useful prognostic biomarker (95, 124, 130).

In follicular lymphoma for instance, these heterozygous *EZH2* gain-of-function mutations occur in more than 25% of patients (127, 129). In DLBCL, particularly the GCB type, it occurs in almost 22% of patients (129). In addition, for melanoma, precisely cutaneous melanoma - the only solid cancer with Tyr646 mutation -, the frequency of this mutation is about 2 - 3% (131, 132). The overexpression of EZH2 has been shown to confer oncogenic potential in lymphoma, for instance natural killer/T-cell lymphoma (119), and other solid tumors such as breast (125), prostate cancer (133) and urothelial carcinoma (134). There is also a close association between EZH2 overexpression and a poor clinical outcome of cancer patients, for

example in patients with gastrointestinal DLBCL (128), prostate, breast and endometrial cancers (126), squamous cell carcinoma of the head and neck (135), as well as colorectal cancer (136). Since mutant *EZH2* as well as overexpressed EZH2 contribute to cancer progression, therapies focusing on inhibiting EZH2 could be promising as alternatives for tumors treatment.

1.2.3 EZH2 inhibitors

Over the years, several small molecule EZH2 inhibitors have been discovered (table 1) and their apoptotic efficacy in NHL cell lines established. Most of these inhibitors however, promote apoptosis mainly in *EZH2*-mutated cell lines (137, 138). These EZH2 inhibitors are mainly direct EZH2 inhibitors with a high selectivity for EZH2 over EZH1 (97). The EZH2 inhibitor EPZ-6438 has been shown to have a remarkable efficacy in lymphomas and is currently in Phase II clinical trials on human subjects. EPZ-6438 however, is described to be more efficacious against lymphomas with mutated *EZH2* (139). 3-Deazaneplanocin-A (DZNep) inhibits EZH2 indirectly, and although it is still in the preclinical phase of drug development, it stands out as having great potential for the treatment of tumors (140-143).

Table 1: A list of EZH2 inhibitors, their mode of EZH2 inhibition and their status in drug development.

Inhibitor	Direct / indirect EZH2 inhibition	Stage of drug development	Reference
EPZ005687	Direct (competes with SAM for binding on EZH2)	Preclinical	(137)
EI1	Direct (competes with SAM for binding on EZH2)	Preclinical	(144)
GSK343	Direct (competes with SAM for binding on EZH2)	Preclinical	(145)
GSK126	Direct (competes with SAM for binding on EZH2)	Clinical (Phase I) NCT02082977	(146)
UNC1999	Direct (competes with SAM for binding on EZH2)	Preclinical	(138)
EPZ-6438	Direct (competes with SAM for binding on EZH2)	Clinical (Phase I&II) NCT01897571; NCT02601950; NCT03010982	(139, 147)
EPZ-011989	Direct (competes with SAM for binding on EZH2)	Preclinical	(148)
CPI-1205	Direct (competes with SAM for binding on EZH2)	Clinical (Phase Ib/II) NCT02395601	(149, 150)
CPI-169	Direct (competes with SAM for binding on EZH2)	Preclinical	(151)
CPI-360	Direct (competes with SAM for binding on EZH2)	Preclinical	(152)
EBI-2511	Direct (competes with SAM for binding on EZH2)	Preclinical	(153)
ZLD1039	Direct (competes with SAM for binding on EZH2)	Preclinical	(154)
DZNep	Indirect (inhibits S-adenosylhomocysteine hydrolase and thus, SAM-dependent methyltransferases)	Preclinical	(155-158)

SAM: S-adenosylmethionine. The above table is an updated version of the list adapted from Kim K. H. and Roberts C. W. M. (97).

1.3 3-Deazaneplanocin A (DZNep) and S-adenosylhomocysteine hydrolase (AHCY)

DZNep is an inhibitor of EZH2 discovered over 30 years ago, and has been associated with its cytotoxic effects in cancer (157, 158). However, preclinical studies on this inhibitor is still ongoing due to questions concerning its specificity, nephrotoxicity and short plasma half-life (159, 160). DZNep indirectly inhibits EZH2 by competitively blocking the activity of AHCY.

AHCY is associated with DNA methylation and it catalyzes the reversible reaction in which SAH is hydrolyzed to adenosine and homocysteine (161, 162). Altered AHCY activity has been linked to diverse outcomes in different cancer entities (163-166). During histone lysine methylation (figure 2), SAM donates methyl groups, and is metabolized to SAH by methyltransferases (162). DZNep directly inhibits AHCY causing buildup of SAH levels within cells, and due to increased SAH, there is a subsequent rise in SAM due to feedback inhibition by SAH on methyltransferases (158, 159, 162). Methyltransferases that require the donation of methyl groups from SAM, such as EZH2 are hence impeded. EZH2 inhibition by DZNep leads to the down regulation of H3K27me3. The lifting of this repressive histone mark from tumor suppressors, differentiation promoting and apoptosis promoting genes is thought to be the mechanism through which DZNep exerts its anti-tumor effects.

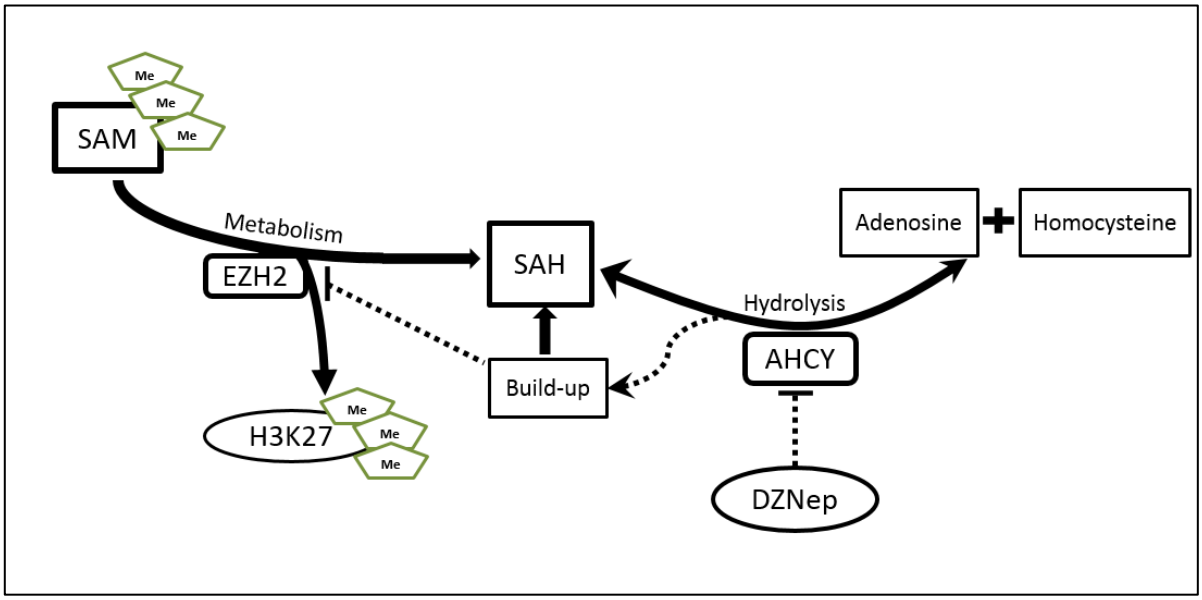

Figure 2: How DZNep indirectly inhibits EZH2. SAM donates methyl (Me) groups during methylation reactions. EZH2 catalyzes the trimethylation of H3K27, while SAM is metabolized to SAH. AHCY catalyzes the reversible hydrolysis of SAH to adenosine and homocysteine. DZNep directly inhibits AHCY, causing buildup of SAH levels within cells, and due to increased SAH, there is a subsequent feedback inhibition of EZH2. Figure was adapted from Miranda T. B. et al., (159).

Indeed, DZNep inhibits EZH2, leading to the lowering of H3K27me3 and induction of apoptosis in different cancer cell lines as well as primary tumor cells (167-171). The histone

demethylation brought about by DZNep revives genes repressed by PRC2 in tumor cells, consequently promoting apoptosis in these cells (167).

We are aware that the inhibitory effects of DZNep on histone methylation are not exclusively specific to EZH2 (97, 159, 172), nevertheless, there is plausibility for its clinical use. For one thing, the changes effected by DZNep are both non-heritable and reversible (159). Moreover, in light of our knowledge of multiple histone methyltransferases whose overexpression have been linked to cancer, as well as the benefit of dual EZH1 and EZH2 inhibition (173-177), DZNep may be a good option in such cases which necessitate the inhibition of more than one of these aberrant histone methyltransferases. In addition, not only does DZNep have better clinical potential in comparison to other AHCY inhibitors but also, the in vivo evaluation of the pharmacokinetic properties of DZNep shows encouraging results for its progress into clinical usage (142, 159).

Despite the number of promising in vitro studies with DZNep, we would not fail to mention the most frequent problem associated with cancer chemotherapy - the issue of drug resistance. Mechanisms of resistance to cancer chemotherapy are well known (178, 179), and they remain a great barrier for many chemotherapeutic regimens. DZNep has already proven to have a good perspective for cancer treatment. However, as more preclinical studies with DZNep evolve, to further explore its potential, one also needs to understand if acquired resistance could occur during its administration. If so, the molecular mechanisms behind this resistance and ways in which this problem could be averted.

1.4 Aims of the study

This study aims to investigate the in vitro effects of DZNep as an EZH2 inhibitor in aggressive B-cell lymphomas. Furthermore, we aim at elucidating the molecular mechanism of resistance to DZNep, and at identifying biomarkers that could be of prognostic relevance for EZH2-based therapy using DZNep.

CHAPTER TWO

MATERIALS AND METHODS

2.1 Cell lines and cell culture

We used seven DLBCL cell lines KARPAS-422 (ACC-32), SU-DHL-10 (ACC-576), CARNAVAL (ACC-724), WSU-DLCL-2 (ACC-575), U-2932 R1, U-2932 R2, HT (ACC-567), five BL cell lines DG-75 (ACC-83), BLUE-1 (ACC-594), BL-2 (ACC-625), CA-46 (ACC-73), BL-41 (ACC-160) as described (180), and one osteosarcoma cell line U-2-OS (ACC 785). The cell lines were obtained from the German collection of microorganisms and cell cultures (DSMZ), Germany. U-2932 R1 and U-2932 R2 were provided by Dr. Hilmar Quentmeier (181), DSMZ, Germany. The lymphoma cell lines were cultured in RPMI 1640 medium (Life Technologies GmbH/ThermoFisher Scientific, Germany) augmented with 20% fetal calf serum (PAN-Biotech, Germany) as described (180). U-2-OS cell line was cultured in Dulbecco's modified Eagle's medium (PAN-Biotech, Germany) supplemented with 10% fetal calf serum and 1% Penicillin-streptomycin (Biochrom GmbH, Germany). Cell lines were screened and confirmed negative for mycoplasma contamination using the MycoAlert Mycoplasma detection kit (Lonza, Germany), and following the manufacturer's recommendations. Cell culture was done under sterile conditions and the cell lines were incubated at 37°C and 5% CO_2.

2.2 Drug preparation

The EZH2 inhibitors DZNep (Selleckchem, Germany) and EPZ-6438 (Selleckchem, Germany) were dissolved in sterile water and dimethyl sulfoxide (DMSO) (SERVA Electrophoresis GmbH, Germany) respectively as described (180).

2.3 Flow cytometry

Flow cytometry was carried out with BD Accuri C6 flow cytometer (BD Biosciences, USA) for determination of the percentage of apoptotic cells, immunophenotyping, proliferation assay and doubling time analysis.

Apoptosis measurement was performed as already described (180). Immunophenotyping for the identification of cell surface cluster of differentiation (CD) markers highly specific for B-cells - CD19 and CD20 - was performed similarly with the method described for the measurement of apoptotic cells, except that in this case, the binding buffer and corresponding anti-CD antibody were mixed at a ratio of 20:1 respectively. Cells were stained with fluorescein isothiocyanate (FITC)-conjugated anti-human CD19 monoclonal antibody (Dako Denmark

A/S, Denmark) and Alexafluor 488-conjugated anti-human CD20 monoclonal antibody (Biolegend, USA). Negative controls used include mouse IgG3 (Dako Denmark A/S, Denmark) and Alexafluor 488 Mouse IgG2b, κ isotype control (Biolegend, USA) respectively. Data was analyzed using the BD Accuri C6 software (BD Biosciences, USA).

Cell proliferation assay was carried out as previously reported (180). Proliferation was also analyzed at the RNA level using synthesized complementary DNA (cDNA) (see description in section 2.7) from the respective cell lines and checking for changes in key proliferation genes. The method is further described in section 2.7.1.

Experiments for the determination of the doubling time of the cell lines was carried out as recorded (see description in Akpa C. A. et al., manuscript in review (appendix C)).

2.4 Generation of a DZNep-resistant BLUE-1 variant

A DZNep-sensitive BL cell line, BLUE-1 was selected for the generation of a DZNep-resistant clone (figure 3) as detailed in Akpa C. A. et al., manuscript in review (appendix C).

Confirmation of the identities of the parent cell line, the generated DZNep-resistant cell line and its control was done at 3 levels: identity based on immunophenotyping, the immunoglobulin heavy chain (IGH) gene rearrangement (described in section 2.8), and short tandem repeat (STR) profile (described in section 2.13).

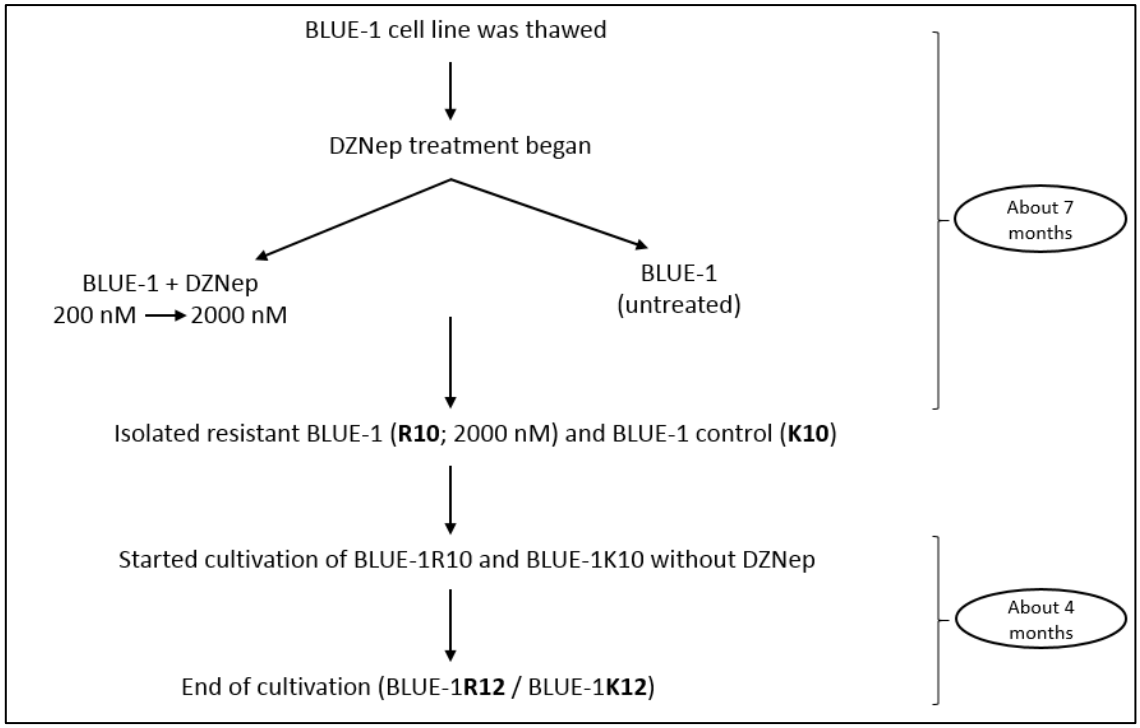

Figure 3. Generation of a DZNep-resistant BLUE-1 clone. The above figure was adapted from Akpa C. A. et al., manuscript in review (see appendix C).

2.5 Inhibitory concentration 50 (IC_{50}) analysis

The IC_{50} was analyzed as described (180). DZNep concentrations above 10 µM were not used in accordance with published information (169, 182) as very large amount of the inhibitor might cause cytotoxic effects rather than programmed cell death induced by the biological consequences of EZH2 inhibition.

2.6 Cell fractionation and Western blotting

Nuclear and cytoplasmic cellular fractions were separated using NE-PER nuclear and cytoplasmic extraction reagents (ThermoFisher Scientific, Germany), adhering to the manufacturer's protocol. Cell lysis and Western blot was performed as described (180). Details of the antibodies used for performing Western blot are listed in table 2.

Table 2. Antibodies used for Western blot, immunophenotyping and immunohistochemistry (IHC).

	Primary antibody				
	Application			**Company**	**Catalogue number**
Target Protein	Western blot	Immunophenotyping	Immunohistochemistry		
CD19		✓		Dako Denmark A/S	F0768
CD20		✓		Biolegend	302316
GAPDH	✓			Cell Signaling Technology	2118S
EZH2	✓			Cell Signaling Technology	5246S
H3K27me3	✓			Cell Signaling Technology	9733S
Beta-actin	✓			Cell Signaling Technology	4967S
Histone 3	✓			Cell Signaling Technology	3638S
Cleaved PARP	✓			Cell Signaling Technology	9541S
AHCY	✓		✓	OriGene	TA332593
Mouse IgG3		✓		Dako Denmark A/S	X954
Mouse IgG2b		✓		Biolegend	400329
Secondary antibody					
Anti-rabbit HRP-conjugated	✓			GE Healthcare	NA934V
Anti-mouse HRP-conjugated	✓			Agilent	P0447

The above table includes (antibody) information adapted from Akpa C. A. et al., (180), and Akpa C. A. et al., manuscript in review (see appendix C).

2.7 RNA extraction and real-time reverse transcriptase polymerase chain reaction (RT-PCR)

RNA isolation and cDNA synthesis were performed as already reported ((180, 183). See method also in Akpa C. A. et al., manuscript in review (appendix C)).

2.7.1 Proliferation assay

To check the impact of DZNep on proliferation, we examined the expression of select genes that play an important role in cellular proliferation. They include proliferating cell nuclear

antigen (*PCNA*) and cyclin-dependent kinase 2 (*CDK2*). Beta 2 microglobulin (*B2M*) gene was used as an endogenous control.

The primers for the above genes were designed with Primer-BLAST, a search tool hosted by the National Center for Biotechnology Information (NCBI), USA as described (180), and were purchased from Eurofins MWG, Germany. Information on the forward and reverse primer sequences for each target can be found in table 3. During the real-time PCR, *B2M* gene was amplified in parallel with both proliferation genes of interest and the run for each sample was performed in triplicates. The comparative $\Delta\Delta C_t$ method (184) was used for relative mRNA quantification.

Table 3. Details of primers used for proliferation assay and mutation validation.

	Target	Forward sequence	Reverse sequence	Application	Company
cDNA Target	PCNA*	5'-GTGTAAACCTGCAGAGCATGGA-3'	5'-GTAGGTGTCGAAGCCCTCAGA-3'	Proliferation assay	Eurofins MWG
	CDK2*	5'-TGGACTAGCCAGAGCTTTTGG-3'	5'-CCACAGGGTCACCACCTCAT-3'	Proliferation assay	Eurofins MWG
	B2M*	5'-TGCTGTCTCCATGTTTGATGTATCT-3'	5'-TCTCTGCTCCCCACCTCTAAGT-3'	Proliferation assay	Eurofins MWG
	EZH2	5'-TGACCTCTGTCTTACTTGTGGAG-3'	5'-GCAGTTTGGATTTACCGAATG-3'	Mutation validation	Eurofins MWG
	AHCY	5'-GGCCGTCCTCATTGAGACC-3'	5'-GCCCGTCCTTGAAGTACAGG-3'	Mutation validation	Sigma-Aldrich
gDNA Target	EZH2	5'-TCCCCAGTCCATTTTCACC-3'	5'-TCATTTCCAATCAAACCCACAG-3'	Mutation validation	Eurofins MWG

* RT-PCR

Table includes *EZH2* primer sequences adapted from Akpa C. A. et al., (180).

2.7.2 *AHCY* gene expression assay

To determine expression of AHCY at the RNA level, the AHCY TaqMan gene expression assay was used. For this assay, B2M, succinate dehydrogenase (SDHA), and AHCY TaqMan gene expression assays, as well as the TaqMan gene expression master mix (all from ThermoFisher Scientific, Germany) were used (see details in table 4). The assay was performed following the manufacturer's protocol and the real-time PCR was done with the StepOnePlus real-time PCR system (ThermoFisher Scientific, Germany). *B2M* and *SDHA* served as reference genes and were amplified in parallel with *AHCY*. Using the Step-One software version 2.3, relative mRNA quantification (RQ) was done using the comparative $\Delta\Delta C_t$ method (184).

Table 4. List of TaqMan assays utilized in analysis of gene expression and copy number variation (CNV).

	Targets	Assay ID	Type	Company
cDNA target	*AHCY*	Hs00898137_g1	Gene expression assay	ThermoFisher Scientific
	*B2M**	Hs00984230_m1	Gene expression assay	ThermoFisher Scientific
	*SDHA**	Hs00417200_m1	Gene expression assay	ThermoFisher Scientific
gDNA target	*AHCY*	Hs02422126_cn	CNV assay	ThermoFisher Scientific
	AHCY	Hs02512802_cn	CNV assay	ThermoFisher Scientific
*Endogenous control				

Details of the gene expression assays and the CNV assay (Hs02422126_cn) were adapted from Akpa C. A. et al., manuscript in review (appendix C).

2.8 DNA extraction, polymerase chain reaction (PCR) and Sanger sequencing

Genomic DNA was extracted with the QIAamp DNA Mini Kit (Qiagen, Germany), following the instructions of the manufacturer as recorded (180).

Design of *EZH2* primers was done with the Primer BLAST tool (NCBI). The forward and reverse primer sequences used for the detection of *EZH2* point mutation at the genomic level can be found in table 3. These primers span the *EZH2* mutation hotspot Tyr646 (product length of 256 base pairs). The primers used to validate the *EZH2* point mutations on the RNA (cDNA) level are also included in table 3. The latter primer sequences interrogates the *EZH2* mutational hotspots Tyr646, Ala682 and Ala692 (product length of 340 base pairs).

To validate the expression of mutated *AHCY* (in the DZNep-resistant cell line HT) at the RNA (cDNA) level, forward and reverse primers spanning the exon 3 region of *AHCY* were designed using the Primer 3 software (185, 186). These primer sequences, which yield a product with a length of 190 base pairs, are included in table 3.

PCR, clean-up of PCR products and Sanger sequencing was performed as described (180).

For the confirmation of the identity of the resistant BLUE-1 clone, B-cell clonality studies was performed for BLUE-1, BLUE-1K10 and BLUE-1R10. To this end, a multiplex PCR using IGH-specific primer sets was performed following the standard protocol of the EuroClonality/BIOMED-2 study, BMH4-CT98-3936 (187). Six primers for the framework (FR) 1 region of the variable (V) IGH gene segment (FR1-V_H), seven FR2-V_H primers and seven FR3-V_H primers were independently mixed with a 6-carboxyfluorescein (6-FAM)-labelled Joining (J_H) primer in three separate combinations. Details on the various primers are available in table 5.

Table 5. Details of the primers used for the confirmation of the B-cell clonality of BLUE-1, BLUE-1K10 and BLUE-1R10.

		Primers	Company of purchase
FR 1	FR1 V IGH	5'-GGCCTCAGTGAAGGTCTCCTGCAAG-3'	TIB MOLBIOL Syntheselabor GmbH
	FR1 V IGH	5'-TCTGGTCCTACGCTGGTGAAACCCA-3'	TIB MOLBIOL Syntheselabor GmbH
	FR1 V IGH	5'-CTGGGGGGTCCCTGAGACTCTCCTG-3'	TIB MOLBIOL Syntheselabor GmbH
	FR1 V IGH	5'-CTTCGGAGACCCTGTCCCTCACCTG-3'	TIB MOLBIOL Syntheselabor GmbH
	FR1 V IGH	5'-CGGGGAGTCTCTGAAGATCTCCTGT-3'	TIB MOLBIOL Syntheselabor GmbH
	FR1 V IGH	5'-TCGCAGACCCTCTCACTCACCTGTG-3'	TIB MOLBIOL Syntheselabor GmbH
FR 2	FR2 V IGH	5'-CTGGGTGCGACAGGCCCCTGGACAA-3'	TIB MOLBIOL Syntheselabor GmbH
	FR2 V IGH	5'-TGGATCCGTCAGCCCCCAGGGAAGG-3'	TIB MOLBIOL Syntheselabor GmbH
	FR2 V IGH	5'-GGTCCGCCAGGCTCCAGGGAA-3'	TIB MOLBIOL Syntheselabor GmbH
	FR2 V IGH	5'-TGGATCCGCCAGCCCCCAGGGAAGG-3'	TIB MOLBIOL Syntheselabor GmbH
	FR2 V IGH	5'-GGGTGCGCCAGATGCCCGGGAAAGG-3'	TIB MOLBIOL Syntheselabor GmbH
	FR2 V IGH	5'-TGGATCAGGCAGTCCCCATCGAGAG-3'	TIB MOLBIOL Syntheselabor GmbH
	FR2 V IGH	5'-TTGGGTGCGACAGGCCCCTGGACAA-3'	TIB MOLBIOL Syntheselabor GmbH
FR 3	FR3 V IGH	5' TGG AGC TGA GCA GCC TGA GAT CTG A 3'	TIB MOLBIOL Syntheselabor GmbH
	FR3 V IGH	5'-CAATGACCAACATGGACCCTGTGGA-3'	TIB MOLBIOL Syntheselabor GmbH
	FR3 V IGH	5'-TCTGCAAATGAACAGCCTGAGAGCC-3'	TIB MOLBIOL Syntheselabor GmbH
	FR3 V IGH	5'-GAGCTCTGTGACCGCCGCGGACACG-3'	TIB MOLBIOL Syntheselabor GmbH
	FR3 V IGH	5'-CAGCACCGCCTACCTGCAGTGGAGC-3'	TIB MOLBIOL Syntheselabor GmbH
	FR3 V IGH	5'-GTTCTCCCTGCAGCTGAACTCTGTG-3'	TIB MOLBIOL Syntheselabor GmbH
	FR3 V IGH	5'-CAGCACGGCATATCTGCAGATCAG-3'	TIB MOLBIOL Syntheselabor GmbH
JH-22 FAM	J IGH	5'-6FAM-CTTACCTGAGGAGACGGTGACC-3'	TIB MOLBIOL Syntheselabor GmbH

Primers used were those from the EuroClonality/BIOMED-2 collaborative study (van Dongen J. J. M. et al., (187)).

2.9 Fluorescence in situ hybridization (FISH) studies

Sections of cell lines that were formalin-fixed and paraffin-embedded (FFPE), as well as cell line cytospins were used for FISH studies as already described (180, 188, 189). This was done in collaboration with Dr. Dido Lenze of the Molecular Pathology department, Charité - University Hospital, Berlin, Germany.

AHCY amplification was detected using *AHCY* gene-specific probe and chromosome 20-control (centromeric) probes (both of which were purchased from Empire Genomics, USA) as detailed in Akpa C. A. et al., manuscript in review (see appendix C).

2.10 Whole exome sequencing (WES)

WES was performed on genomic DNA obtained from BLUE-K10 and BLUE-1R10 at the core facility Genomics, Berlin Institute of Health (BIH), Berlin, Germany. Next generation sequencing libraries, cluster generation, template sequencing, data analysis and copy number variation analysis were carried out as reported (Akpa C. A. et al., manuscript in review (appendix C)). Data analysis was carried out in collaboration with the research group of Dr. Dieter Beule (BIH/Charité Core Unit Bioinformatics, Berlin, Germany).

2.11 Copy number variation (CNV) assay

AHCY CNV assay was carried out with high-quality genomic DNA using 2 independent Taqman assays (see details in table 4), one (assay ID: Hs02422126_cn), overlapping intron 7 and exon 8 and the other (assay ID: Hs02512802_cn) overlapping intron 3 and exon 3 (both on reference genome GRCh37). *AHCY* CNV analysis was also carried out using primary patient DNA samples. For the use of patient samples a positive statement from the Institutional Review Board of Charité - Berlin (EA4/104/11) was obtained. The TaqMan CNV assay and data analysis was performed as recorded (Akpa C. A. et al., manuscript in review (appendix C)).

CNV analysis was also done using genome-wide DNA methylation array data (refer to section 2.12). The 'conumee' R package in Bioconductor (190) was used for the production of copy number plots as recorded (Akpa C. A. et al., manuscript in review (appendix C)). This analysis was performed in collaboration with Prof. David Capper from the Institute of Neuropathology, Charité - University Hospital, Berlin, Germany. Details of the methods for this analysis has been published (191).

2.12 Global DNA methylation analysis

Two methods were used to detect global changes in the DNA methylation status of the cell lines, BLUE-1, BLUE-1K10 and BLUE-1R10.

Initially, the percentage of DNA methylation was evaluated using the MethylFlash Global DNA methylation (5-mC) enzyme-linked immunosorbent assay (ELISA) Easy Kit (Colorimetric) purchased from EpiGentek, USA. The product protocol was followed accordingly, and global methylated DNA quantification was done following a colorimetric approach by reading the absorbance at 450 nm wavelength with the Emax plus microplate spectrophotometer (Molecular devices, USA).

Subsequently, genome-wide DNA methylation analysis was done in collaboration with Prof. David Capper (Neuropathology, Charité - University Hospital, Berlin, Germany) with the Infinium MethylationEPIC BeadChip (Illumina, USA) (191). Methylation data from concerned lymphoma cell lines were analyzed and compared with the methylation data from primary DLBCL and plasmacytomas from skull and spinal lesions (192) using R (193). Bioinformatics.Expert UG, Berlin, Germany, performed further analysis of Infinium EPIC datasets, including data processing, differential methylation analysis, and comparison of differentially methylated probes. Differentially methylated probes were defined by having an adjusted p-value of below 0.01.

2.13 Cytogenetics, OncoScan CNV assay and metabolomics assay

The authenticity of BLUE-1, BLUE-1K10 and BLUE-1R10 were confirmed by determining the STR profile as already published (194). While cytogenetic investigation was performed on these three cell lines as described (195), OncoScan CNV assays were done as reported (194). The criteria used to define a copy number alteration include chromosomal changes covering a minimum of 20 probes, having a size of 100kb or more, showing a median log2Ratio of +/- 0.3, and possessing a copy number neutral loss of heterozygosity (CNN-LOH) of more than 5Mb (194). STR profiling, conventional cytogenetics and OncoScan CNV analysis was carried out in collaboration with the research group of Prof. Reiner Siebert at the Institute of Human Genetics, University of Ulm, Germany. Intermediates of methionine and polyamine metabolism in BLUE-1, BLUE-1K10, BLUE-1R10, BLUE-1K12 and BLUE-1R12 were analyzed in collaboration with the research group of Prof. Peter J. Oefner of the Institute of Functional Genomics, University of Regensburg, Regensburg, Germany. The metabolites were measured using a procedure already reported (196). The methods for STR profiling of the cell lines, cytogenetics, OncoScan CNV analysis and metabolomics studies have already been reported (Akpa C. A. et al., manuscript in review (appendix C)).

2.14 Immunohistochemistry (IHC)

Immunohistochemistry for the analysis of AHCY protein expression was performed on FFPE sections of cell lines as described (197). The anti-AHCY antibody used for IHC is shown in table 2.

2.15 Stable AHCY transfection of cell lines

Human AHCY ORF mammalian expression plasmid and pCMV3-C-FLAG negative control plasmid (both from Biozol Diagnostica Vertrieb GmbH, Germany) were used to transfect cell lines. Both plasmids, which are under the control of a CMV promoter, carry the Kanamycin and Hygromycin resistance genes. Competent DH5α *E. coli* cells were transformed using both plasmids. Selection of potent plasmids was done using a medium with Kanamycin. The plasmid DNA was isolated and purified using the Qiagen Plasmid Maxi kit (Qiagen, Germany).

2.15.1 AHCY Knockdown

Mission endoribonuclease-prepared small interfering RNA (esiRNA) (from Sigma-Aldrich/Merck, Germany) targeting human *AHCY*, and an ON-TARGETplus Non-targeting negative control pool (ThermoFisher Scientific/Dharmacon, Germany) were used to transfect $5x10^6$ vital BLUE-1R10 cells in a 6-well cell culture plate. Using program D-23 on the Nucleofector 2b Device (Lonza Group AG, Germany) and following the manufacturer's protocol, the Amaxa Cell line Nucleofector Kit C (Lonza Group AG, Germany) was used for the electroporation procedure. Knockdown efficiency was analyzed using Western blot while gene expression analysis following *AHCY* knockdown was done by real-time RT-PCR using AHCY and B2M TaqMan gene expression assays (see table 4).

2.15.2 AHCY overexpression

Overexpression of AHCY was performed in collaboration with the research group of Prof. Claus Scheidereit (Max-Delbrück-Centrum for Molecular Medicine, Berlin, Germany). The respective lymphoma cell lines as well as the osteosarcoma cell line (U-2-OS) were transfected with the respective plasmids (described in 2.15) using Lipofectamine 2000 transfection reagent (ThermoFisher Scientific, Germany) following the reagent protocol of the manufacturer. Stably transfected clones overexpressing the insert were selected using 200 µg/ml hygromycin B (Sigma-Aldrich/Merck, Germany). The hygromycin B-resistant cells were propagated in hygromycin B-positive medium for at least 10 days. They were harvested afterwards, and AHCY overexpression was confirmed by Western blotting.

2.16 Statistical analysis

GraphPad Prism 5 (GraphPad Software, California, USA) was used to perform statistical analysis. Comparisons between two groups were done using the Mann-Whitney U test (two-tailed) while group comparisons were done with one-way ANOVA (Tukey post-hoc test). Regarded significant are p values less than 0.05.

CHAPTER THREE

RESULTS

3.1. DZNep causes apoptosis in lymphoma cell lines

To determine the apoptotic effect of DZNep in lymphoma cells, we treated selected cell lines with increasing DZNep concentrations (0 - 10 µM). We recorded a gradual increase in the percentage of apoptotic cells measured with increasing DZNep concentrations (figure 4A). Subsequent treatment of cell lines was carried out with 5 µM DZNep since the percentage of apoptotic cells recorded (and the expression of cleaved poly (ADP-ribose) polymerase (PARP, a known molecular indicator of apoptosis induction)) were only minimal between DZNep concentrations of 5 µM and 10 µM.

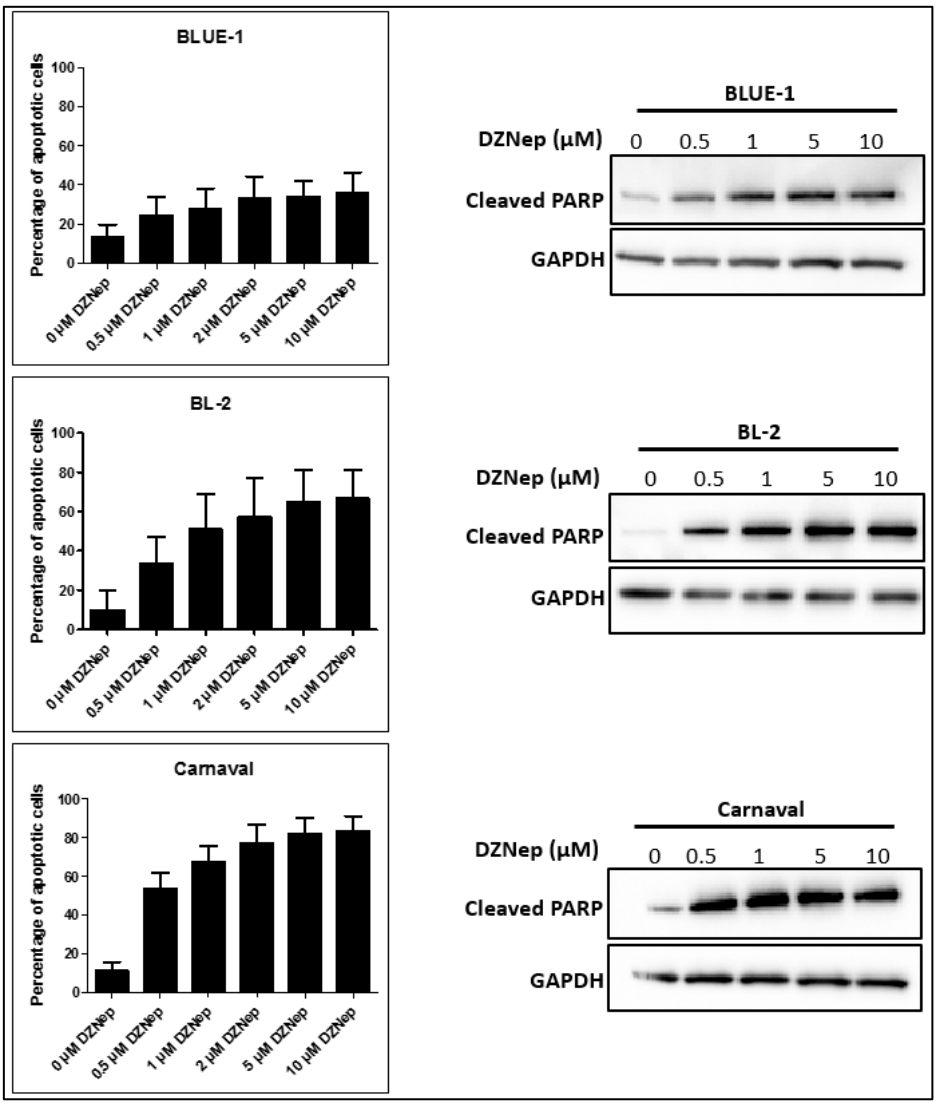

Figure 4A. DZNep-mediated apoptosis depends on the drug concentration. Three cell lines that undergo apoptosis upon treatment with DZNep (BLUE-1, BL-2 and Carnaval) were treated with increasing concentrations of the inhibitor for 72 hours. Flow cytometry was employed for the measurement of the percentage of apoptotic cells. The results of three independent experiments are shown, and data is presented as mean plus standard deviation (SD). Figure was adapted from Akpa C. A. et al., (180).

To show the time dependence of apoptosis mediated by DZNep, 12 lymphoma cell lines (consisting of BLs and DLBCLs) were treated with 5 µM DZNep. Measurement of apoptotic cells was done at 24 hours, 48 hours and 72 hours following treatments. At 72 hours, we could clearly observe greater than 20% apoptotic cells measured for many DZNep-sensitive cell lines (Carnaval, U-2932 R2, BL-41, BL-2, SU-DHL-10, WSU-DLCL-2, KARPAS-422 and BLUE-1) (figure 4B). Some cell lines (CA-46 and DG-75) however, showed a low percentage of apoptotic cells even at 72 hours after DZNep treatment. We thus made further DZNep treatments for 72 hours since after this time, there was a high tendency that the cell number of the untreated controls could exceed the maximum density stipulated by the DSMZ for optimal growth of the cells.

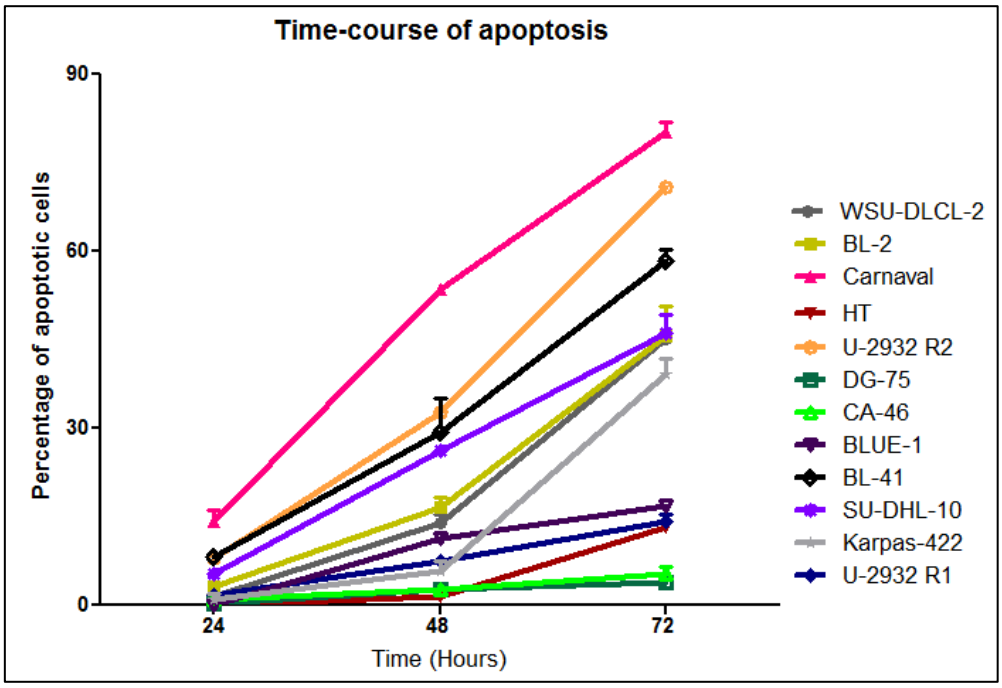

Figure 4B. DZNep-mediated apoptosis is time-dependent. 5 µM DZNep was administered to 12 B-cell lymphoma cell lines, and the percentage of apoptotic cells measured using flow cytometry at 24 hours, 48 hours and 72 hours as reported (180). The values shown were normalized with those of the controls. Figure was adapted from Akpa C. A. et al., (180).

Having established the optimal concentration and time point for DZNep treatment, the 12 lymphoma cell lines, were administered 5 µM DZNep for 72 hours. Upon measurement of the percentage of apoptotic cells, we observed a gradation in the response of the cell lines to apoptosis (figure 4C).

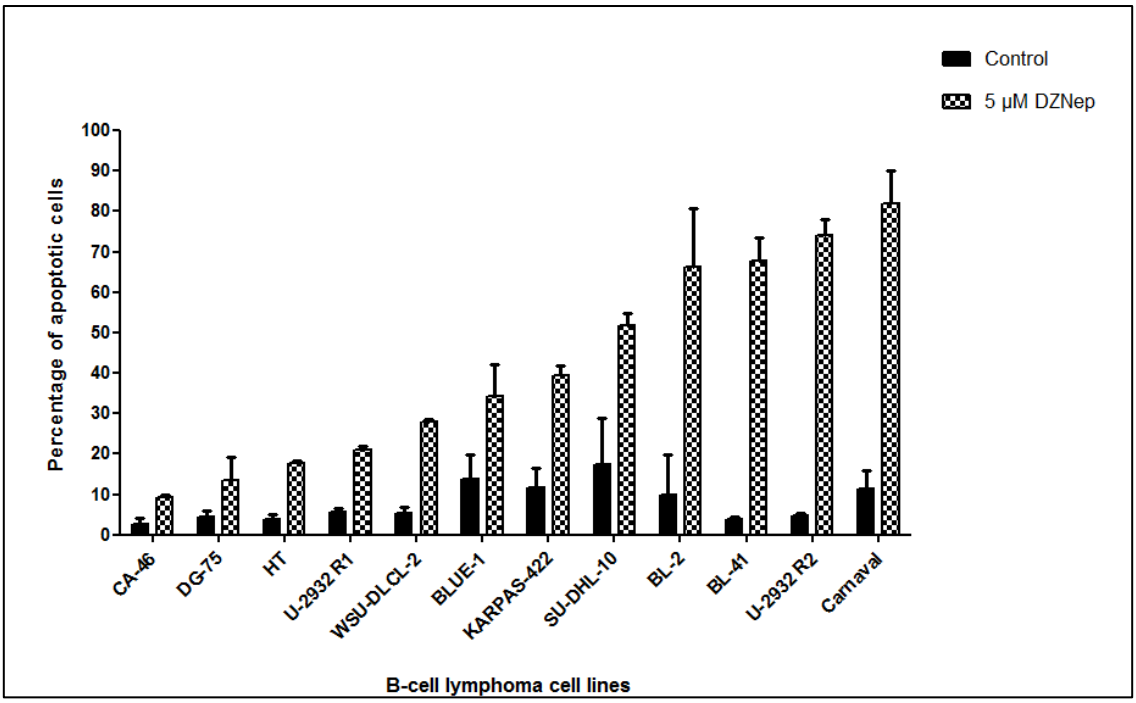

Figure 4C. Effect of DZNep on apoptosis in B-cell lymphoma cell lines. 12 lymphoma cell lines were either untreated or treated for 72 hours with 5 µM DZNep, and apoptosis was measured afterwards with flow cytometry. The above data is presented as mean plus SD from 3 independent replicates. Figure adapted from Akpa C. A. et al., (180).

The need to better classify the cell lines as DZNep-sensitive or DZNep-resistant arose following the observation that some cell lines only reacted weakly to apoptosis following DZNep exposure using already established culture conditions. To achieve this, we determined the IC_{50}. Based on our IC_{50} definition (180), 7 cell lines were grouped as DZNep-sensitive (IC_{50} between 2 – 10 µM), 3 cell lines were grouped as DZNep-resistant (IC_{50} > 15 µM), while 2 cell lines fell within an intermediate group (IC_{50} between 10 – 15 µM) (figure 4D). We are aware that these groups demonstrate gradual concentration differences. However, to correlate the reactivity of the cell line to DZNep treatment a clustering of cell lines with similar behavior is required.

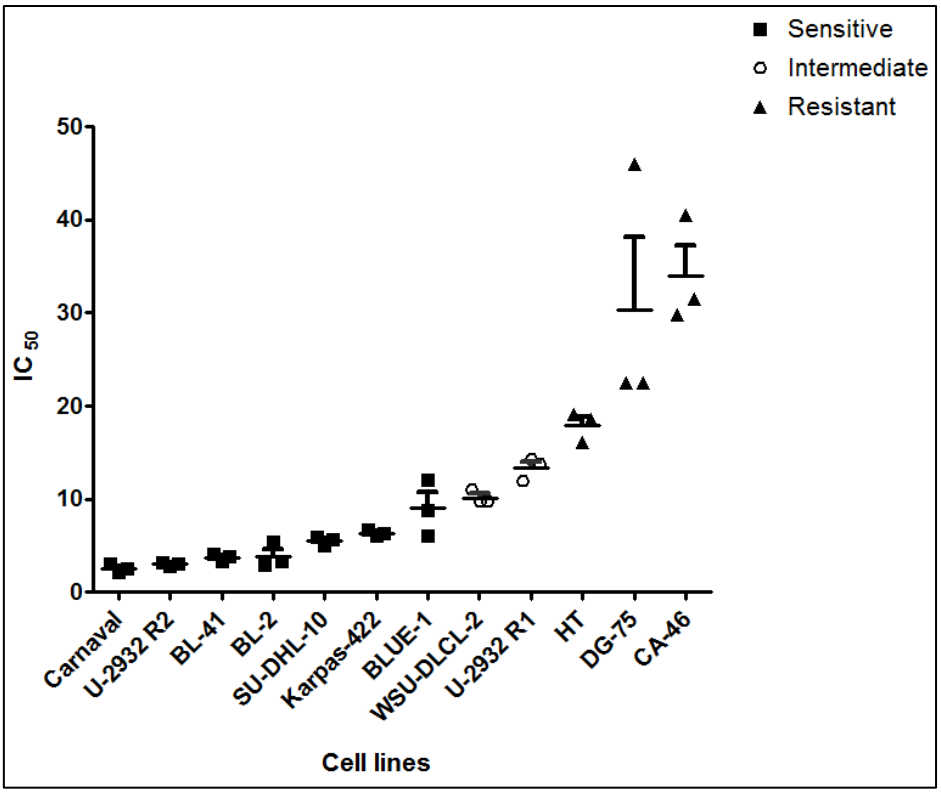

Figure 4D. DZNep-sensitive and DZNep-resistant cell lines based on IC_{50}. The IC_{50} for each cell line was determined, and the cell lines were grouped into a DZNep-sensitive, a DZNep-resistant and an intermediate group. The above measurement is presented as mean plus SD of triplicate experiments. Figure adapted from Akpa C. A. et al., (180).

To use another method for confirmation that cell lines designated as DZNep-resistant based on the IC_{50} results were indeed resistant, Western blot showing PARP cleavage expression was performed using two representative DZNep-resistant cell lines. These cell lines, CA-46 and HT were treated with increasing DZNep concentrations until 10 µM. The cells were harvested, the percentage of apoptotic cells determined with flow cytometry, and total cell protein lysate from the cells used for Western blot analysis. The results showed that both DZNep-resistant cell lines display minimal changes in the level of cleaved PARP expression after DZNep treatment in relation to their untreated controls (figure 4E).

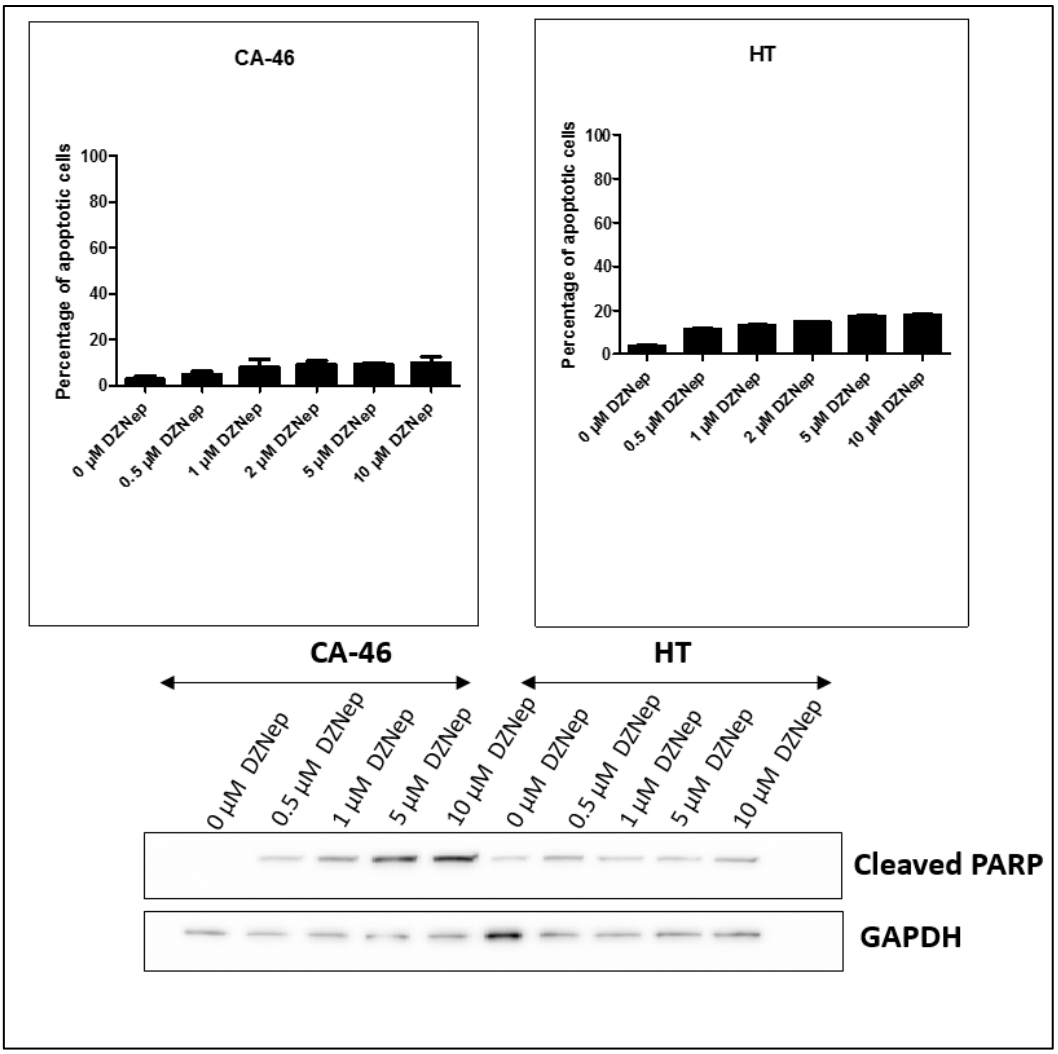

Figure 4E. DZNep-resistant cell lines (as determined by IC_{50} values) CA-46 and HT show minimal apoptotic cells and comparable cleaved PARP expression following exposure to DZNep. The upper panel shows the percentage of apoptotic cells as measured by flow cytometry. The lower panel shows the Western blot result following the analysis of protein lysate isolated from DZNep treated cells and their controls. Glyceraldehyde 3-phosphate dehydrogenase (GAPDH) was used as a loading control.

3.2. Sensitivity to DZNep is independent of the *EZH2* mutation status, lymphoma type, and *MYC*, *BCL2* and *BCL6* translocations

Having shown that DZNep possesses a robust in vitro apoptotic capacity, we sought to address whether the sensitivity or resistance of the cell lines to DZNep depends on the type of lymphoma, the *EZH2* mutation status or the presence of *MYC*, *BCL2* or *BCL6* translocations.

We first determined the *EZH2* mutation status of the cell lines, focusing on the frequently reported *EZH2* mutation sites already known (Tyr646, Ala682 and Ala692). In 4 out of the 12 cell lines analyzed, the Tyr646 mutation was detected (figure 5A). This mutation was expressed in these cell lines at the RNA (cDNA) level as demonstrated by Sanger sequencing. The amino acid change from Tyrosine to Phenylalanine was observed in the cell lines SU-DHL-10,

Carnaval and WSU-DLCL-2, while a change from Tyrosine to Asparagine was noted in KARPAS-422. None of the cell lines had *EZH2* mutated at Ala682 and Ala692 hotspots.

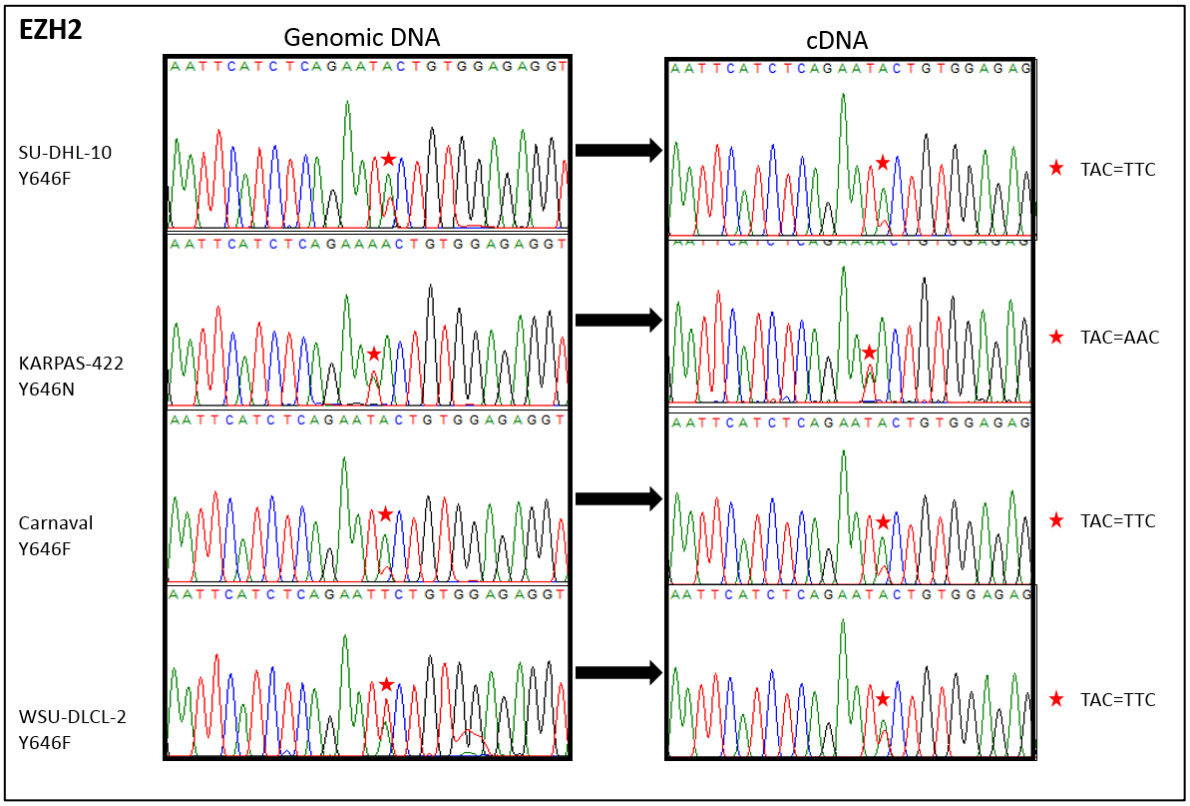

Figure 5A. Summary of *EZH2* mutations detected in the cell lines at the *EZH2* mutation hotspot Tyr646. Results of the lymphoma cell lines that expressed *EZH2* Tyr646 mutation (SU-DHL-10, KARPAS-422, Carnaval and WSU-DLCL-2) as determined by Sanger sequencing. Figure adapted from Akpa C. A. et al., (180).

We also performed FISH analysis on sections of FFPE cell line blocks and cytospins of cell lines to determine cell lines which have or which do not have *MYC*, *BCL2* and *BCL6* translocations. The results (figure 5B) reveal cell lines which harbor (+) or do not harbor (-) the respective translocations. *MYC* translocations for the cell lines DG-75, CA-46 and SU-DHL-10 was confirmed from the DSMZ information on the cell lines (found on DSMZ website with the cell line identification numbers: ACC 83, ACC 73 and ACC 576 respectively). *MYC* translocation status of the cell lines HT and WSU-DLCL-2 was not investigated since this is already known (198, 199).

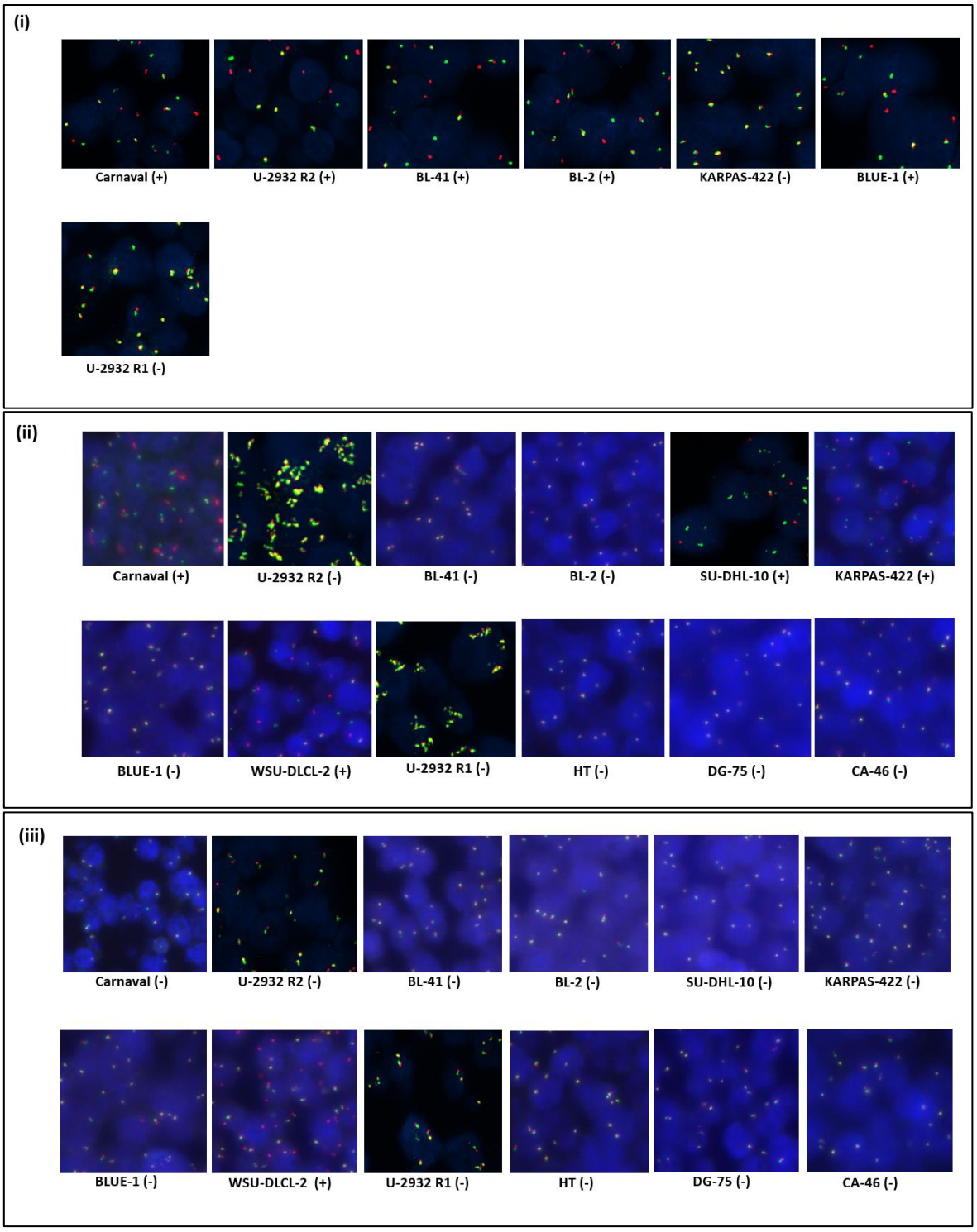

Figure 5B. FISH data showing cell lines which harbor (+) or do not harbor (-) (i) *MYC* (ii) *BCL2* and (iii) *BCL6* translocations. Figure adapted from Akpa C. A. et al., (180).

Integrating the data from the lymphoma type, the *EZH2* mutation status and *MYC*, *BCL2* and *BCL6* translocation status, there was no correlation between DZNep sensitivity or resistance and these mentioned factors. Nonetheless, we observed that the Tyr646 mutation is expressed predominantly in *BCL2*-translocated DLBCLs (table 6).

Table 6. Association between the lymphoma type, the *EZH2* mutation status, the *MYC*, *BCL2* and *BCL6* translocation status and DZNep sensitivity.

Cell line	Lymphoma type	*EZH2* Tyr646 mutation	Type of Tyr646 mutation	*MYC* translocation	*BCL2* translocation	*BCL6* translocation	DZNep-sensitive	IC_{50}
Carnaval	DLBCL	+	TAC→TTC (Tyr641Phe)	+	+	-	+	2.5
U-2932 R2	DLBCL	-	-	+	-	-	+	3.0
BL-41	BL	-	-	+	-	-	+	3.8
BL-2	BL	-	-	+	-	-	+	3.8
SU-DHL-10	DLBCL	+	TAC→TTC (Tyr646Phe)	+	+	-	+	5.4
KARPAS-422	DLBCL	+	TAC→AAC (Tyr646Asn)	-	+	-	+	6.3
BLUE-1	BL	-	-	+	-	-	+	8.7
WSU-DLCL-2	DLBCL	+	TAC→TTC (Tyr646Phe)	+	+	+	+	10.1
U-2932 R1	DLBCL	-	-	-	-	-	+	13.2
HT	DLBCL	-	-	-	-	-	-	17.8
DG-75	BL	-	-	+	-	-	-	27.4
CA-46	BL	-	-	+	-	-	-	33.4

The table was adapted from Akpa C. A. et al., (180).

Further grouping of the cell lines with focus on the strength of apoptosis measured upon DZNep treatment and their *EZH2* mutation status (Tyr646) showed low correlation between these two variables. Nevertheless, we showed that cell lines resistant to DZNep (with no to weak apoptosis) did not have *EZH2* mutated at Tyr646 (figure 5C).

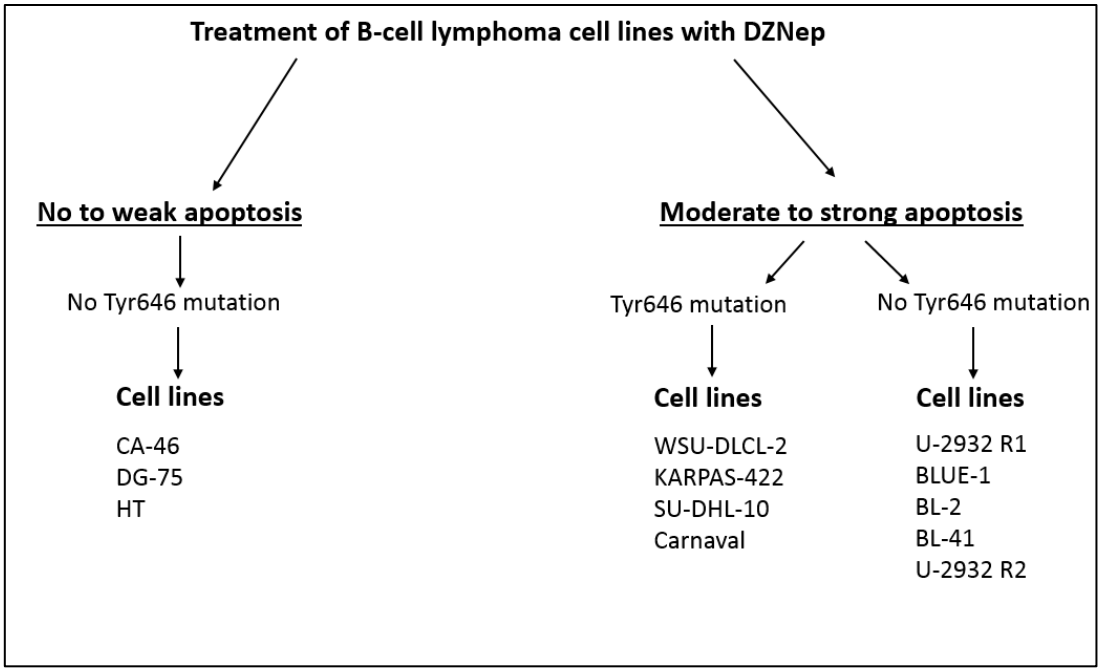

Figure 5C. Grouping of the 12 lymphoma cell lines based on the strength of apoptosis measured following DZNep administration and the *EZH2* mutation status. Figure adapted from Akpa C. A. et al., (180).

3.3 Consequence of mutated *EZH2* on H3K27me3 in B-cell lymphoma cell lines

To check the impact of *EZH2* mutation on H3K27me3 mark in the genome, we performed Western blot assay with extracted protein lysates from *EZH2*-mutated and wild-type *EZH2* lymphoma cell lines. We showed that this gain-of-function mutation is associated with an increased H3K27me3 in the cell, as cell lines with the Tyr646 mutation had increased H3K27me3 protein expression (figure 6).

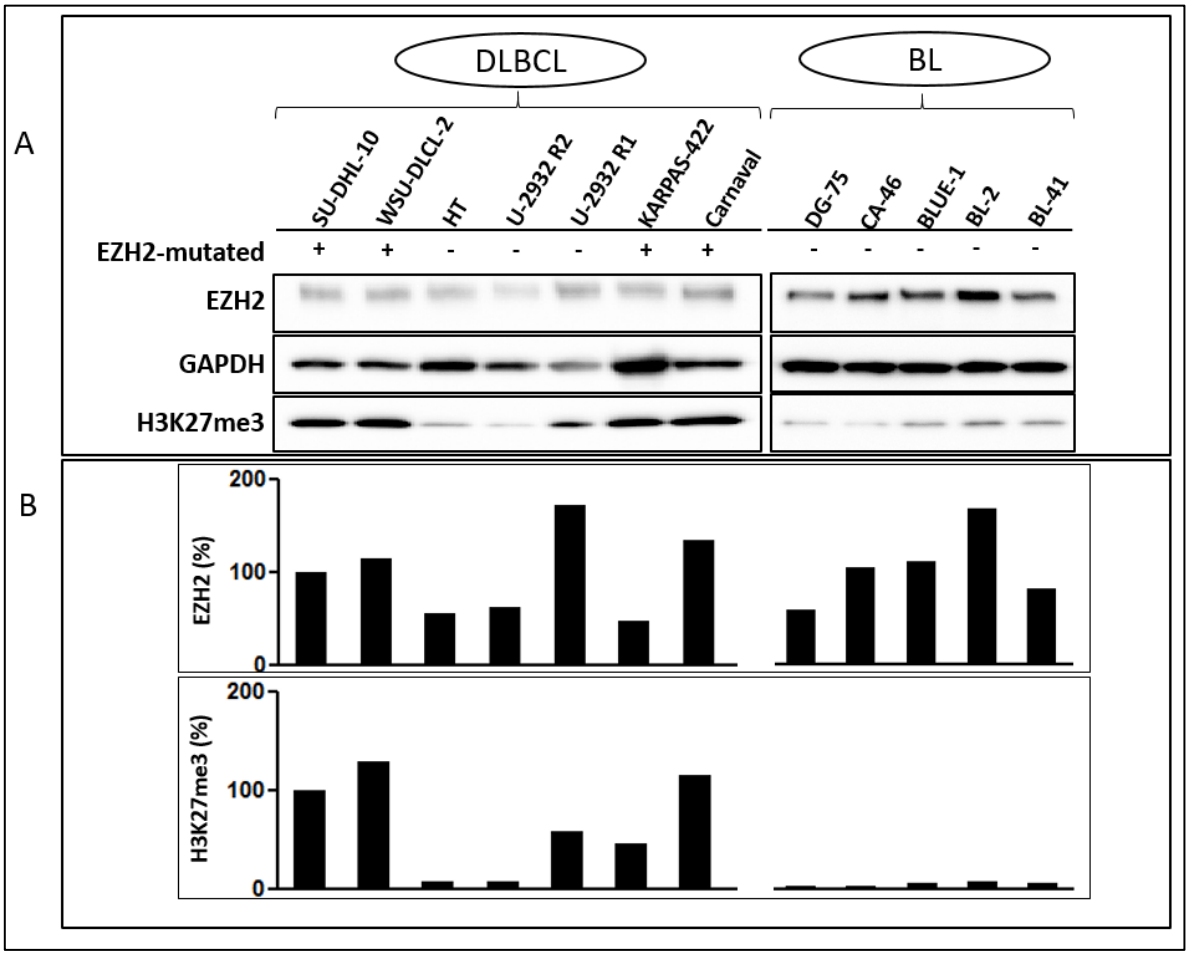

Figure 6. **Cell lines with mutated *EZH2* have H3K27me3 overexpression relative to cell lines with wild-type *EZH2*.** (A) Western blot of whole cell protein lysates from the 12 lymphoma cell lines used in this work, showing EZH2 and H3K27me3 expression. GAPDH used as a loading control. (B) EZH2 and H3K27me3 densitometric quantification (SU-DHL-10 served as a reference cell line while GAPDH was used for data normalization). Figure adapted from Akpa C. A. et al., (180).

3.4 DZNep induces apoptosis by the inhibition of EZH2 and downregulation of H3K27me3 in lymphoma

To understand whether DZNep indeed inhibits EZH2 and causes subsequent H3K27me3 downregulation, 3 cell lines, one *EZH2*-mutated cell line (KARPAS-422) and two wild-type *EZH2* cell lines (BL-2 and BLUE-1) were treated with increasing concentrations of DZNep. Total protein lysates were prepared from the cells and used for Western blot analysis. The

results showed a decrease in EZH2 expression and a concomitant downregulation of H3K27me3 levels in the cells with increasing concentrations of DZNep (figure 7A).

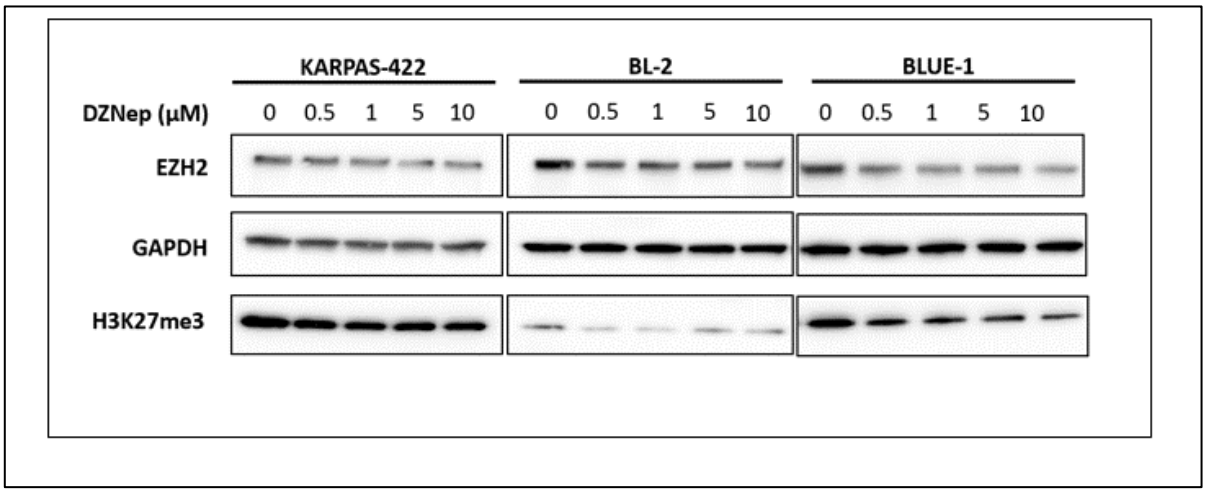

Figure 7A. Western blot showing progressive downregulation of H3K27me3 in lymphoma cell lines treated with gradually increasing DZNep concentrations. Figure adapted from Akpa C. A. et al., (180).

To investigate whether DZNep has to capacity to reduce H3K27me3 level despite this protein being overexpressed in *EZH2*-mutated lymphoma cell lines, we treated 4 cell lines with DZNep. 2 of these cell lines represent *EZH2*-mutated cell lines (WSU-DLCL-2 and Carnaval), and the other 2 representative of wild-type *EZH2* cell lines (BL-2 and BLUE-1). Western blot with whole cell protein lysate from the cells was performed showing PARP cleavage, EZH2 and H3K27me3 expression. The results indicate that there is increased H3K27me3 in cell lines having the *EZH2* Tyr646 mutation, however, DZNep decreases this histone trimethylation mark, promoting apoptotic death of the cells (figure 7B).

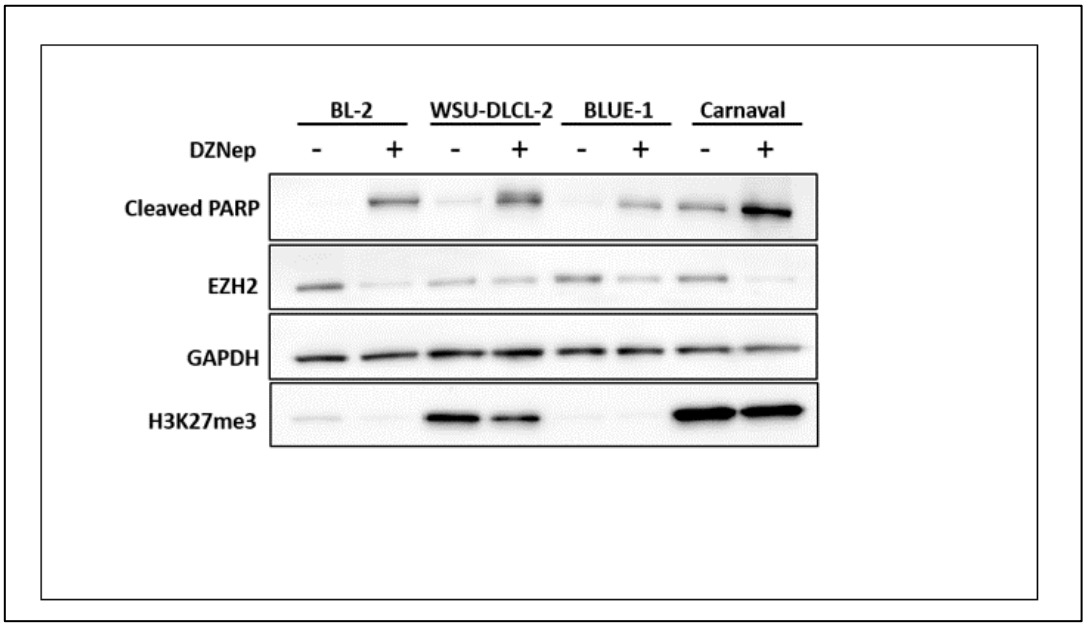

Figure 7B. Decrease in H3K27me7 in *EZH2*-mutated cell lines treated with DZNep. Figure adapted from Akpa C. A. et al., (180).

3.5 DZNep suppresses the proliferation of lymphoma cells

Considering that DZNep possesses a strong capacity to induce apoptosis in lymphoma cells, we considered looking into its effect on lymphoma cell proliferation. First, we analyzed the expression of proliferation-associated genes - proliferating cell nuclear antigen (*PCNA*) and cyclin dependent kinase 2 (*CDK2*) - in 7 cell lines including the generated DZNep-resistant clone and its control, in the presence and absence of DZNep pressure. The results displayed a decrease in the expression of these two proliferation markers in the DZNep-treated cell lines when compared to the untreated controls (figure 8A).

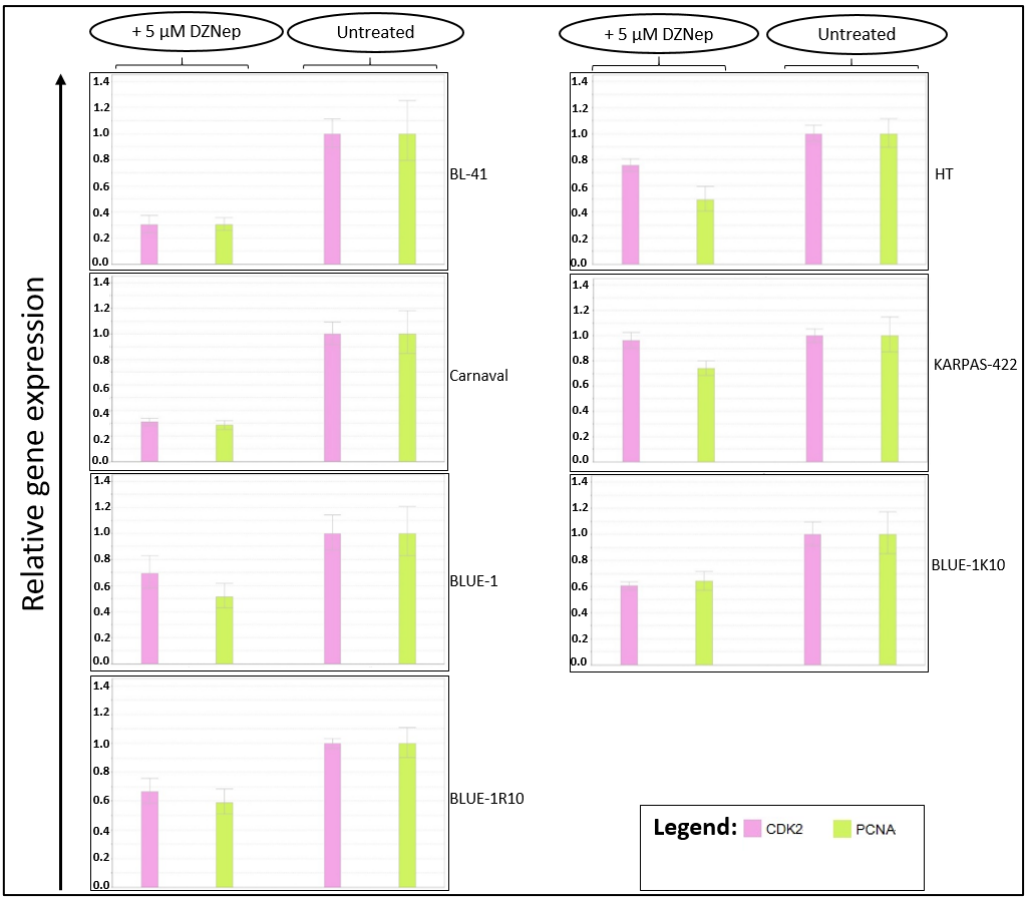

Figure 8A. DZNep decreases the expression of the proliferation genes *PCNA* and *CDK2* in lymphoma cell lines. Lymphoma cell lines were either untreated or treated with 5µM DZNep for 72 hours. Cells were harvested and RNA extracted from them. This was followed by cDNA synthesis and analysis of relative *PCNA* and *CDK2* gene expression by real-time RT-PCR. The untreated samples were used as reference while *B2M* was used as an endogenous control.

Since the above analysis was made without exclusion of the dead and apoptotic cell population from the total cells used for RNA synthesis, we also used flow cytometry to confirm the effect of DZNep on proliferation. Using this method, the number of vital cells present in the culture was counted, while excluding the dead and apoptotic cells present under DZNep-treated and untreated conditions. The results showed a time-dependent decrease in the proliferation rate of the cell lines in presence of DZNep (figure 8B). At 72 hours, we could notice a clear decrease

in the number of vital cells present in the culture under DZNep pressure in comparison to the untreated cultures.

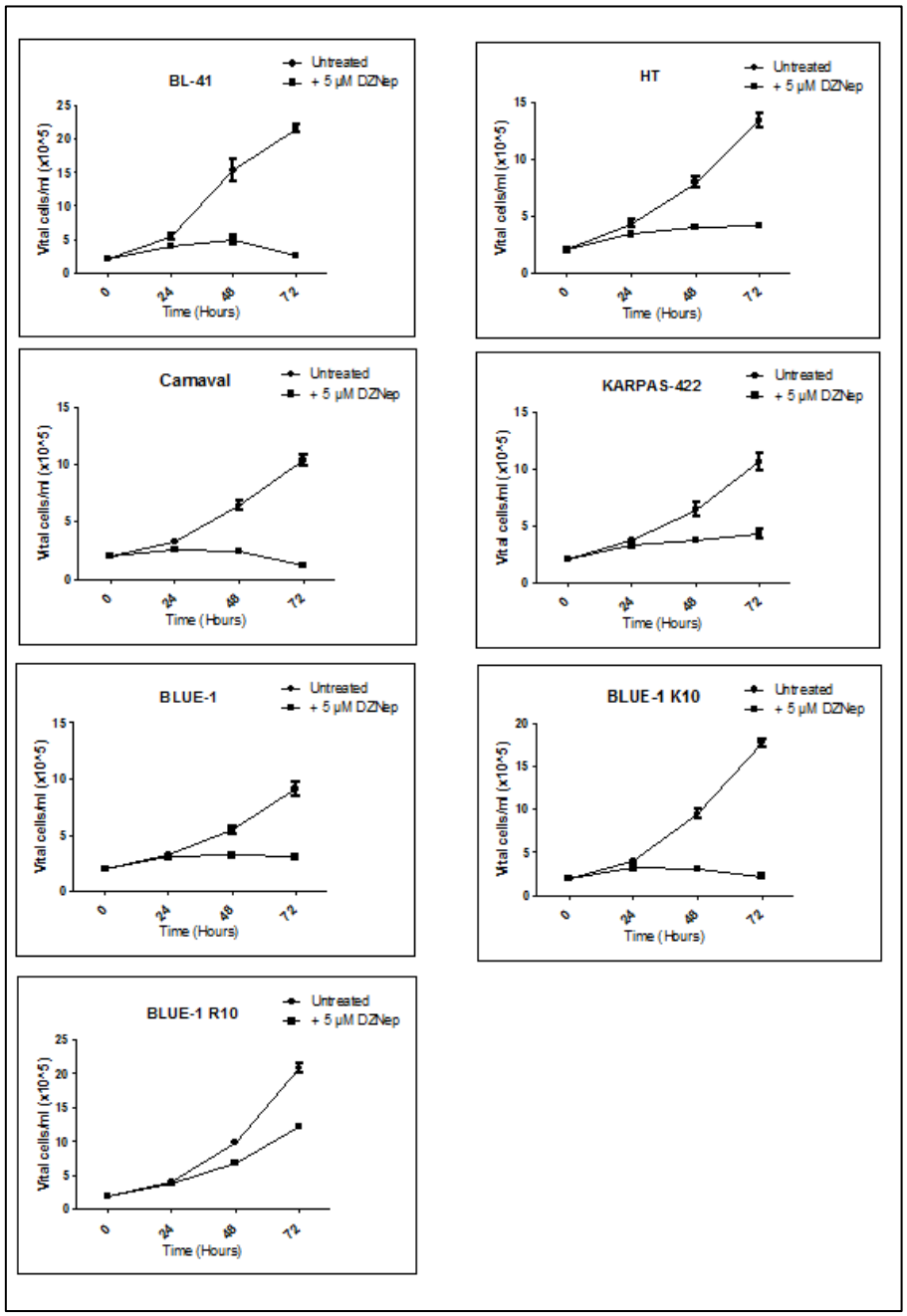

Figure 8B. DZNep inhibits proliferation of lymphoma cell lines. We measured proliferation of *EZH2*-mutated (Carnaval and KARPAS-422) and *EZH2* wild-type (BL-41, HT, BLUE-1, BLUE-1R10 and BLUE-1K10) cell lines either treated or untreated with 5 µM DZNep for 24, 48 and 72 hours. Figures for BL-41, KARPAS-422, HT, Carnaval and BLUE-1 were adapted from Akpa C. A. et al.,(180).

3.6 Comparison of the apoptotic effect of DZNep and EPZ-6438

We analyzed the efficacy of DZNep and EPZ-6432 - a direct EZH2 inhibitor currently tested in clinical trials (phase II) - in mediating apoptosis. Initially, 2 *EZH2*-mutant and 2 *EZH2* wild-type cell lines were treated with 5 µM of both DZNep and EPZ-6438 respectively. The results obtained following measurement of the number of apoptotic cells indicate that DZNep exhibited

no inclination towards causing apoptosis in either types of cell lines (figure 9A). The percentage of apoptosis caused by 5 µM EPZ-6438 however, was obviously lower in comparison to that measured in presence of 5 µM DZNep. Even the cell line classified as DZNep-resistant (HT) showed about 10% more apoptotic cells in comparison to EPZ-6438 under identical culture conditions.

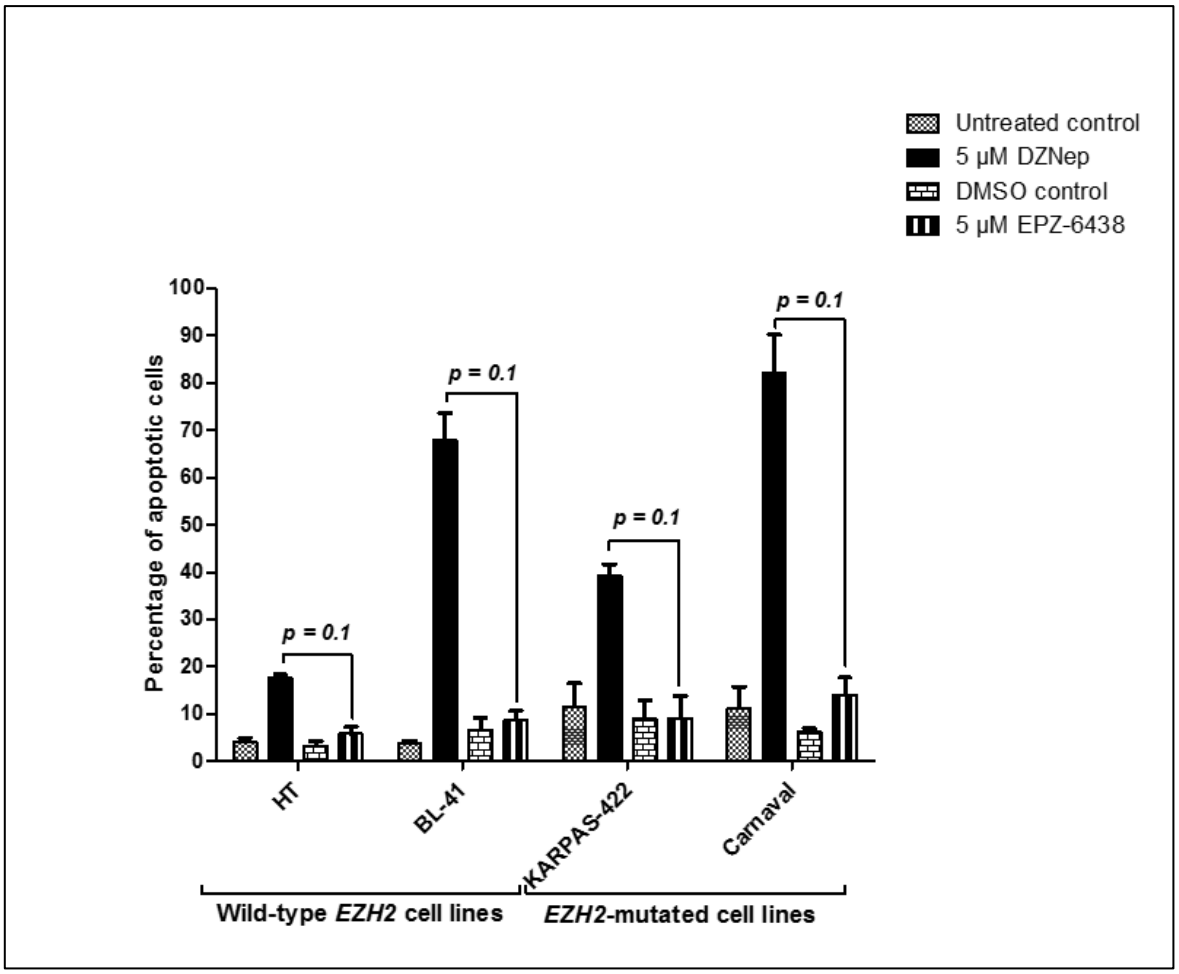

Figure 9A. Stronger apoptosis is measured within a short time after DZNep treatment in comparison with that observed after EPZ-6438 treatment. Each of the cell lines was treated for 72 hours with 5 µM DZNep and 5 µM EPZ-6438 respectively. The percentage of apoptotic cells were measured afterwards by flow cytometry. Data is presented as mean plus SD from three independent measurements. Figure adapted from Akpa C. A. et al.,(180).

Prolonged EPZ-6438 treatment of the same cell lines used in figure 9A (HT, BL-41, KARPAS-422 and Carnaval) was performed based on a previous report (139). In this case, the cell lines were treated for up to 13 days with both 5 µM and 10 µM EPZ-6438 as described (180). We noticed (figure 9B) that the DZNep-sensitive *EZH2*-mutant and wild-type *EZH2* cell lines exhibited an almost similar percentage of apoptosis after treatment with this drug even at 13 days post-exposure. The concentration of the inhibitor used did not seem to make a huge difference as to the percentage of apoptosis measured. However, HT cell line, which is DZNep-

resistant, exhibited a robust proportion of apoptotic cells, which was obvious after the third day following EPZ-6438-treatment.

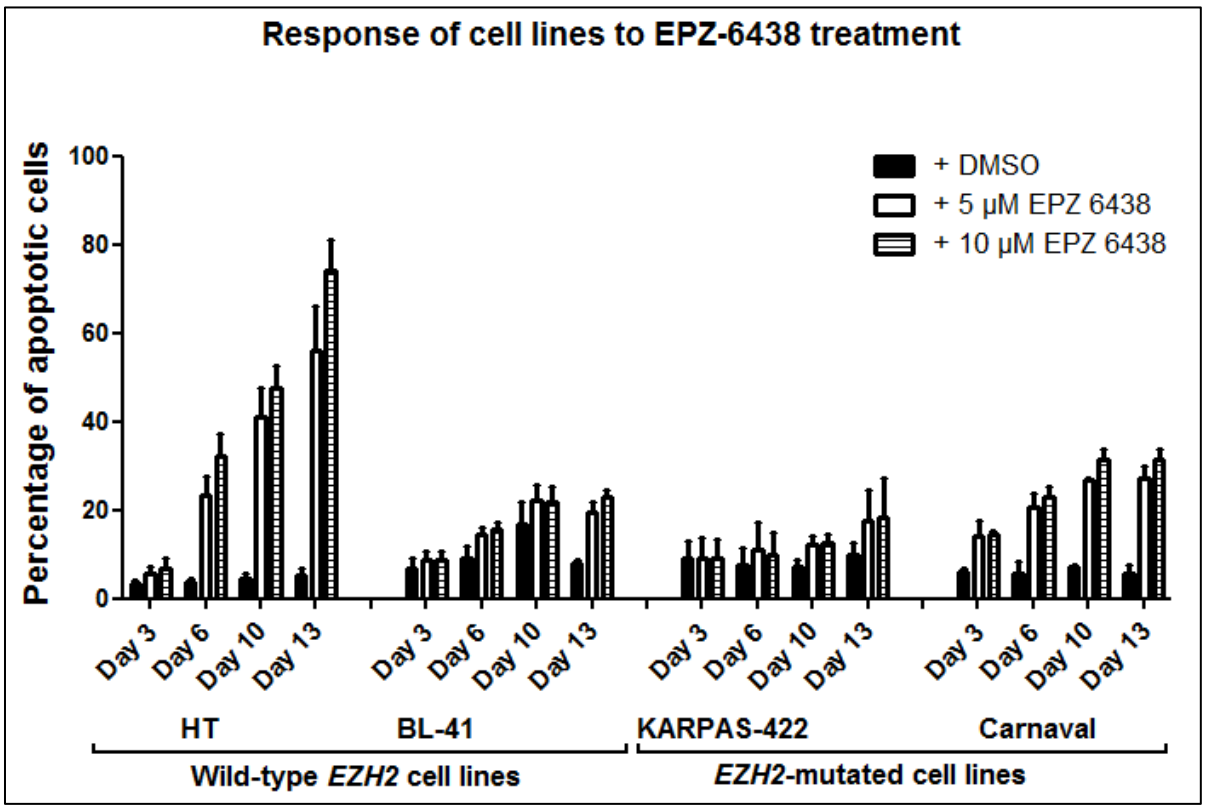

Figure 9B. EPZ-6438 causes apoptosis in both DZNep-sensitive and DZNep-resistant cell lines upon long-term exposure. HT, BL-41, KARPAS-422 and Carnaval cell lines were administered 5 µM and 10 µM EPZ-6438 for a duration of 13 days. The cells were split, apoptosis was measured, and culture medium was replaced every third to fourth day. The respective amounts of the inhibitor was replaced in the culture medium following medium change. The equivalent amount of DMSO was also replaced in the culture medium of the negative control (as this was the solvent for EPZ-6438). The percentage of apoptotic cells as determined by flow cytometry is shown as mean plus SD from 3 independent measurements. Figure adapted from Akpa C. A. et al.,(180).

To investigate the apoptotic effect of EPZ-6438 on the generated DZNep-resistant clone, its corresponding control and the parent cell line from which it was generated (BLUE-1), a similar experiment to that performed in figure 9B was set up. This time, we treated the cell lines BLUE-1, BLUE-1K10 and BLUE-1R10 with 10 µM EPZ-6438 for up to 13 days accordingly. We showed that BLUE-1 as well as the generated clone and corresponding control were resistant to EPZ-6438 (figure 9C).

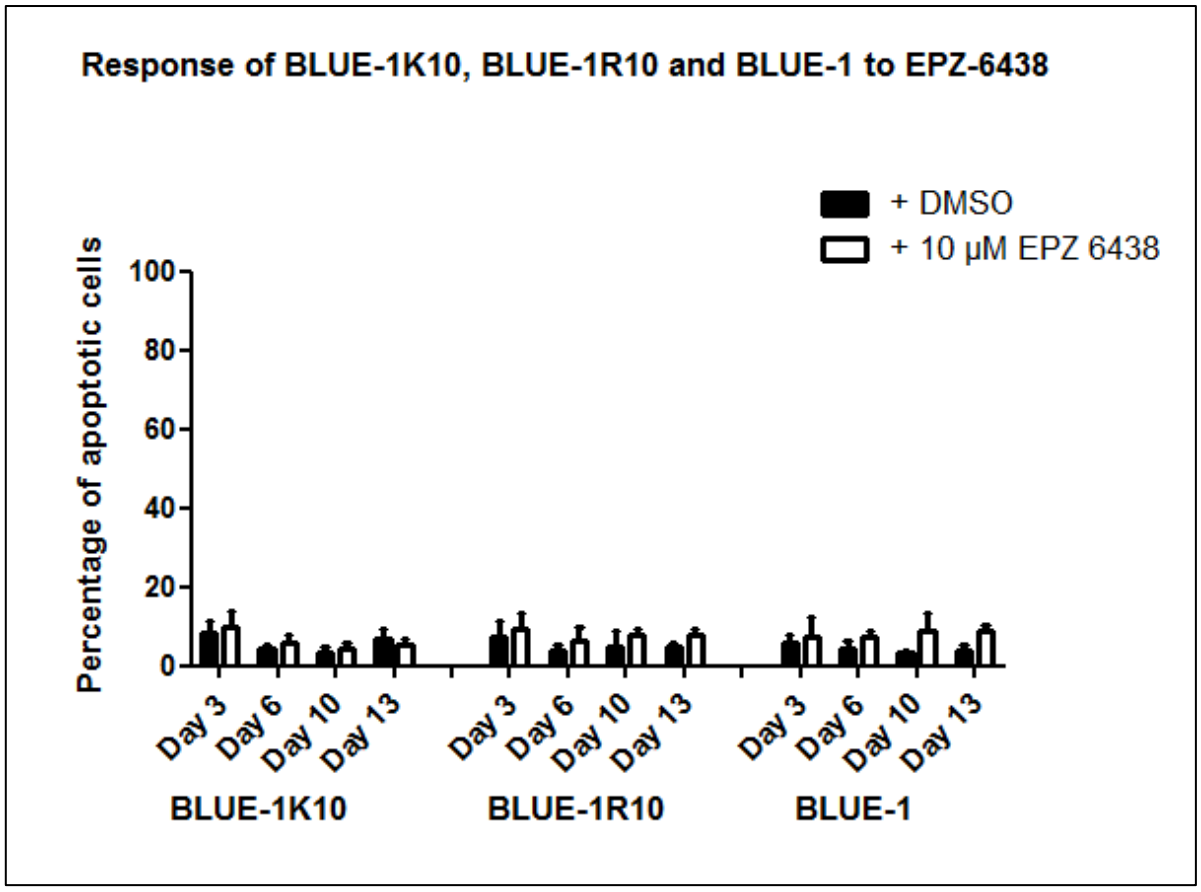

Figure 9C. The DZNep-resistant clone is also resistant to EPZ-6438. The DZNep-sensitive BLUE-1 cell line, the generated DZNep-resistant cell line BLUE-1R10 as well as its corresponding control BLUE-1K10 were treated with 10 µM EPZ-6438 for up to 13 days. The cells were split, apoptosis was measured, and the culture medium was replaced every third to fourth day. 10 µM EPZ-6438 was replaced in the culture medium following medium change. The controls received the same concentration of DMSO (10 µM). The above data is presented as mean plus SD from triplicate measurements.

3.7 Characterization of the generated DZNep-resistant clone

Because some cell lines are resistant to DZNep despite its strong apoptotic capacity, we aimed to probe the molecular mechanism behind this resistance and to detect biomarkers, which could be predictive of the therapeutic success of EZH2 inhibition with DZNep. To this end, we generated a DZNep resistant cell line as described in section 2.4 and characterized it alongside its corresponding control and the parent cell line BLUE-1.

First, we determined that this clone and control actually derived from the parent BLUE-1 cell line. One way this was done was by checking for the expression of distinct B-cell surface markers CD19 and CD20 to confirm cell lineage identity. This was done by immunophenotyping (described in section 2.3). As expected, both cell lines expressed CD19 but not CD20, just like the parent cell line (figure 10A).

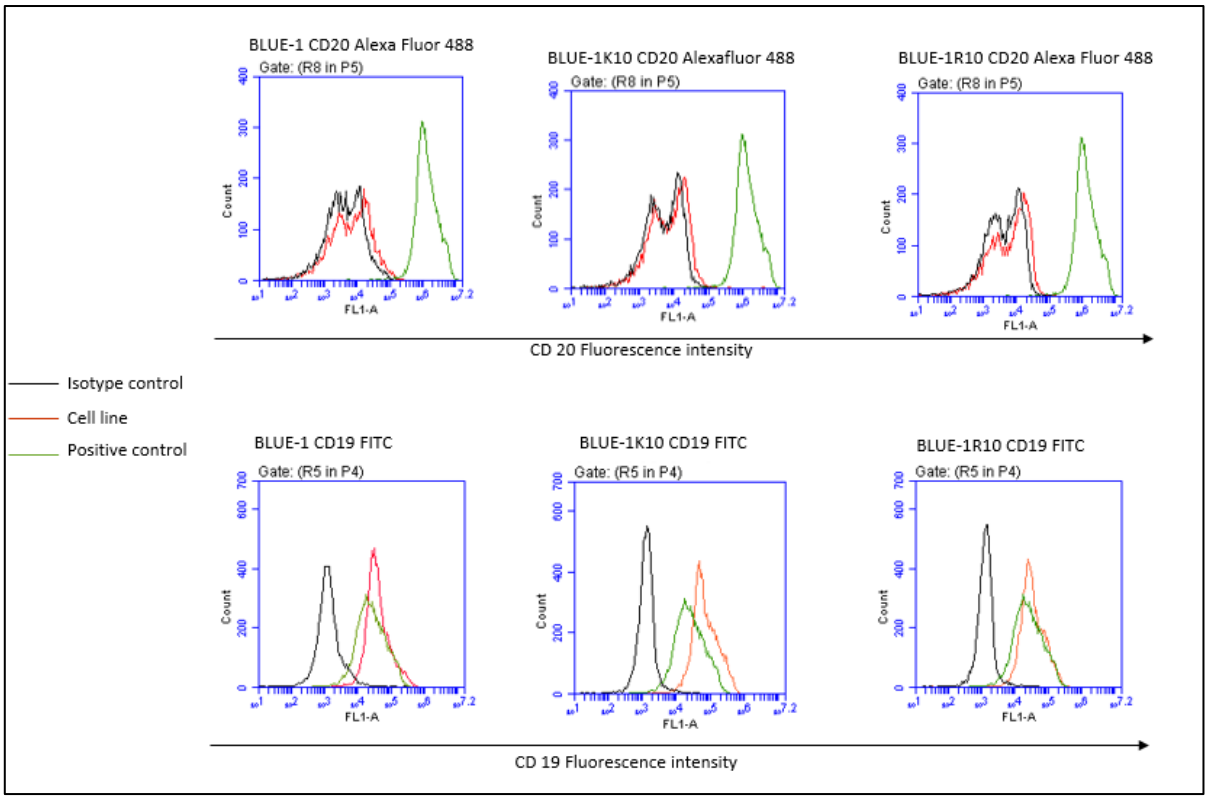

Figure 10A. Flow cytometry histograms showing cell surface expression of CD19 and CD20 in BLUE-1, BLUE-1K10 and BLUE-1R10. The cells were stained with the respective fluorescent-labelled antibodies against CD19 and CD20. Using flow cytometry, the fluorescence intensity of cells expressing the CD markers was detected. The dashed red line shows the respective cell line of interest, the dashed black line shows the isotype / negative control, and the dashed green line highlights the positive control (U-2932 R1 cell line).

In addition, we performed clonality studies to confirm the identity of the generated resistant clone and its control. This was done by checking the IGH gene rearrangement in the resistant clone, its corresponding control and cell line of origin. The results obtained showed that the IGH gene rearrangement for the three cell line clones (BLUE-1, BLUE-1R10 and BLUE-1K10) were identical (figure 10B).

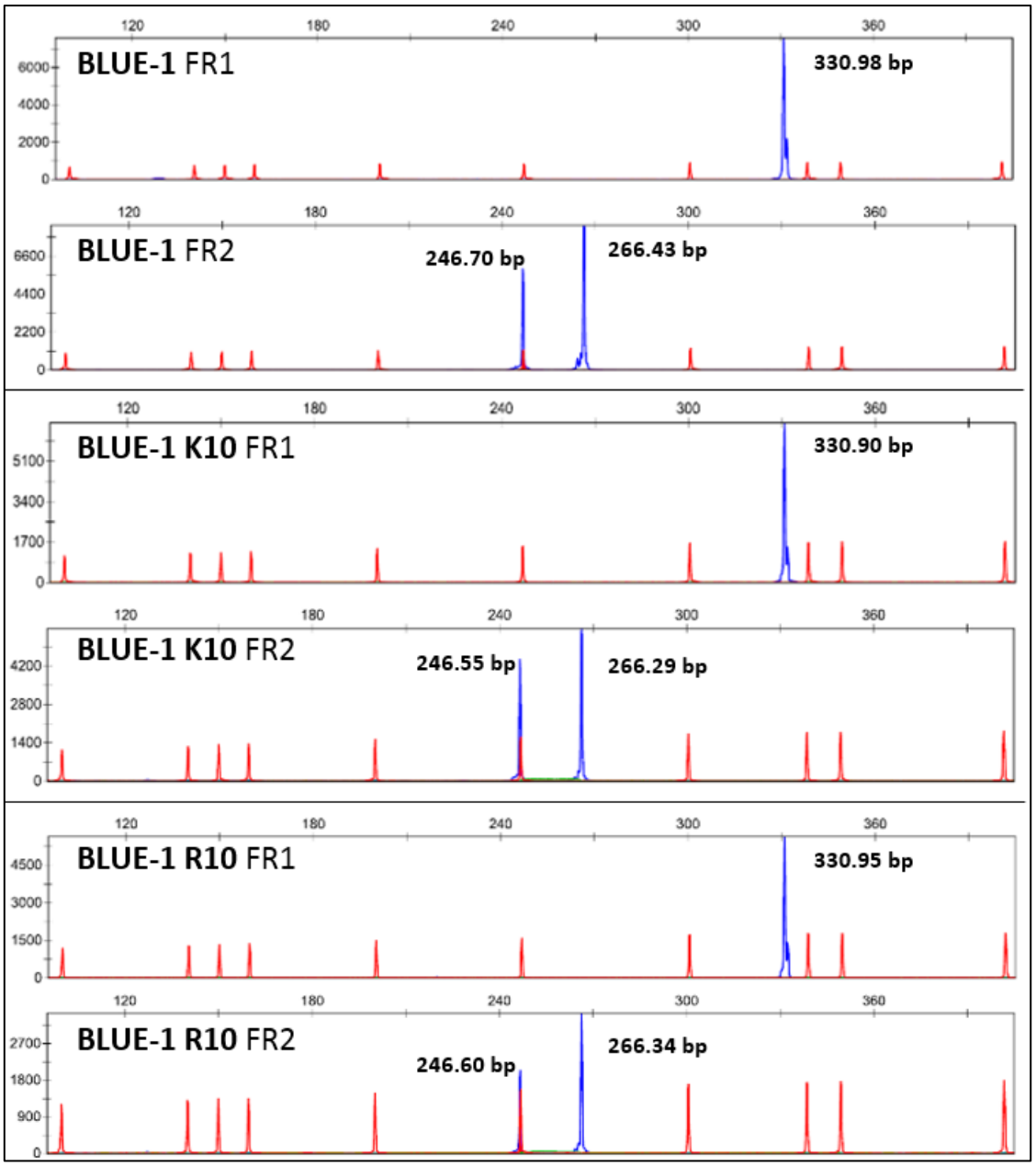

Figure 10B. BLUE-1, BLUE-1K10 and BLUE-1R10 exhibit identical B-cell clonality following multiplex PCR and accompanying GeneScan analysis of the resultant FR1 and FR2 sequences. FR1 sequences of the IGH gene for the three cell lines show monoallelic rearrangements (with one dominant blue peak) while FR2 sequences show biallelic rearrangements (two dominant blue peaks) as determined by GeneScan analysis. Figure adapted from Akpa C. A. et al., manuscript in review (appendix C).

Furthermore, the authenticity of the parent BLUE-1 cell line, the resistant clone and its control was verified and all three cell lines showed a short tandem repeat (STR) profile of a BLUE-1 cell line. The results of the chromosome analysis (karyotyping) for the three cell lines was also determined and shown in figure 10C.

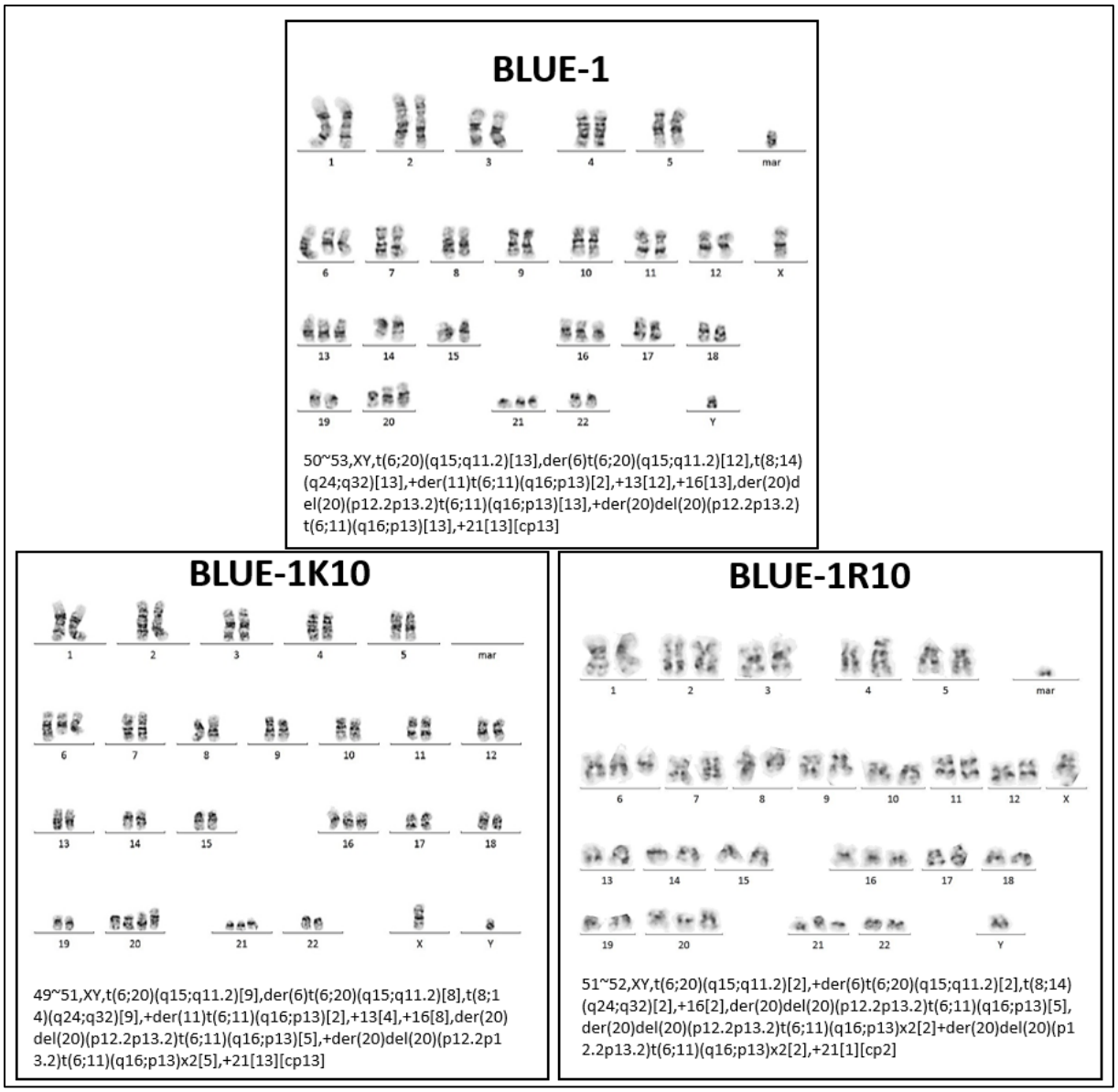

Figure 10C. Karyotypes of BLUE-1, BLUE-1K10 and BLUE-1R10. The karyotype was written with the international nomenclature (ISCN) 2013.The analysis was performed in collaboration with the research group of Prof. Reiner Siebert. Figure adapted from Akpa C. A. et al., manuscript in review (appendix C).

We further characterized the resistant clone by determining the doubling time in comparison to the corresponding control and the parent cell line. We showed that both BLUE-1K10 and BLUE-1R10 proliferate faster and have shorter doubling times than the parent cell line BLUE-1, which had a doubling time of about 35 hours (figure 10D).

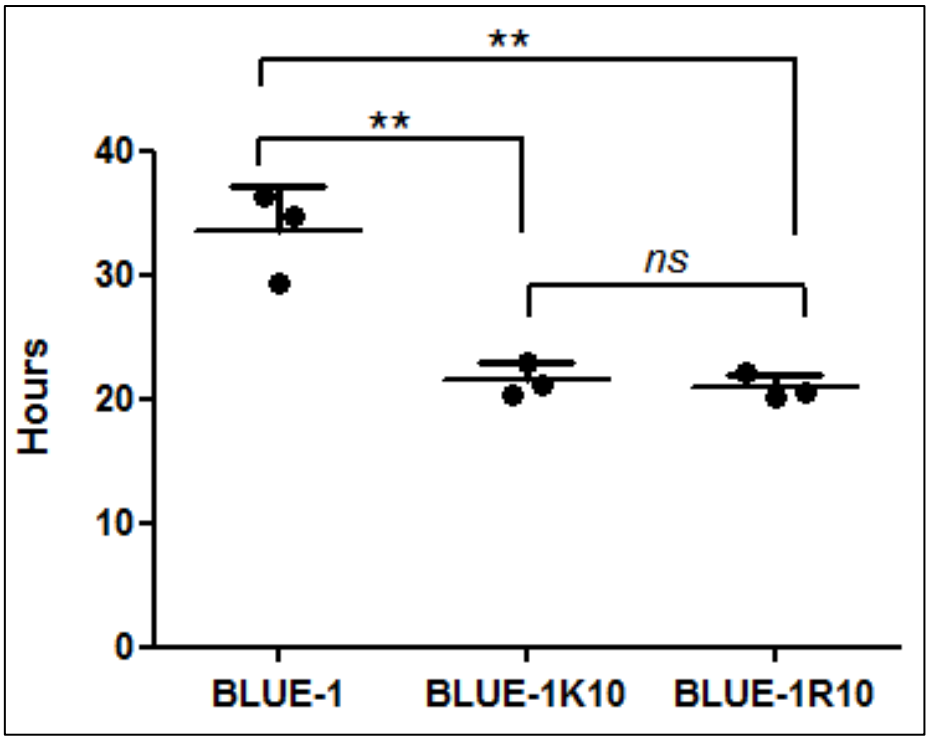

Figure 10D. BLUE-1, BLUE-1K10 and BLUE-1R10 proliferation rate analysis. The doubling time for BLUE-1, BLUE-1R10 and BLUE-1K10 cell lines was determined using measurements of the number of vital cells at 0 hours (beginning of incubation time) and at 48 hours (end of incubation time). The result is shown as mean plus SD from three measurements. ns means not significant. Figure adapted from Akpa C. A. et al., manuscript in review (appendix C).

More so, we analyzed the response of the generated DZNep-resistant clone and its corresponding control to DZNep treatment. In comparison with BLUE-1R10, BLUE-1K10 exhibited about 40% more apoptotic cells upon treatment of both cell lines for 72 hours with 5 µM DZNep (figure 10E). In addition, Western blot analysis of total protein lysates derived from both cell lines treated with 2 µM and 5 µM DZNep for 72 hours showed an increased cleaved PARP expression in BLUE-1K10, which is not the case in BLUE-1R10 (figure 10E).

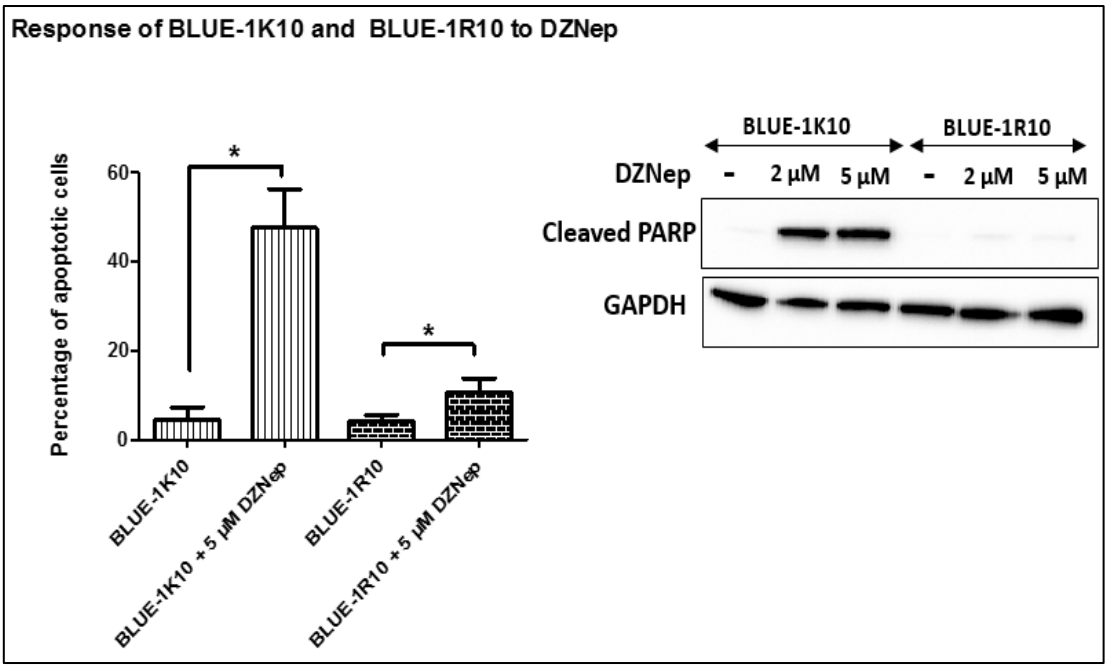

Figure 10E. BLUE-1K10 undergoes apoptosis when treated with DZNep while BLUE-1R10 is resistant to DZNep. Left: The fraction of apoptotic cells was determined following treatment of both cell lines for 72 hours with 5 µM DZNep. The controls were left untreated in culture. Flow cytometry was used for determination of the fraction of apoptotic cells. Data is presented as mean plus SD from three independent measurements. **Right:** Western blot showing the expression of cleaved PARP upon treatment of both cell lines with DZNep. GAPDH served as a loading control. Figure adapted from Akpa C. A. et al., manuscript in review (appendix C).

3.8 Identification of biomarkers underlying the resistance of BLUE-1R10

A microarray-based whole-genome copy number assay (OncoScan) was done to detect genomic changes such as copy number gains or losses and copy number neutral losses of heterozygosity in the cell lines BLUE-1K10, BLUE-1R10 and BLUE-1. The copy number alterations detected in the chromosomes are shown in figure 11A. As expected, all three cell lines harbored a deletion in 14qter which overlaps with the immunoglobulin heavy chain (IGH) locus which indicates a clonal rearrangement of these loci. A comparison of the copy number aberrations (CNA) in all three BLUE-1 derivatives as determined by OncoScan is shown in table 7.

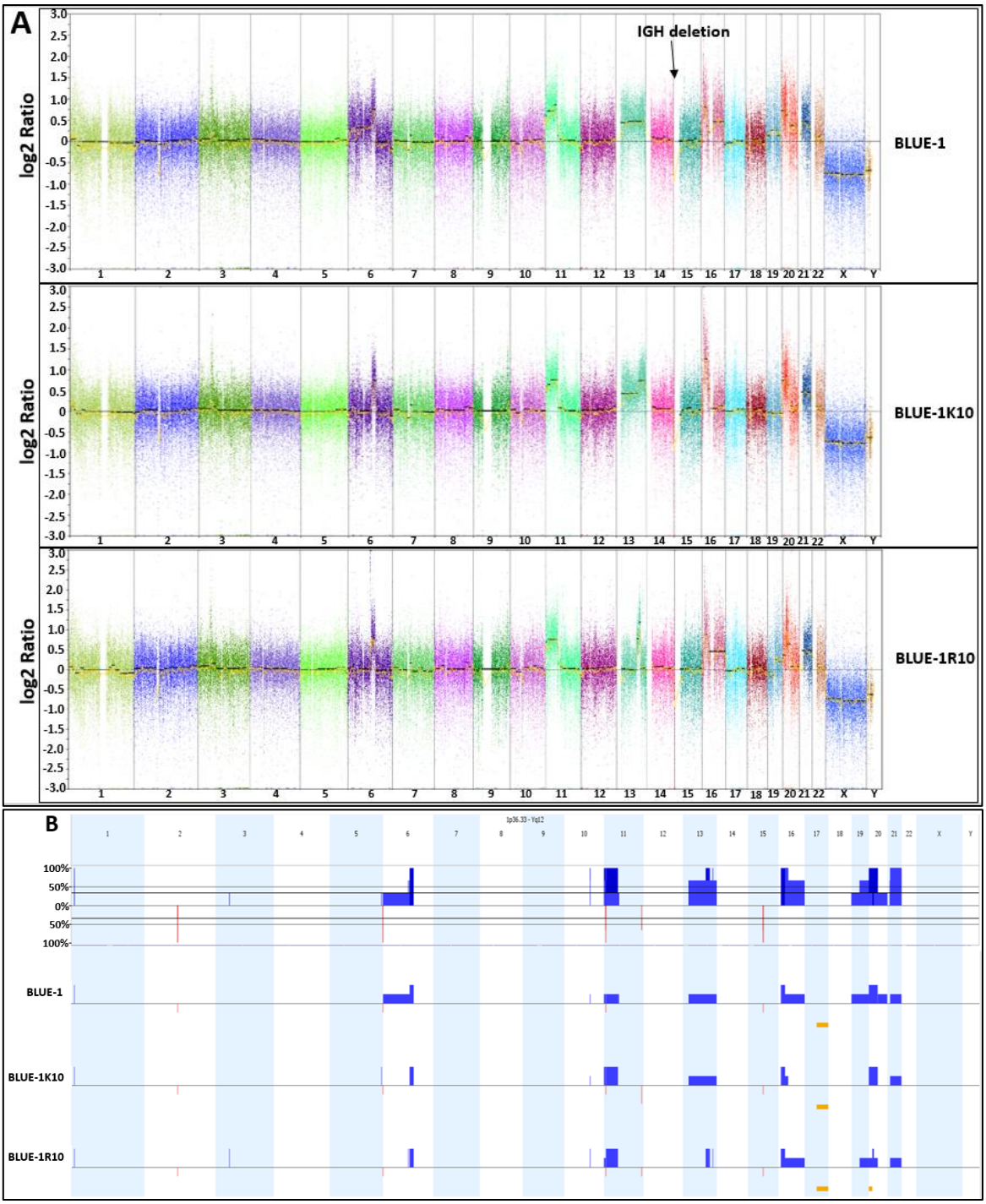

Figure 11A. Analysis of copy number alterations in the three BLUE-1 cell lines. In **panel A** are the log2 ratios for all three BLUE-1 samples depicted. Values centered around 0 indicate no aberrations whereas, an increased log2 ratio indicates a copy number gain and a decreased log2 ratio, a copy number loss. Of note, copy number neutral losses of heterozygosity (CNN-LOH) cannot be observed by log2 ratio. **Panel B** depicts the results of the chromosomal imbalance profiling for all three cell lines. The upper row shows the frequency of every alteration while the lower rows depict the CNA separately for all cell lines. Copy number gains are shown with blue bars, losses with red bars and CNN-LOH in orange bars. This picture clearly depicts that the majority of the CNA are shared between all BLUE-1 cell lines. The analysis was performed in collaboration with the research group of Prof. Reiner Siebert.

Table 7. Comparative copy number alterations (CNA) detected in BLUE-1, BLUE-1K10 and BLUE-1R10 as identified by OncoScan analysis.

Aberration	Genomic region (hg19)	Size (kbp)	Ensembl Gene Count	Cell lines
Loss	chr4:53960195-54283313	323.118	4	BLUE-1-R10
Gain	chr6:204908-28013410	27808.502	396	BLUE-1
High copy gain	chr6:86373374-87809402	1436.028	9	BLUE-1-R10
Gain	chr13:19084822-115103150	96018.328	968	BLUE-1 & BLUE-1K10*
Gain	chr16:8947035-11210415	2263.38	176	BLUE-1 & BLUE-1R10
Gain	chr16:11229588-23143876	11914.288	787	BLUE-1 & BLUE-1R10
Gain	chr16:23156450-90158005	67001.555	4049	BLUE-1 & BLUE-1R10
Gain	chr19:18306750-59093239	40786.489	1597	BLUE-1
Gain	chr19:247231-18101830	17854.599	866	BLUE-1
Gain	chr19:27754572-59093239	31338.667	1419	BLUE-1 & BLUE-1R10
CN-LOH	chr20:69093-11891608	11822.515	213	BLUE-1-R10

CN-LOH indicates copy neutral loss of heterozygosity. *aberration is recognized as two events by the software. The above table was generated in collaboration with the research group of Prof. Reiner Siebert. Table was adapted from Akpa C. A. et al., manuscript in review (appendix C).

Copy number variant analysis was also done on the WES data from BLUE-1R10 and BLUE-1K10 as described (section 2.10). On chromosome 6, we detected a high copy number gain for the *SNHG5*, *SMIM11P1*, *HTR1E* and *CGA* genes (left of figure 11B). On chromosome 20, we detected a prominent gain in the copy number for the *AHCY* gene; this gain extending until the adjoining section of *ITCH* gene (right of figure 11B).

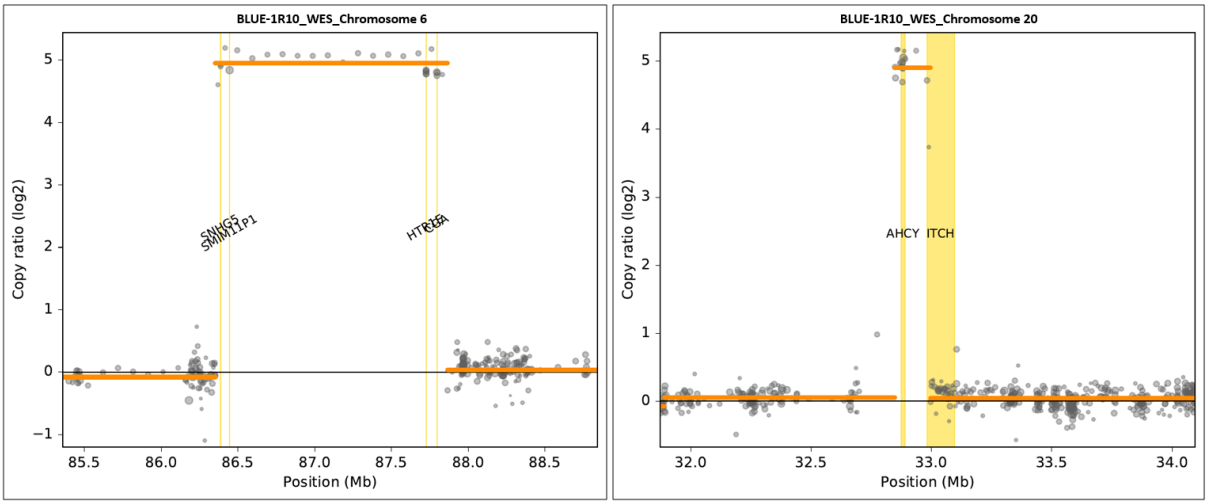

Figure 11B. Copy ratio plot (log2) of CNV regions in BLUE-1R10 when compared with BLUE-1K10. Individual genes are represented with the yellow bars while copy ratio values are represented with the gray dots. Copy number plots were generated in collaboration with the research group of Dr. Dieter Beule. The copy ratio plot for chromosome 20 was adapted from Akpa C. A. et al., manuscript in review (appendix C).

3.9 Validation of the detected *AHCY* copy number gain

3.9.1 Validation of *AHCY* copy number gain at the DNA level

From the listed targets, *AHCY* seemed most promising for further validation since it is the direct target of DZNep. Validation was performed using different techniques. One technique we used was the TaqMan CNV assay. This was performed on genomic DNA from all 12 cell lines, including BLUE-1R10 and BLUE-1R12 and their corresponding controls. The results show an increase in the *AHCY* copy number in BLUE-1R10, with about two-fold increase in BLUE-1R12 (figure 12A). We did not observe a profound *AHCY* copy number gain in the other lymphoma cell lines (including the other DZNep-resistant ones) used in this work.

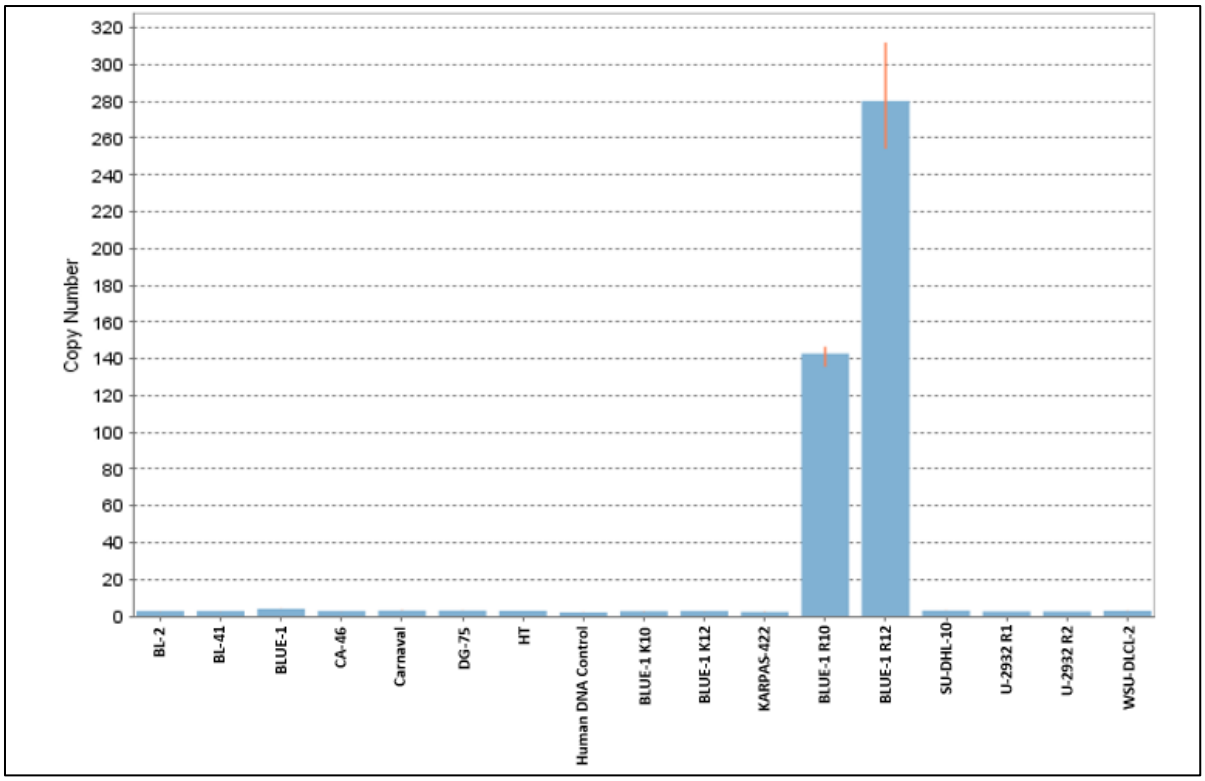

Figure 12A. Copy number variation profile of the lymphoma cell lines. The AHCY TaqMan CNV assay (ID: Hs02422126_cn) was utilized for the analysis of genomic DNA derived from the respective cell lines. CopyCaller software was used to perform data analysis. A commercially available human genomic DNA control (ThermoFisher Scientific, Germany) was used to calibrate the assay.

Having shown the profound increase in the copy number of *AHCY* in the DZNep-resistant clone, we sought to trace the time point at which the resistant clone evolved with this copy number aberration. For this purpose, we performed the TaqMan CNV assay on extracted DNA from the cell lines acquired at different points during the evolution of the clone. We demonstrate a clear gain in the *AHCY* copy number starting from BLUE-1R6, this gain increasing progressively during subsequent months. During the month when DZNep pressure was withdrawn from the cells (from BLUE-1R9 to BLUE-1R10), we observed a doubling of the number of copies of *AHCY* in the resistant clone (figure 12B).

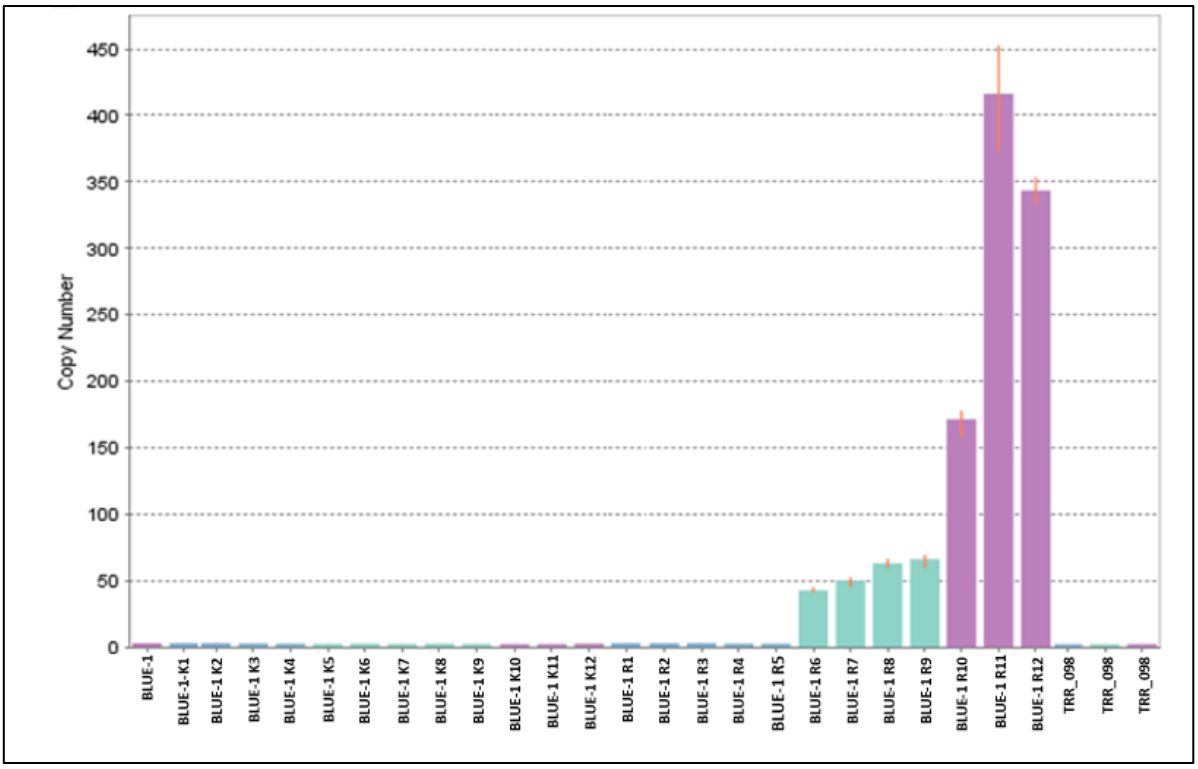

Figure 12B. *AHCY* copy number evolution in the DZNep-resistant clone. The AHCY TaqMan CNV assay (ID: Hs02422126_cn) was used for the analysis of genomic DNA derived from the respective cell lines. The CopyCaller software was used for copy number analysis. A primary tonsil sample (TRR_098) was used as a reference sample for the assay. Data was adapted from Akpa C. A. et al., manuscript in review (appendix C).

We repeated this experiment with a different AHCY TaqMan CNV assay to ensure that we were really detecting the gene of interest. This assay (ID: Hs02512802_cn) was designed to detect a region of *AHCY* overlapping intron 3 and exon 3, in contrast to the former assay which recognizes a region of *AHCY* overlapping intron 7 and exon 8. The results obtained (figure 12C) followed a similar pattern with that obtained in figure 12B.

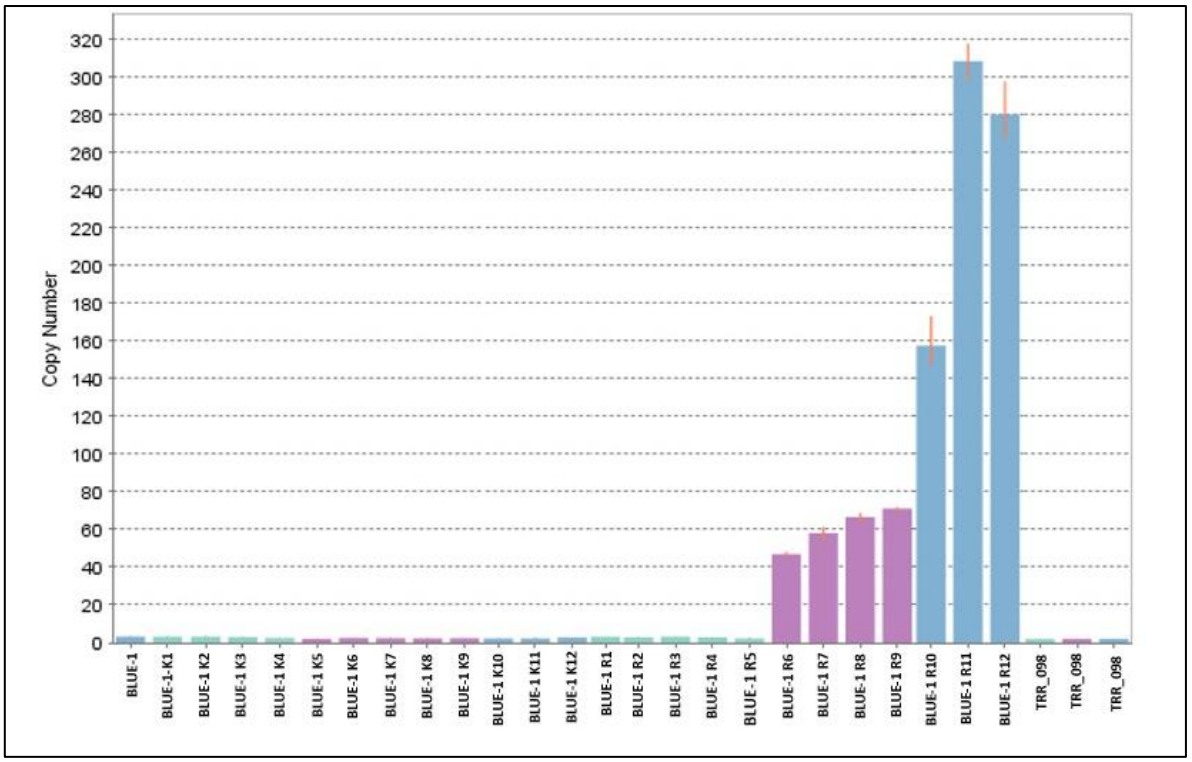

Figure 12C. *AHCY* copy number evolution in the DZNep-resistant clone (use of a different assay). The AHCY TaqMan CNV assay (ID: Hs02512802_cn) was used to interrogate genomic DNA from the individual cell lines. Copy number analysis was done using the CopyCaller software. DNA from a primary tonsil sample (TRR_098) served as a reference for the assay.

We also performed CNV analysis using generated DNA methylation data (refer to section 2.11). The result of the analysis showed an increased *AHCY* copy number in BLUE-1R10, which was absent in BLUE-1 and BLUE-1K10 (figure 12D).

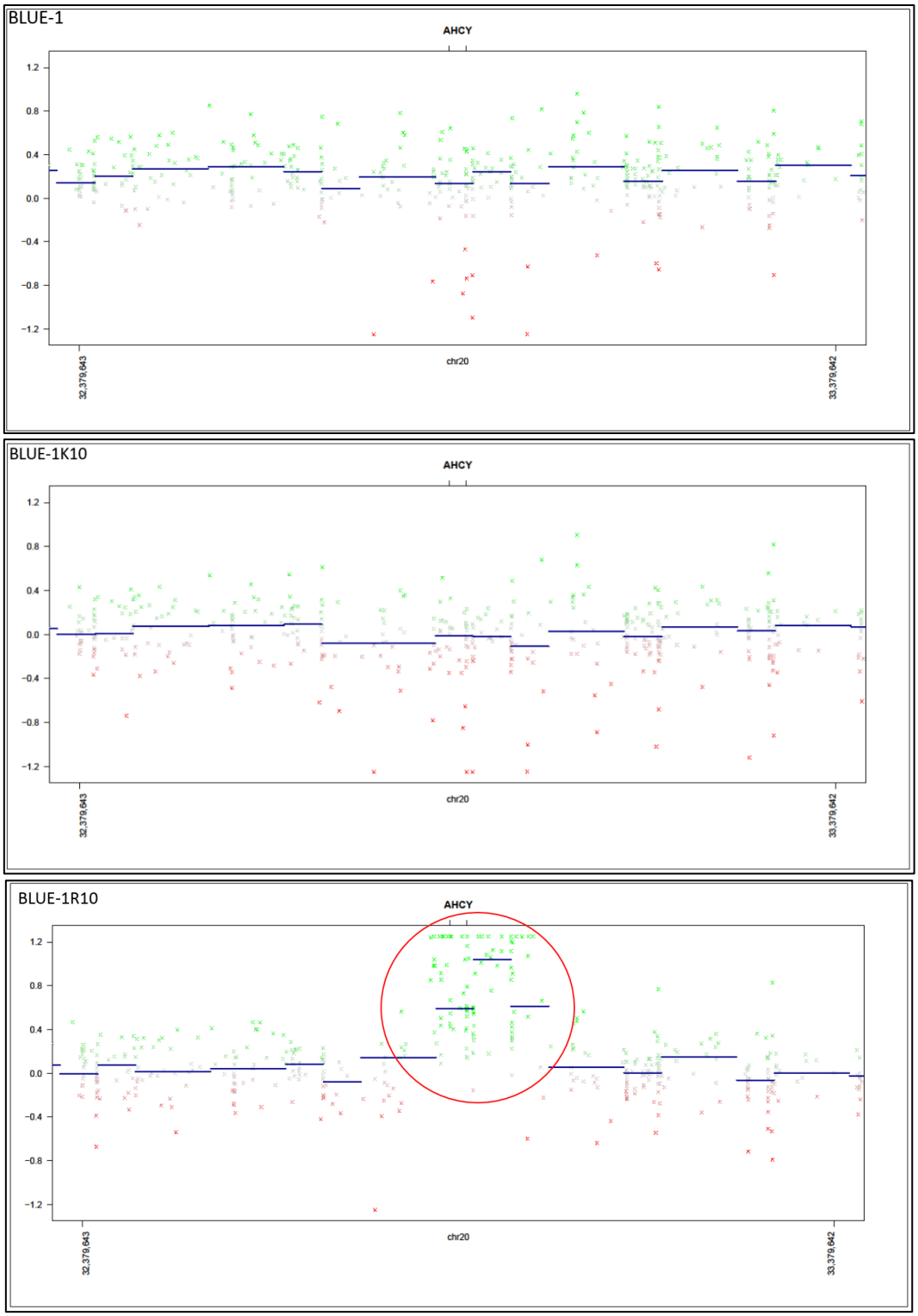

Figure 12D. *AHCY* gain depicted using CNV plots derived from global DNA methylation data. Log2 copy number ratio is shown on the y-axis. *AHCY* copy number gain in BLUE-1R10 is shown in the area within the red circle. CNV analysis of the methylation data was performed in collaboration with the research group of Prof. David Capper. Figure adapted from Akpa C. A. et al., manuscript in review (appendix C).

Upon manual analysis of the OncoScan CNV assay (*AHCY* genomic region) that was initially performed in section 3.8, the result (figure 12E) confirmed the high copy number gain of *AHCY* in BLUE-1R10, not visible in other BLUE-1 derivatives. It is worthy to note that due to the

filtering criteria used for detection of CNA (see section 2.13), this alteration was not picked up in the initial analysis due to the small size of this genomic region and low probe coverage.

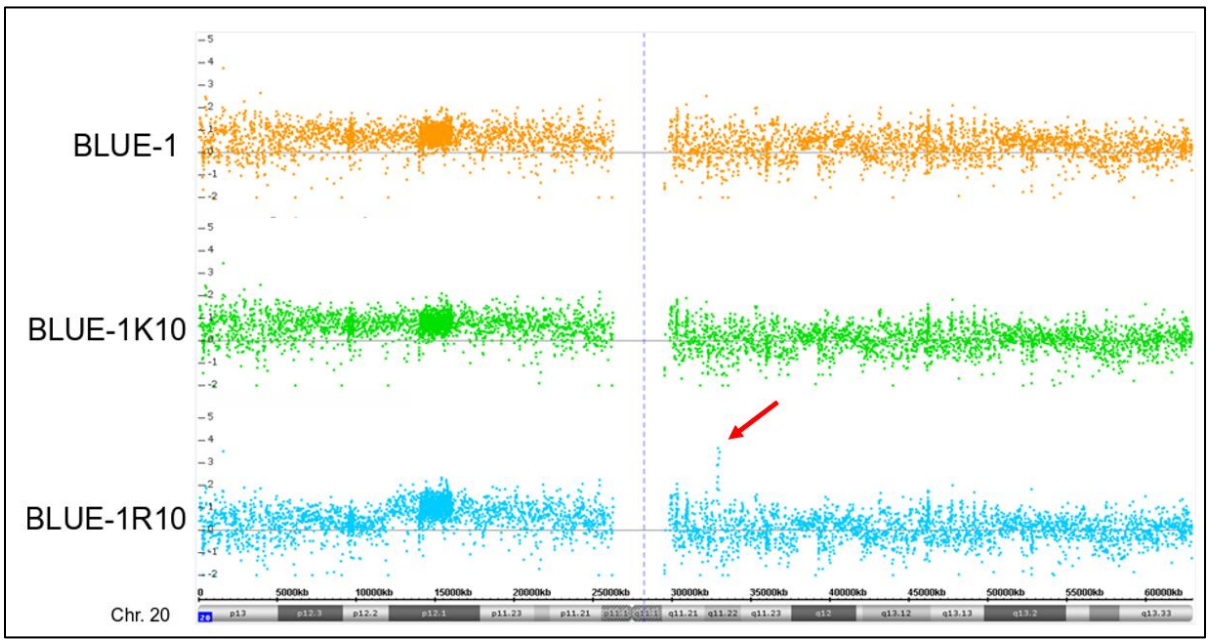

Figure 12E. Validation of the *AHCY* CNV in BLUE-1R10 using OncoScan CNV assay. OncoScan CNV assay results showing on chromosome 20, the log2 ratios for BLUE-1, BLUE-1K10 and BLUE-1R10. The region highlighted with a red arrow shows the *AHCY* copy number gain. OncoScan CNV analysis was done in collaboration with the research group of Prof. Reiner Siebert. Figure adapted from Akpa C. A. et al., manuscript in review (appendix C).

3.9.2 Validation of *AHCY* copy number gain at the chromosomal level

We performed FISH analysis using *AHCY*-specific probes to detect *AHCY* amplification in the resistant clone at the chromosomal level. The result (figure 12F) displayed cluster-type amplification of *AHCY* appearing as homogeneously stained regions in BLUE-1R10 cells in comparison with BLUE-1K10 cells. This amplification, corroborating the results of the CNV assay, was more in BLUE-1R12 when compared with BLUE-1R10.

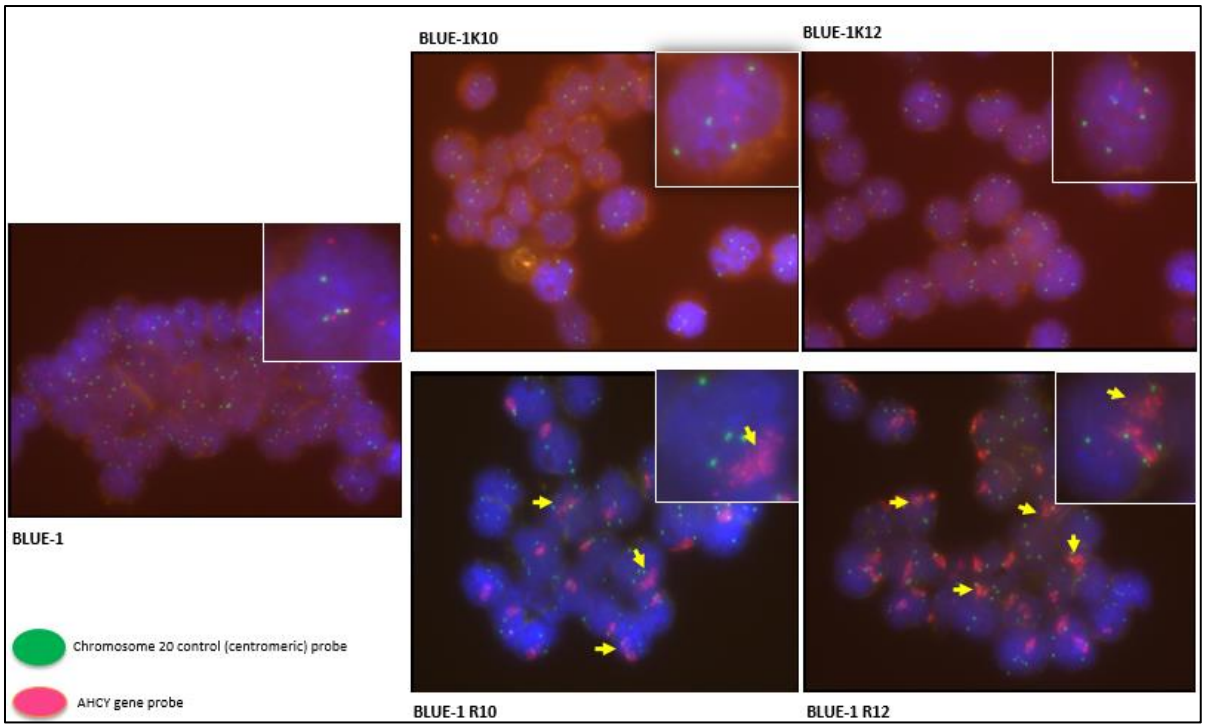

Figure 12F. Validation of *AHCY* copy number gain on the chromosomal level by FISH analysis. The yellow arrows show *AHCY* amplification (in pink clusters). Chromosome 20 centromere is shown in green dots. The blue color (DAPI stain) highlights the cell nucleus. FISH analysis was performed in collaboration with Dr. Dido Lenze. Figure adapted from Akpa C. A. et al., manuscript in review (appendix C).

3.9.3 Validation of *AHCY* copy number gain at the transcriptional level

To validate the expression of AHCY, real-time RT-PCR was performed on RNA from the cell lines using the AHCY TaqMan gene expression assay kit. Consistent with the preceding results, AHCY was overexpressed in the resistant clone but not the corresponding controls. Moreover, the expression of AHCY in BLUE-1R12 was about 2-times greater than the expression of AHCY in BLUE-1R10. Amplification of AHCY was not detected in the other 12 lymphoma cell lines used in this work (figure 12G).

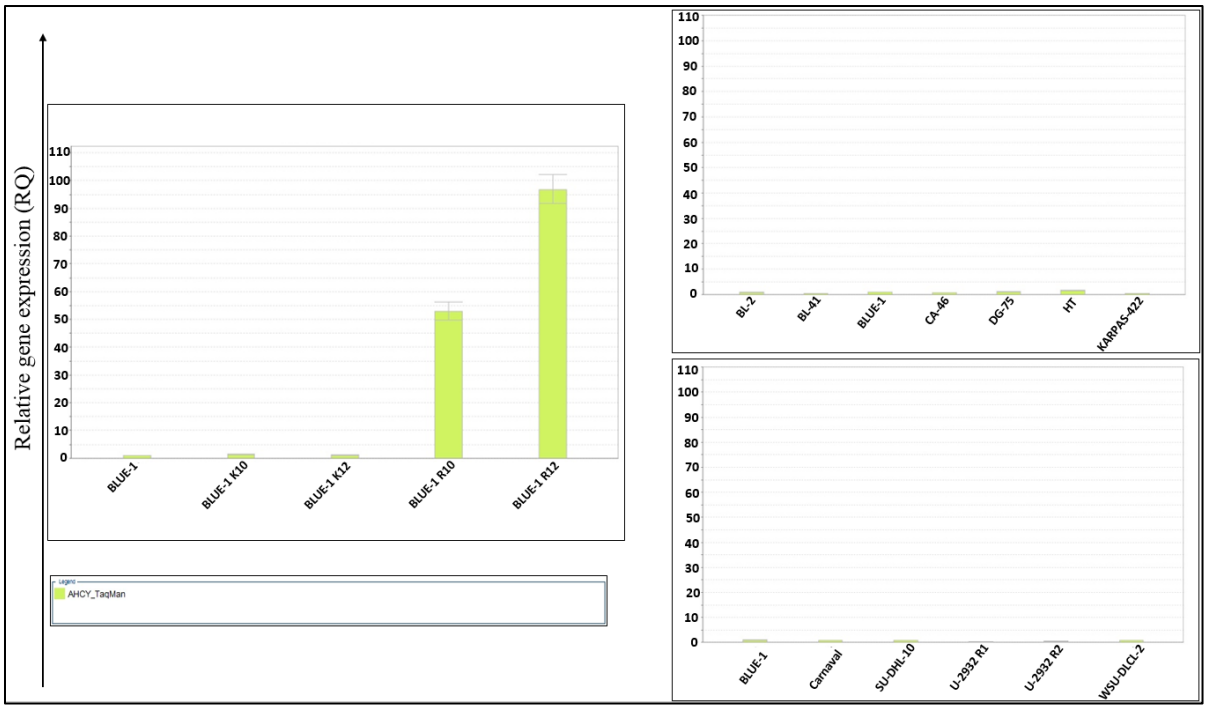

Figure 12G. Expression of AHCY at the transcriptional level. Real-time RT-PCR was performed on RNA extracted from the respective cell lines. The y-axis indicates the relative gene expression. *AHCY* TaqMan gene expression assay was used for mRNA quantification. The data for BLUE-1, BLUE-1K10, BLUE-1K12, BLUE-1R10 and BLUE-1R12 were adapted from Akpa C. A. et al., manuscript in review (appendix C).

3.9.4 Validation of *AHCY* copy number gain at the protein level

AHCY protein expression in the cell lines was investigated using IHC and Western blot. IHC results revealed AHCY overexpression in BLUE-1R12 in relation with BLUE-1K12 and BLUE-1 (figure 12H). Upon treatment of BLUE-1R12 with DZNep, the expression of AHCY protein seemed even more in comparison to BLUE-1R12 without DZNep pressure. Furthermore, BLUE-1R12 showed a more cytoplasmic AHCY immunostaining in comparison to BLUE-1K12, where there seemed to be a more nuclear AHCY immunostaining of the cells. Other lymphoma cell lines analyzed for their AHCY expression did not show a strong AHCY staining like that observed in the resistant clone (BLUE-1R12).

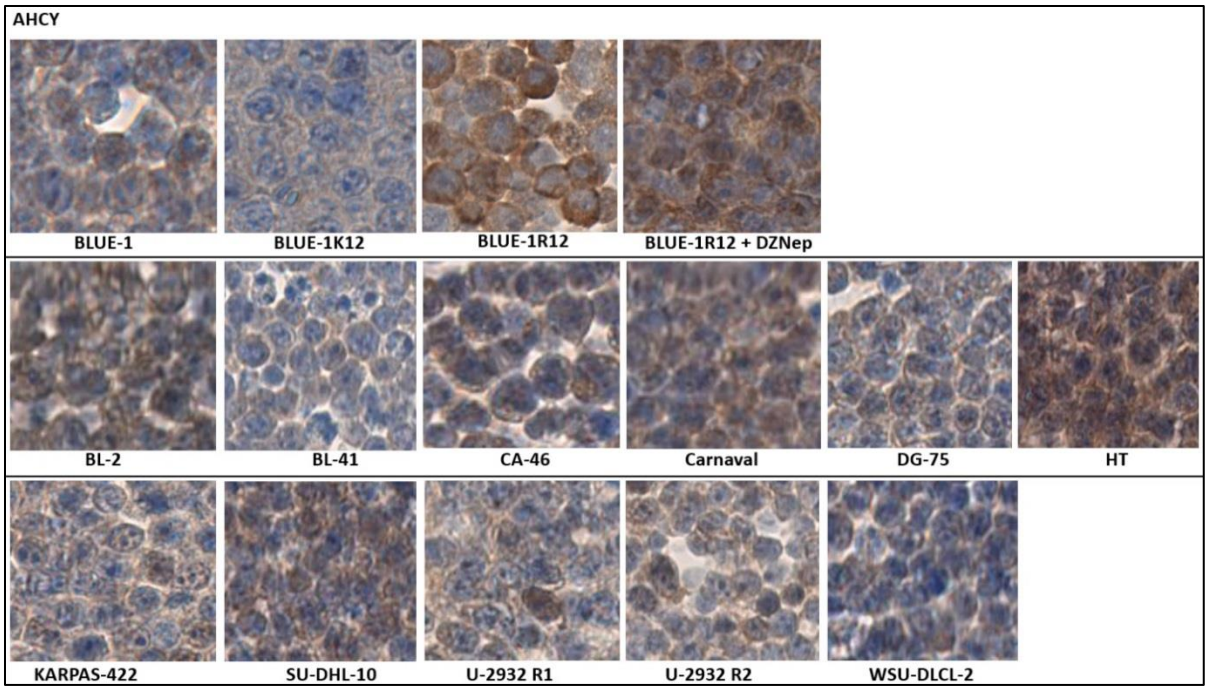

Figure 12H. IHC results of lymphoma cell lines. Anti-AHCY antibody was used to stain FFPE sections of the individual cell lines. IHC results for BLUE-1, BLUE-1K12 and BLUE-1R12 were adapted from Akpa C. A. et al., manuscript in review (appendix C).

Western blot was also performed to check for overexpression of AHCY at the protein level using whole cell protein lysates derived from all 12 lymphoma cell lines, as well as the resistant clone and their respective controls. The protein expression profile revealed AHCY overexpression in BLUE-1R10, with a further increase in BLUE-1R12. The other lymphoma cell lines only showed a basal expression of AHCY protein, similar to that seen in a HeLa cell line used as a positive control for AHCY in this experiment (figure 12I).

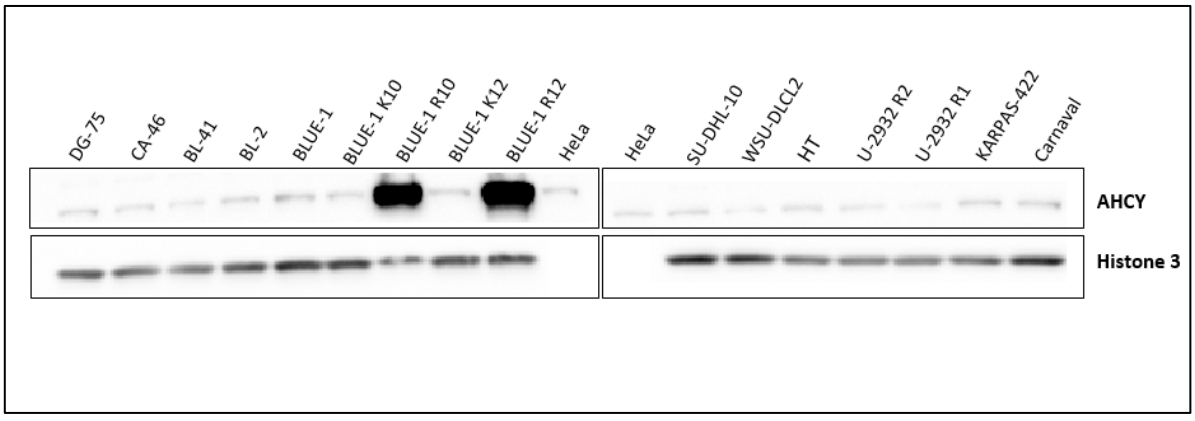

Figure 12I. AHCY is overexpressed in the DZNep-resistant clone. Total cell protein lysate extracted from the respective cell lines were analyzed with Western blot. Protein lysate from a HeLa cell line was used as a positive control for AHCY. Histone 3 served as the loading control. The Western blot figure for the cell lines BLUE-1, BLUE-1K10, BLUE-1R10, BLUE-1K12 and BLUE-1R12 was adapted from Akpa C. A. et al., manuscript in review (appendix C).

As mentioned in the IHC results of figure 12H, there seemed to be a more cytoplasmic AHCY immunostaining in BLUE-1R12 in comparison to BLUE-1K12, which appeared to show a more

nuclear AHCY immunostaining. This led to the speculation that AHCY may display different subcellular localizations in presence and absence of DZNep. To clarify if it could be the case that perhaps, treatment of cell lines with DZNep causes the drift of AHCY from the nucleus to the cytoplasmic cellular compartment, we separated the nuclear and cytoplasmic fractions of the resistant clone BLUE-1R10, its control BLUE-1K10 and another lymphoma cell line BL-2. We then performed a Western blot analysis to show the cytoplasmic distribution of AHCY before and after DZNep treatment. We observed in all cases that AHCY was more in the cytoplasm under conditions of DZNep pressure and without DZNep pressure (figure 12J).

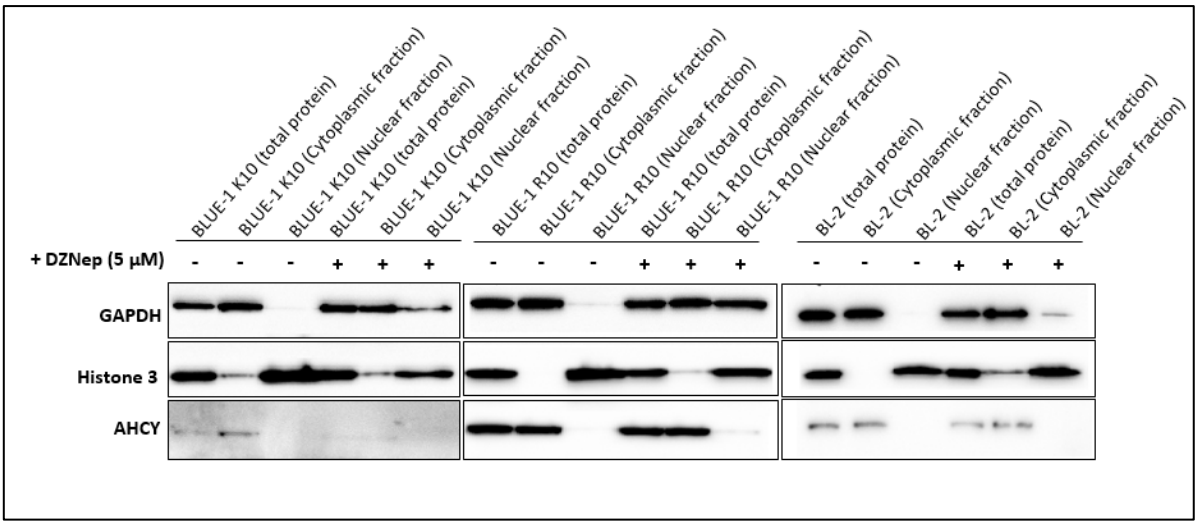

Figure 12J. AHCY is mainly distributed in the cytoplasm of the cell irrespective of DZNep pressure. Whole cell protein lysates as well as protein lysates from the cytoplasmic and nuclear fractions of the respective cell lines, either untreated or treated with DZNep were used for the Western blot. GAPDH served as a positive control for the cytoplasmic fraction and Histone 3 served as a positive control for the nuclear cell fraction. The blots were stripped and incubated with anti-AHCY primary antibody.

3.9.5 Validation of *AHCY* copy number in primary patient samples

To validate *AHCY* copy number variation in patient samples, we analyzed a diverse group of 11 primary lymphoma samples made up of BL, DLBCL, follicular lymphoma, PMBL and anaplastic large cell lymphoma. Genomic DNA was isolated from the tissue sections and subjected to the *AHCY* TaqMan CNV assay (ID: Hs02422126_cn). The *AHCY* copy number as determined by the CopyCaller software was 2 copies for all except one of the samples with a predicted loss of one copy of *AHCY* (figure 12K).

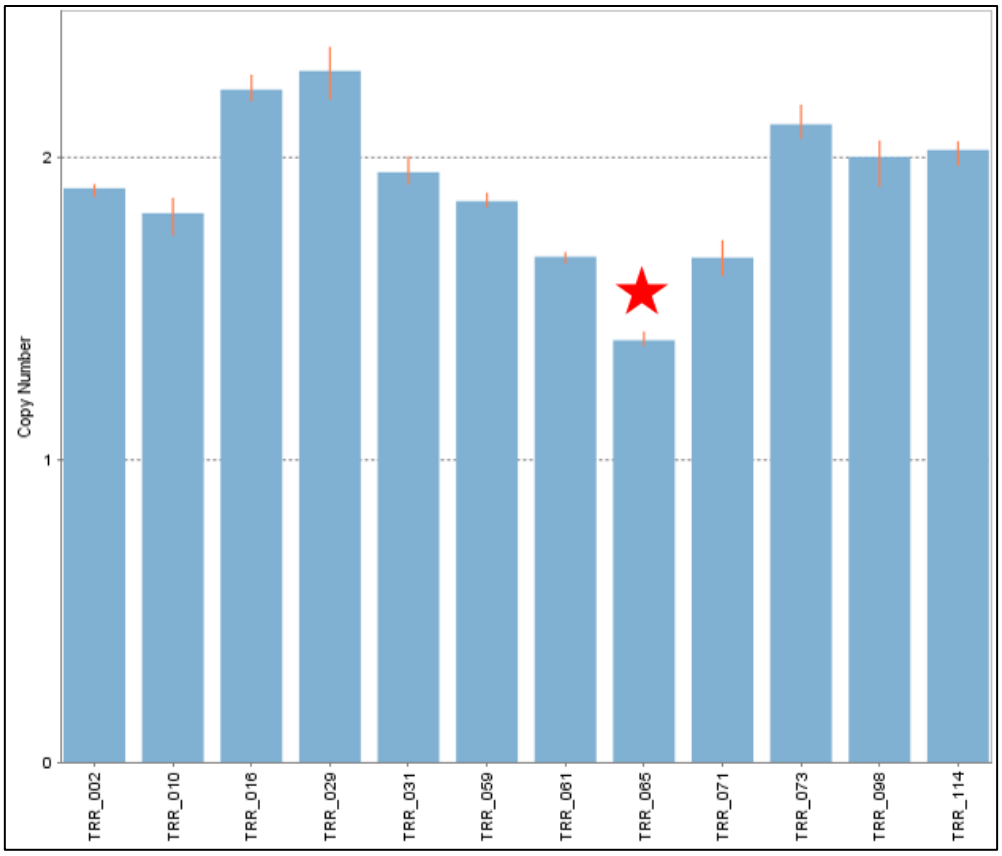

Figure 12K. Validation of *AHCY* CNV in primary patient samples. The AHCY TaqMan CNV assay (assay ID: Hs02422126_cn) was used for the copy number analysis, with a human tonsil sample (TRR_098) serving as a reference for the assay. The CopyCaller software was used for data analysis. Highlighted in red is the sample predicted by the software to have one copy of the *AHCY* gene deleted. Data adapted from Akpa C. A. et al., manuscript in review (appendix C).

3.10 Effect of DZNep on AHCY expression

Although DZNep is a known AHCY inhibitor, we sought to investigate the effect of DZNep on AHCY expression at the RNA level. To this end, we treated cell lines with 5 µM DZNep for 72 hours and measured the AHCY RNA expression in the cells using real-time RT-PCR. We used two DZNep-resistant cell lines, BLUE-1R10 and HT, and 3 DZNep sensitive cell lines, BL-41, BLUE-1 and BLUE-1K10. Our results showed a decrease in expression of AHCY upon treatment with DZNep in all the cell lines (figure 13A & 13B).

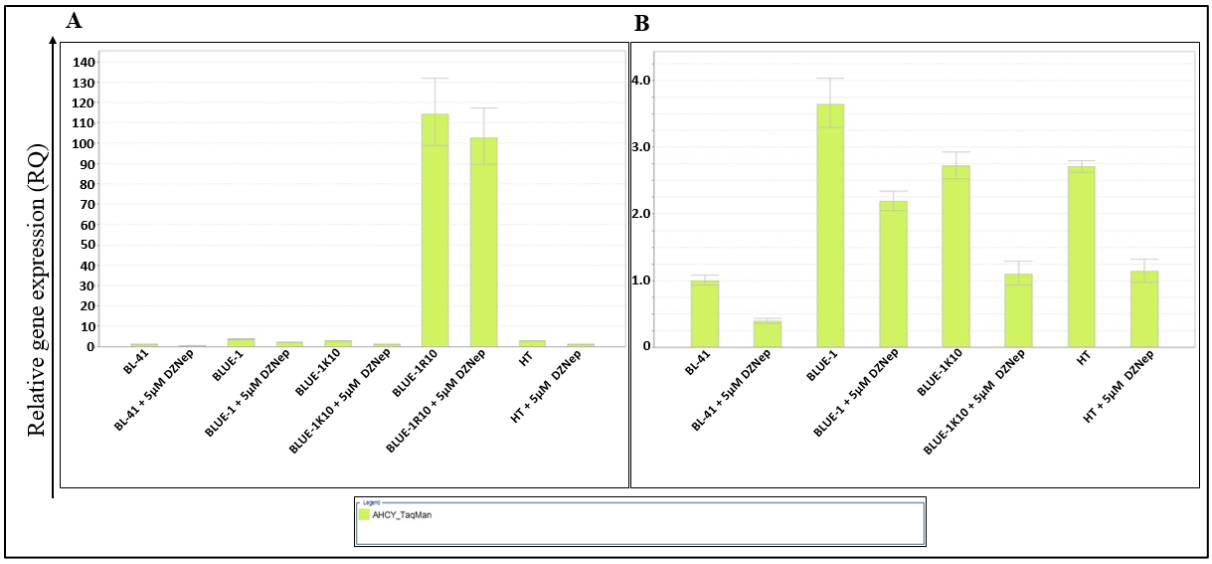

Figure 13: Expression of AHCY in DZNep-resistant and DZNep-sensitive cells upon treatment with DZNep. (A) $2x10^5$ cells from each of the cell lines were cultured in 6 well plates, and either untreated or treated with 5 µM DZNep for 72 hours. Cells were harvested, RNA extracted and real-time RT-PCR performed to determine AHCY expression. The *AHCY* TaqMan gene expression assay was used to analyze AHCY expression, with *B2M* serving as an endogenous control. The y-axis represents the relative *AHCY* gene expression **(B)** Due to the very high AHCY expression in BLUE-1R10, we excluded it from the analysis to take a closer look at the AHCY expression (in presence and absence of DZNep) for the DZNep-sensitive cell lines (BL-41, BLUE-1, BLUE-1K10) and the DZNep-resistant cell line (HT).

3.11 Metabolomics

We analyzed the concentrations of selected metabolites of methionine (SAH, adenine and adenosine) when lymphoma cells are treated with DZNep. We investigated the cell lines BLUE-1, BLUE-1K10, BLUE-1R10, BLUE-1K12 and BLUE-1R12 as described in section 2.13. We observed that the three metabolites were distributed in a similar manner in BLUE-1, BLUE-1K10 and BLUE-1K12. In BLUE-1R10 treated with DZNep, we clearly observed an increase in SAH. However, in the resistant clone without DZNep pressure (BLUE-1R12), there was a prominent rise in both adenine and adenosine (figure 14).

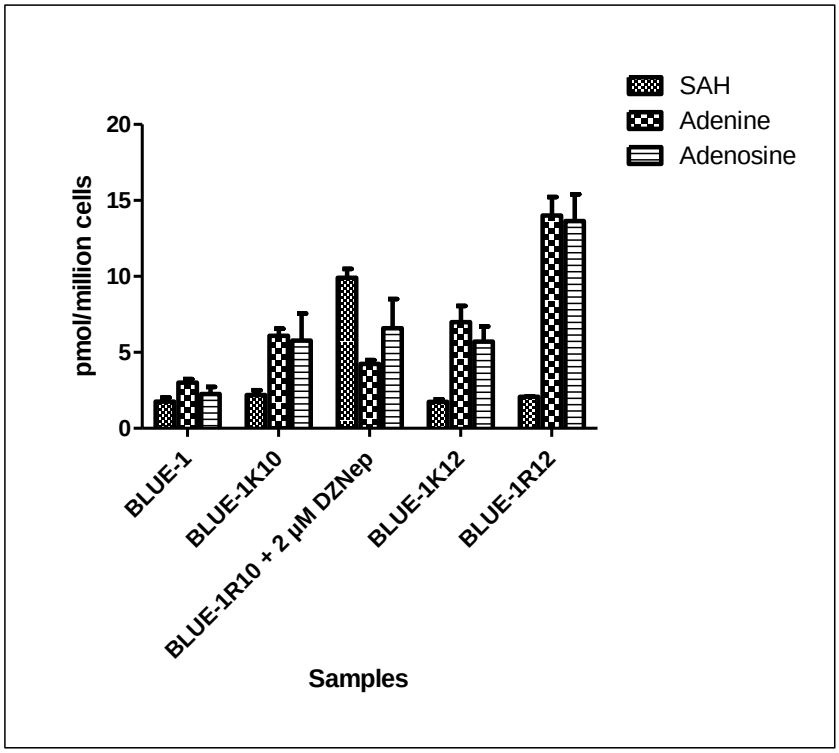

Figure 14. Quantification of metabolites of s-adenosylmethionine (SAM). SAH: S-adenosylhomocysteine. Metabolomics analysis was performed in collaboration with the research group of Prof. Peter J. Oefner. Data of BLUE-1, BLUE-1K12 and BLUE-1R12 was adapted from Akpa C. A. et al., manuscript in review (appendix C).

3.12. Global DNA methylation profile of BLUE-1, BLUE-1K10 and BLUE-1R10

We looked into the global DNA methylation status of the lymphoma cell lines BLUE-1, BLUE-1K10 and BLUE-1R10, with and without DZNep pressure. We first analyzed this using a colorimetric approach - the MethylFlash Global DNA methylation (5-mC) ELISA Easy Kit assay. This assay was performed two independent times on similar samples. We noticed from the results of the first experiment (figure 15A (I)), a higher methylation level (percentage of 5-methylcytocine (5-mC)) for all the cell lines analyzed in comparison to the results of the replicate analysis (figure 15A (II)). In the latter experiment, we observed a much lower percentage of 5-mC, with varying levels in all the samples analyzed. Due to the inconsistencies and non-reproducibility encountered with this colorimetric assay, we applied an array-based method to analyze our samples.

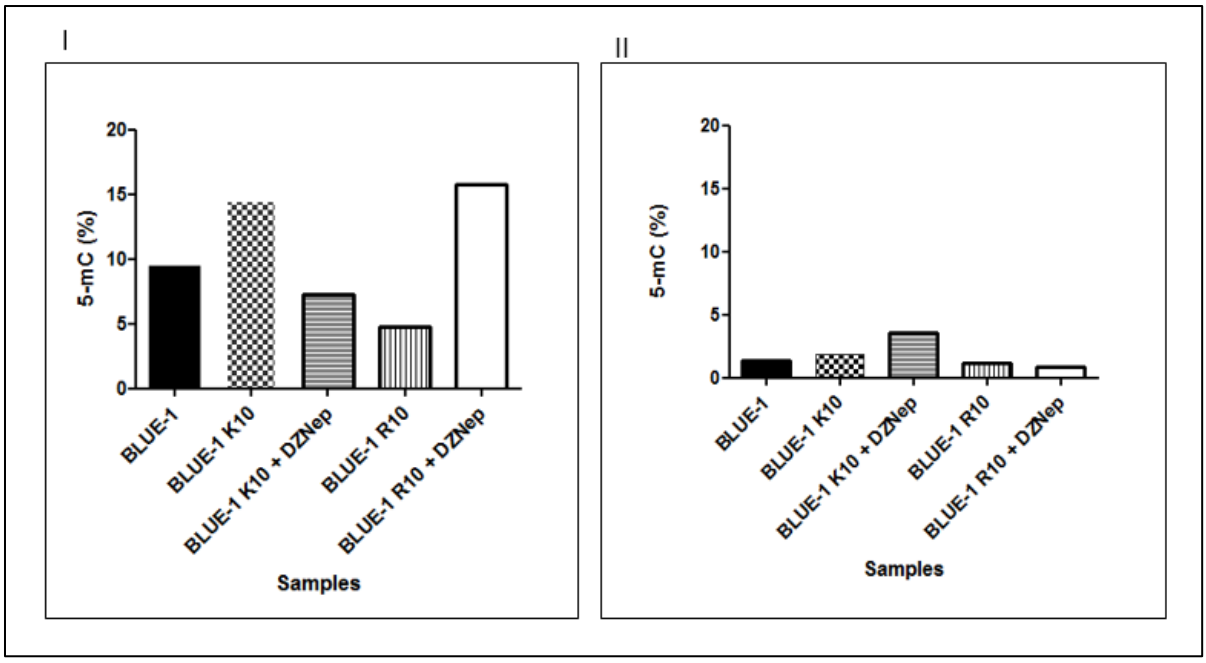

Figure 15A. Global DNA methylation status of BLUE-1, BLUE-1K10 and BLUE-1R10, with and without DZNep pressure. ELISA-based colorimetric determination of the global DNA methylation profile of the respective cell lines. **(I)** First experiment performed on the respective cell line DNA samples. DZNep treated cells received 5 µM DZNep for 72 hours. **(II)** Replication of the first experiment.

We utilized the Infinium MethylationEPIC BeadChip Kit, a microarray-based method, capable of examining thousands of methylation sites throughout the genome with high resolution (200). We adopted this method, with the purpose of providing a deeper and more concise understanding of the genome-wide methylation pattern of individual genes.

Hierarchical clustering as well as principal component analysis (PCA) was performed on the 25000 most variant probes (methylation sites) to show the similarities between the methylation data of the cell lines (BLUE-1, BLUE-1K10, BLUE-1K10 treated with DZNep, BLUE-1R10 and BLUE-1R10 treated with DZNep) and their replicates. We also compared the methylation data obtained from the cell lines with those of primary tumor samples. From the clustering results and PCA (figures 15B and 15C respectively), we noticed similarity in the methylation patterns of the DZNep-treated cell lines, as well as more clustering together of untreated cell lines. Comparing the cell lines' methylation data with those of primary tumor samples, we observed that the methylation patterns of each type of primary sample (lymphoma and plasmacytoma) are much similar to each other. The cell lines, even with the intra-group differences, show more similarity (clustering together).

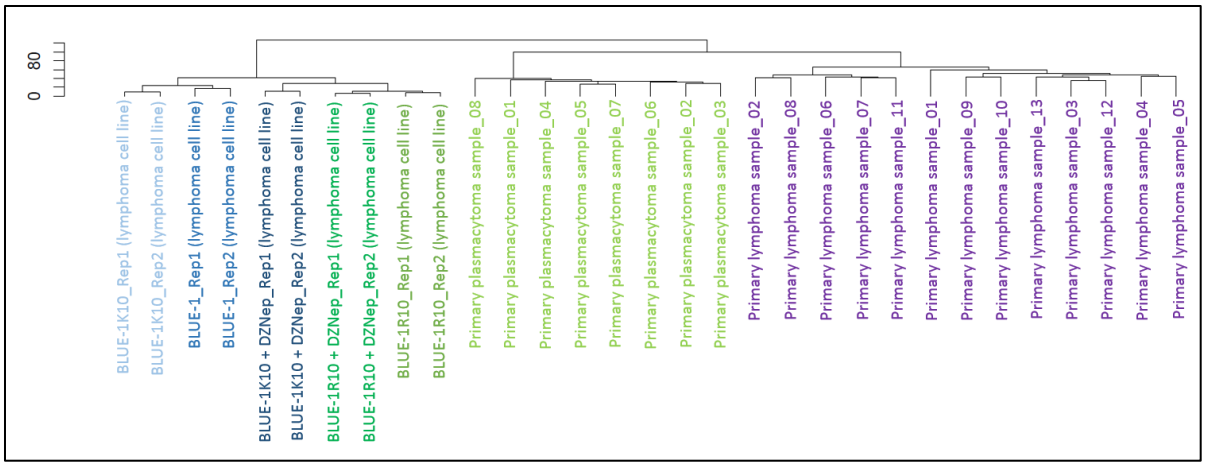

Figure 15B. Dendrogram shows hierarchical clustering results of the methylation dataset of the respective cell lines, plasmacytoma and lymphoma patient samples. Rep1 indicates the first set of samples while Rep2 denotes the replicate sample used for the data analysis. Included are the 13 primary lymphoma and 8 primary plasmacytoma patient samples. Methylation data was analyzed in collaboration with the research group of Prof. David Capper.

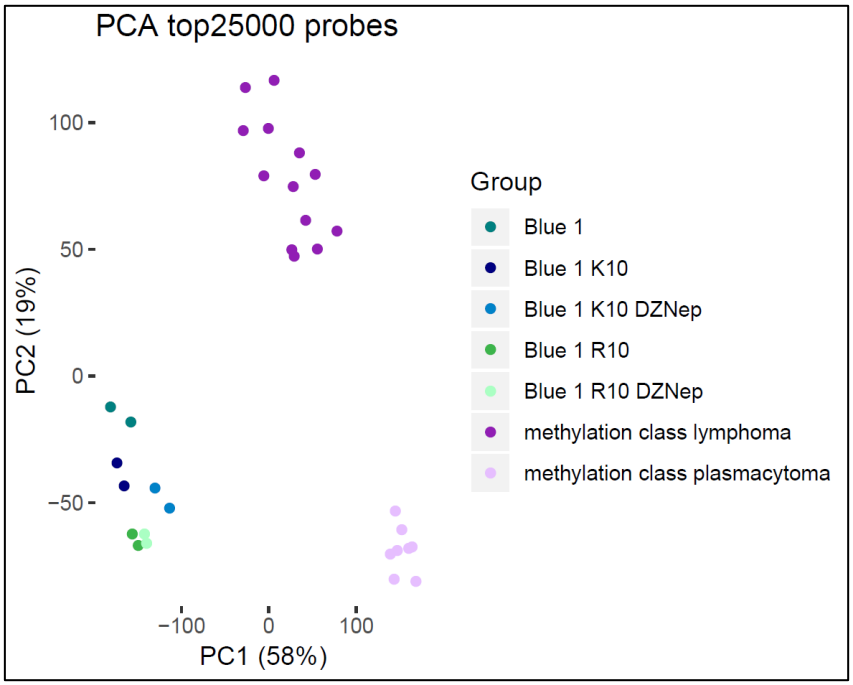

Figure 15C. Depicted are the first two dimensions of a PCA of the 25000 most variably methylated probes of cell lines and primary lymphoma patient samples (methylation class lymphoma and methylation class plasmacytoma). Methylation data was analyzed in collaboration with the research group of Prof. David Capper.

Further analysis of the methylation data was done to determine genes differentially methylated between BLUE-1K10 and BLUE-1R10 (group 1) as well as between 2 DZNep-sensitive (Carnaval and BL-41) and 2 DZNep-resistant (HT and CA-46) cell lines (group 2). A Venn diagram showing the overlap between genes which were differentially methylated in both groups was created using the Venny 2.1 software (201). We identified around 5036 overlapping genes comprising about 24% of the identified differentially methylated targets between the two groups (figure 15D).

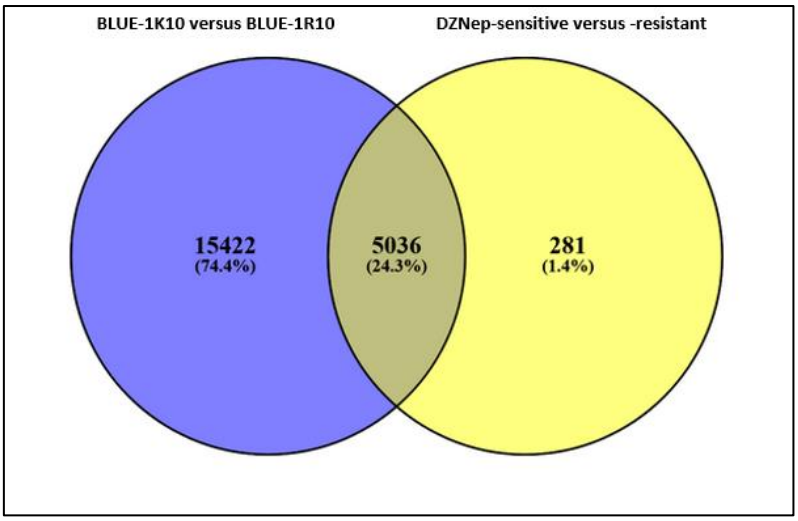

Figure 15D. Differentially methylated targets in BLUE-1K10 versus BLUE-1R10 and DZNep-sensitive (Carnaval and BL-41) versus DZNep-resistant (HT and CA-46) cell lines. Differentially methylated probes were defined by having an adjusted p-value of below 0.01.

To probe the effect of DZNep on the global methylation profile of BLUE-1K10 and BLUE-1R10, we investigated differentially methylated genes in these cell lines before and upon treatment with 5 µM DZNep. Upon examination of BLUE-1K10 in presence and absence of DZNep pressure (group 3), we identified 21359 differentially methylated targets (figure 15E).

Analysis of the DZNep-resistant clone BLUE-1R10 yielded no differentially methylated genes under DZNep-treated and untreated conditions based on the criteria for defining differentially methylated probes (adjusted p-value < 0.01).

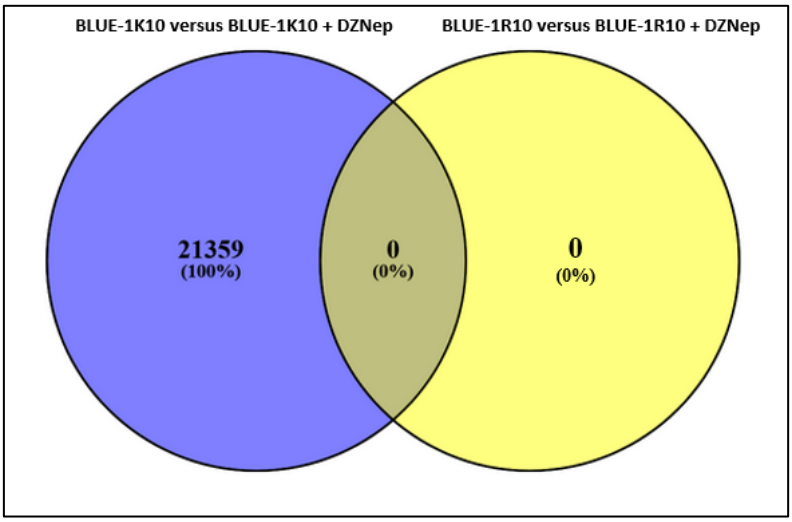

Figure 15E. Differentially methylated targets in BLUE-1K10 versus BLUE-1K10 + DZNep. There were no differentially methylated targets detected when comparing BLUE-1R10 under untreated and DZNep-treated conditions. Differentially methylated probes were defined by having an adjusted p-value of below 0.01.

Sequel to this, a pathway analysis to determine differentially methylated genes involved in the apoptosis signaling pathway was done, focusing the overlapping genes from groups 1, 2 and 3. Out of 1942 pathway hits, 38 differentially methylated genes were identified using the

PANTHER classification system (202) as being involved in the apoptosis signaling pathway (table 8).

Table 8. List of differentially methylated genes involved in the apoptosis signaling pathway, identical to group 1 (BLUE-1K10 versus BLUE-1R10), group 2 (DZNep-sensitive versus DZNep-resistant cell lines) and group 3 (BLUE-1K10 versus BLUE-1K10 + DZNep).

	Gene Name	**Gene Symbol**
1	Protein kinase C eta type	*PRKCH*
2	Mitogen-activated protein kinase kinase kinase kinase 4	*MAP4K4*
3	TNF receptor-associated factor 2	*TRAF2*
4	Mitogen-activated protein kinase kinase kinase kinase 2	*MAP4K2*
5	DNA replication licensing factor MCM5	*MCM5*
6	Proto-oncogene c-Fos	*FOS*
7	Protein kinase C delta type	*SDK1*
8	Heat shock 70 kDa protein 6	*HSPA6*
9	BCcl-2-related ovarian killer protein	*BOK*
10	Cyclic AMP-dependent transcription factor ATF-7	*ATF7*
11	Mitogen-activated protein kinase 1	*MAPK1*
12	Mitogen-activated protein kinase kinase kinase kinase 5	*MAP4K5*
13	Protein kinase C epsilon type	*PRKCE*
14	Transcription factor p65	*RELA*
15	Protein kinase C theta type	*PRKCQ*
16	Cyclic AMP-dependent transcription factor ATF-6 beta	*ATF6B*
17	Mitogen-activated protein kinase kinase kinase kinase 3	*MAP4K3*
18	CASP8 and FADD-like apoptosis regulator	*CFLAR*
19	Caspase-3	*CASP3*

20	Cyclic AMP-dependent transcription factor ATF-6 alpha	*ATF6*
21	Apoptosis regulator Bcl-2	*BCL2*
22	Eukaryotic translation initiation factor 2 subunit 1	*EIF2S1*
23	MAP kinase-activating death domain protein	*MADD*
24	Interferon-inducible double-stranded RNA-dependent protein kinase activator A	*PRKRA*
25	RAC-gamma serine/threonine-protein kinase	*AKT3*
26	Bcl-2-like protein 2	*BCL2L2*
27	Cyclic AMP-dependent transcription factor ATF-3	*ATF3*
28	RAC-alpha serine/threonine-protein kinase	*AKT1*
29	cAMP-responsive element modulator	*CREM*
30	Mitogen-activated protein kinase kinase kinase 14	*MAP3K14*
31	Protein kinase C alpha type	*PRKCA*
32	Tumor necrosis factor receptor superfamily member 1B	*TNFRSF1B*
33	Phosphatidylinositol 4,5-bisphosphate 3-kinase catalytic subunit delta isoform	*PIK3CD*
34	Caspase-10	*CASP10*
35	Tumor necrosis factor receptor type 1-associated DEATH domain protein	*TRADD*
36	Inhibitor of nuclear factor kappa-B kinase subunit beta	*IKBKB*
37	Death domain-associated protein 6	*DAXX*
38	RAC-beta serine/threonine-protein kinase	*AKT2*

The list of differentially methylated targets from group 1, group 2 and group 3 is shown in the supplementary file S1.

3.13. Functional validation of *AHCY* copy number gain (AHCY knockdown assays)

To validate the functional relevance of increased *AHCY* gene expression observed in BLUE-1R10, we sought to knock down *AHCY* in this resistant clone and to check if it would regain sensitivity to apoptosis upon treatment with DZNep. We first performed an assay to establish

optimal conditions for the transfection of BLUE-1R10 cell line. Following the assay set-up shown in table 9A, and using the method described in section 2.15.1, we tested various programs designed for transfection of BLUE-1R10 with the Nucleofector 2b Device.

Table 9A: Plate set-up for the experiment to determine the optimal conditions for transfection of BLUE-1R10.

Sample	Cell culture medium	pmaxGFP; 0.5 µg/µl	Program
Sample 01 [NTC]	4 ml (6-well plate)	-	Q-06
Sample 02 [+ GFP]	4 ml (6-well plate)	+ 4 µl GFP	D-28
Sample 03 [+ GFP]	4 ml (6-well plate)	+ 4 µl GFP	O-07
Sample 04 [+ GFP]	4 ml (6-well plate)	+ 4 µl GFP	O-06
Sample 05 [+ GFP]	4 ml (6-well plate)	+ 4 µl GFP	D-23
Sample 06 [+ GFP]	4 ml (6-well plate)	+ 4 µl GFP	Q-06

NTC means no template control. GFP: Green fluorescent protein

The 'test' transfection was done using green fluorescent protein (pmaxGFP) vector (Lonza Group AG, Germany). At the end of transfection (48 hours), the lowest number of apoptotic cells and the highest percentage of GFP positive cells were obtained using the program D-23 (figure 16A and table 9B). This program was then utilized for subsequent experiments involving the transfection of BLUE-1R10 with the electroporation technique.

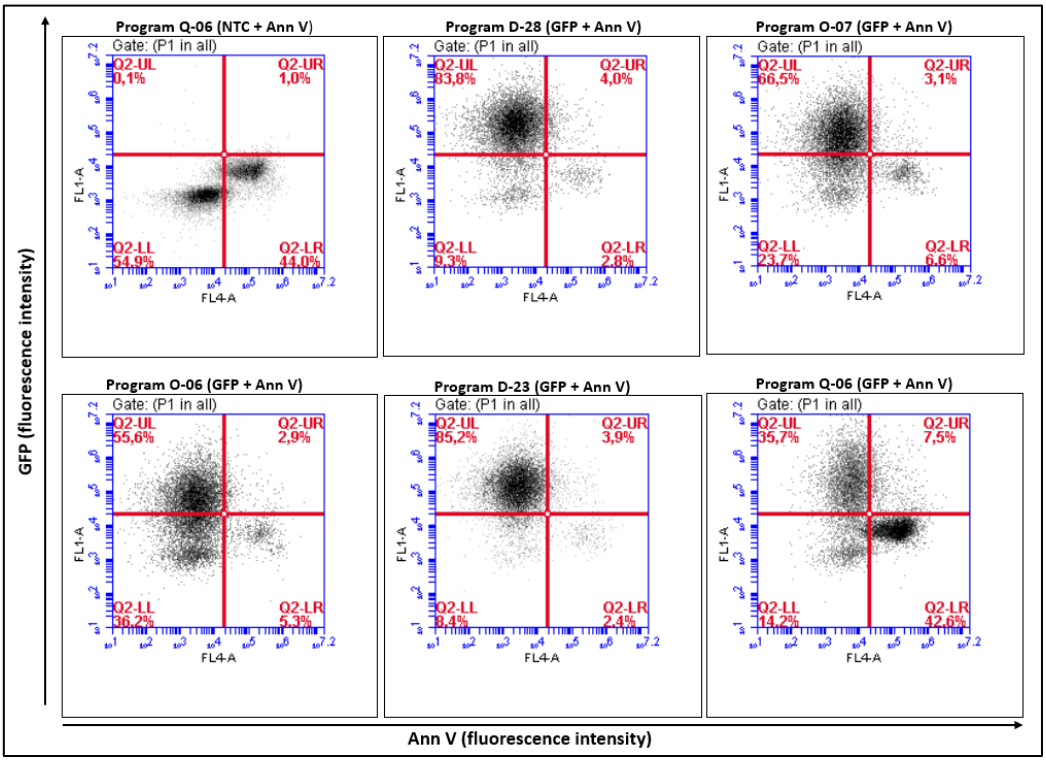

Figure 16A. Flow cytometry gating to determine the percentage of vital and GFP-positive cells. BLUE-1R10 was transfected with pmaxGFP vector for 48 hours. The cells were counted and Annexin V (Ann V) - stained following transfection. The Ann V- stained cells indicate the apoptotic cells. The fluorescence intensity of GFP (percentage of GFP-positive cells) was measured using flow cytometry in the FL1 channel while that of Ann V (Ann V-positive cells) was measured in the FL-4 channel.

Table 9B: Table showing the number of vital cells and GFP-positive cells present in the culture upon transfection of BLUE-1R10 with GFP vector using various electroporation programs.

Sample	Total cell count (x 10^5) / ml	GFP - positive cells (%)	GFP + Ann V -positive cells (%)	Ann V - positive cells (%)
Sample 01 [Q-06/NTC]	7.7	-	-	44.0
Sample 02 [D-28/GFP]	21.4	83.8	4.0	2.8
Sample 03 [O-07/GFP]	20	66.5	3.1	6.6
Sample 04 [O-06/GFP]	23.1	55.6	2.9	5.3
Sample 05 [D-23/GFP]	25.0	85.2	3.9	2.4
Sample 06 [Q-06/GFP]	8.8	35.7	7.5	42.6

NTC means no template control.

After determining the best conditions to use for transfection, we utilized 200 pmol/µl of both Mission AHCY esiRNA (human) and an ON-TARGETplus Non-targeting negative control pool for the transfection of BLUE-1R10. The percentage of apoptotic cells was determined 48 hours later using flow cytometry and the results shown in table 9C. We noticed that the sample transfected with AHCY esiRNA (without DZNep treatment) had a similar number of vital cells when compared with the no template control. Upon treatment with 5 µM DZNep, the percentage of apoptotic cells (Ann V / propidium iodide (PI)-positive cells) measured was greater in comparison to the AHCY-transfected cells without DZNep treatment. This was also the case for the no template control treated with DZNep as well as the non-target controls.

Table 9C: Flow cytometry read-out showing the percentage of vital cells and apoptotic cells present in the culture upon transfection of BLUE-1R10 with AHCY esiRNA.

Sample	Total cell count (x10^5) / ml	Vital cell count (x10^5) / ml	Ann V/PI-positive cells (%)
Sample 01 [NTC]	7.7	6.0	22.1
Sample 02 [esiRNA_AHCY]	7.1	5.1	29.2
Sample 03 [esiRNA_AHCY + DZNep]	4.3	1.1	74.7
Sample 04 [NTC + DZNep]	3.1	0.3	92.0
Sample 05 [non-target_siRNA]	4.5	1.7	61.4
Sample 06 [non-target_siRNA + DZNep]	5.0	0.8	83.7

NTC means no template control.

To check for transfection efficiency of the samples, Western blot using whole cell protein lysate from the cultured cells (in table 9C) was performed and antibodies detecting cleaved PARP, AHCY and Histone 3, were used to show expression of respective proteins (figure 16B). Our results showed that in comparison with the no template control (sample 01), the expression of AHCY was lower, but relatively similar in all the samples (samples 02 - 06).

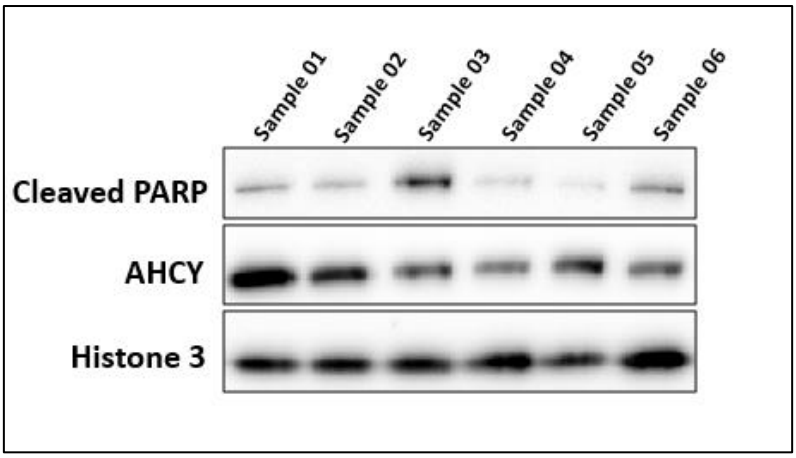

Figure 16B. Western blot showing the transfection efficiency of BLUE-1R10 with AHCY esiRNA (using non-target negative control siRNA). Whole cell protein lysate of the samples from table 9C showing AHCY and cleaved PARP protein expression in the respective cells. Histone 3 served as a loading control.

To check for reproducibility of the obtained result, the experiment was repeated. This time, we used an ON-TARGETplus human GAPDH control pool (ThermoFisher Scientific/Dharmacon, Germany) as a negative control rather than the non-targeting control pool, since we were unsure of its specificity. We also adjusted the duration of transfection (harvesting the cells 48 hours and 72 hours post-transfection) to check for the optimal time point for *AHCY* knockdown. The percentage of apoptotic cells and vital cells counted following transfection are shown in table 9D.

Table 9D: Flow cytometry results showing the percentage of vital cells and apoptotic cells present in the culture upon transfection of BLUE-1R10 with AHCY esiRNA.

Sample	Total cell count ($x10^5$) / ml	Vital cell count ($x10^5$) / ml	Ann V/PI-positive cells (%)
Sample 01 [NTC_48h]	4.5	3.1	32.4
Sample 02 [NTC + DZNep_48h]	3.9	1.8	53.3
Sample 03 [esiRNA_AHCY_48h]	11.5	10.0	13.5
Sample 04 [esiRNA_AHCY + DZNep_48h]	7.3	4.4	39.7
Sample 05 [esiRNA_AHCY_72h]	21.4	19.9	7.3
Sample 06 [esiRNA_AHCY + DZNep_72h]	6.8	4.8	30.3
Sample 07 [siRNA_GAPDH_48h]	5.3	4.1	21.3
Sample 08 [siRNA_GAPDH + DZNep_48h]	4.2	2.0	51.8
Sample 09 [Unpulsed]	13.6	12.4	9.2
Sample 10 [Unpulsed + DZNep_48h]	9.4	7.4	21.1

NTC means no template control and siRNA targeting GAPDH was used as a negative control.

Subsequent validation of the transfection efficiency of the cells using Western blot was done using whole cell protein lysate from the samples. Our results showed no obvious change in the level of AHCY expression in all the samples. However, samples 07 and 08 transfected with GAPDH siRNA showed a somewhat lower level of GAPDH expression in comparison with other samples (figure 16C).

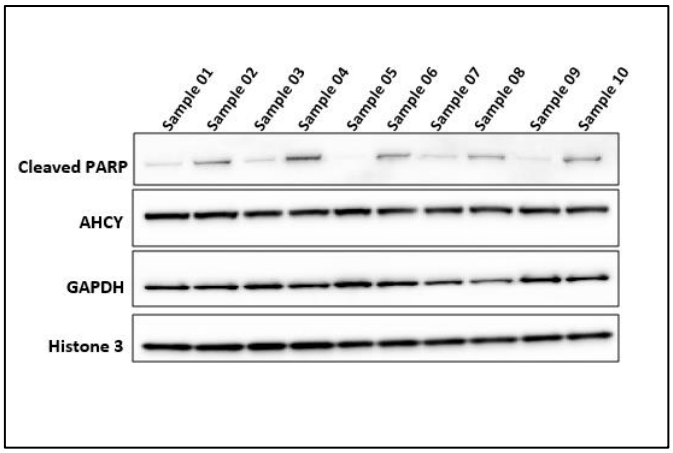

Figure 16C.**Western blot showing the transfection efficiency of BLUE-1R10 transfected with AHCY esiRNA (using GAPDH negative control siRNA).** Whole cell protein lysate from the samples of table 9D showing cleaved PARP, AHCY and GAPDH expression in the respective cells. Histone 3 served as a loading control.

Since AHCY is overexpressed in BLUE-1R10, we adjusted the concentration of the esiRNA used (using 2 fold more than that previously applied) for transfection. The concentration of the AHCY esiRNA used this time was increased to 400 pmol/µl, and the transfection performed as already described for 48 hours. Upon analysis of the transfection efficiency of the cells using Western blot, no significant downregulation of AHCY was observed in the cells at the protein level (figure 16D).

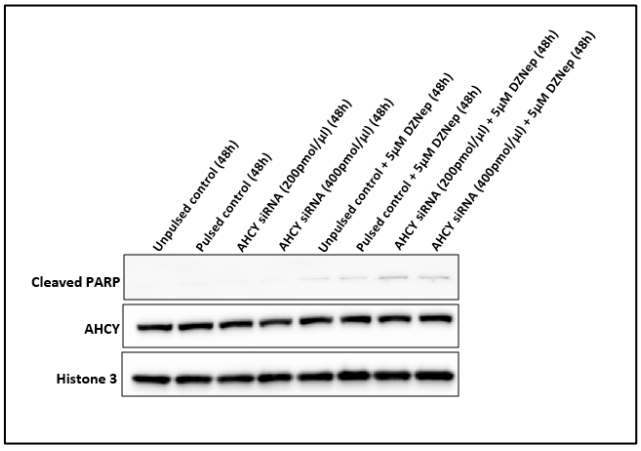

Figure 16D. Western blot showing the transfection efficiency of BLUE-1R10 transfected with AHCY esiRNA (varying the esiRNA concentration). Cells were cultured in 6-well plates at a seeding density of $5x10^6$ cells/ml. Electroporation of the transfected cells were carried out using 200 pmol/µl AHCY esiRNA and 400 pmol/µl AHCY esiRNA. Transfection as well as DZNep treatment of both the samples and controls with 5 µM DZNep was done for a duration of 48 hours. Cells were harvested and counted afterwards using flow cytometry. Protein lysate was prepared from the cells of each sample and Western blot made to determine the efficiency of transfection. The blot was incubated with antibodies for cleaved PARP, AHCY and Histone 3. Histone 3 served as a loading control.

The preceding result led to the presumption that AHCY is downregulated at an earlier time point than 48 hours. We thus reduced the transfection time to 16 and 24 hours. Western blot of the transfected samples was made and the expression of AHCY protein determined. In both cases, the results showed a poor AHCY knockdown efficiency (figure 16E). The siRNA

targeting GAPDH however, showed a good transfection efficiency, with GAPDH knocked down in BLUE-1R10 at both 16 hours and 24 hours after transfection.

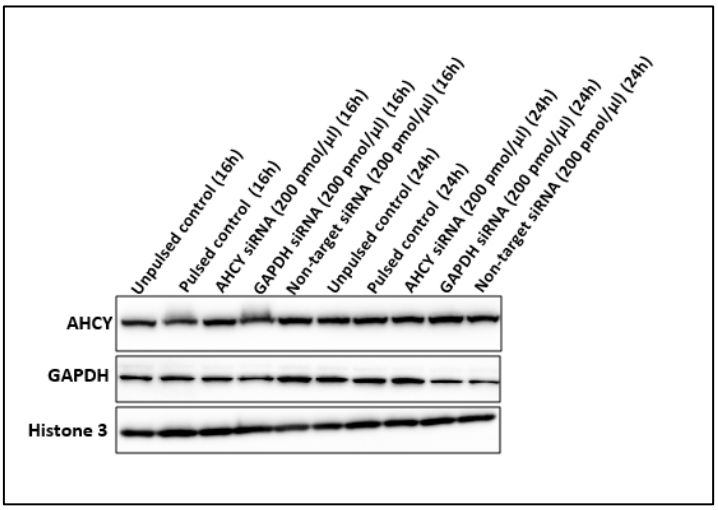

Figure 16E. Western blot showing the transfection efficiency of BLUE-1R10 transfected with AHCY esiRNA (varying the time of transfection). Cells were cultured in 6-well plates at a seeding density of $5x10^6$ cells/ml. Electroporation of the transfected cells were carried out using 200 pmol/µl AHCY esiRNA. Transfection using 200 pmol/µl GAPDH negative control siRNA and the Non-target negative control pool siRNA were performed as controls in parallel. Transfection was performed for 16 hours as well as 24 hours, after which the cells were harvested and counted. 3 x 10^6 cells were lysed and total protein lysate prepared from the cells of each sample. Western blot to examine the level of AHCY and GAPDH expression after transfection was performed with Histone 3 serving as a loading control for the experiment.

Having given several attempts to knockdown AHCY in the resistant BLUE-1R10 cell line without success, we hypothesized that AHCY expression in BLUE-1R10 may be so high that large concentrations of AHCY esiRNA would not be able to reduce it to an extent observable at the protein level using the Western blot assay. To check if this was the case, we examined the expression of AHCY at the RNA level following transfection with the AHCY esiRNA. Cells were transfected once again according to the set-up in table 9E.

Table 9E. Plate set-up for the transfection of BLUE-1R10 with esiRNA targeting AHCY (validation of transfection efficiency at the RNA level).

Sample	Medium	esiRNA AHCY	Program	Time
Sample 01 [NTC]	4 ml (6-well plate)	-	D-23	24 hours
Sample 02	4 ml (6-well plate)	+ 10 µl AHCY esiRNA (200 pmol/µl)	D-23	24 hours
Sample 03	4 ml (6-well plate)	+ 20 µl AHCY esiRNA (400 pmol/µl)	D-23	24 hours
Sample 04	4 ml (6-well plate)	+ 4 µl non-target siRNA (200 pmol/µl)	D-23	24 hours
Sample 05 [NTC]	4 ml (6-well plate)	-	D-23	48 hours
Sample 06	4 ml (6-well plate)	+ 10 µl AHCY esiRNA (200 pmol/µl)	D-23	48 hours
Sample 07	4 ml (6-well plate)	+ 20 µl AHCY esiRNA (400 pmol/µl)	D-23	48 hours
Sample 08	4 ml (6-well plate)	+ 4 µl non-target siRNA (200 pmol/µl)	D-23	48 hours

NTC means no template control. The transfection times were 24 hours and 48 hours respectively, with 200 pmol/µl and 400 pmol/µl of the esiRNA targeting AHCY. The non-target control pool was used as a negative control for the transfection.

At the end of transfection, cells were harvested and the number of vital cells analyzed using flow cytometry. All transfected cell cultures had an average percentage of apoptotic cells less than 15%. RNA was isolated from the cells of each sample and subjected to real-time RT-PCR analysis to determine *AHCY* gene expression. Our results confirmed that there was a decrease in the expression of AHCY in the cells following knockdown with increasing concentrations of the AHCY esiRNA at 24 hours (figure 16F). At 48 hours post-transfection this decrease was even more in the AHCY esiRNA-transfected cells. Despite the high concentration of AHCY esiRNA (400 pmol/µl) used for transfection of BLUE-1R10, the expression level of AHCY in a basic lymphoma cell line (BLUE-1) was not reached after knockdown. This explains why decreased AHCY expression was not evident in the cells at the protein level by Western blot.

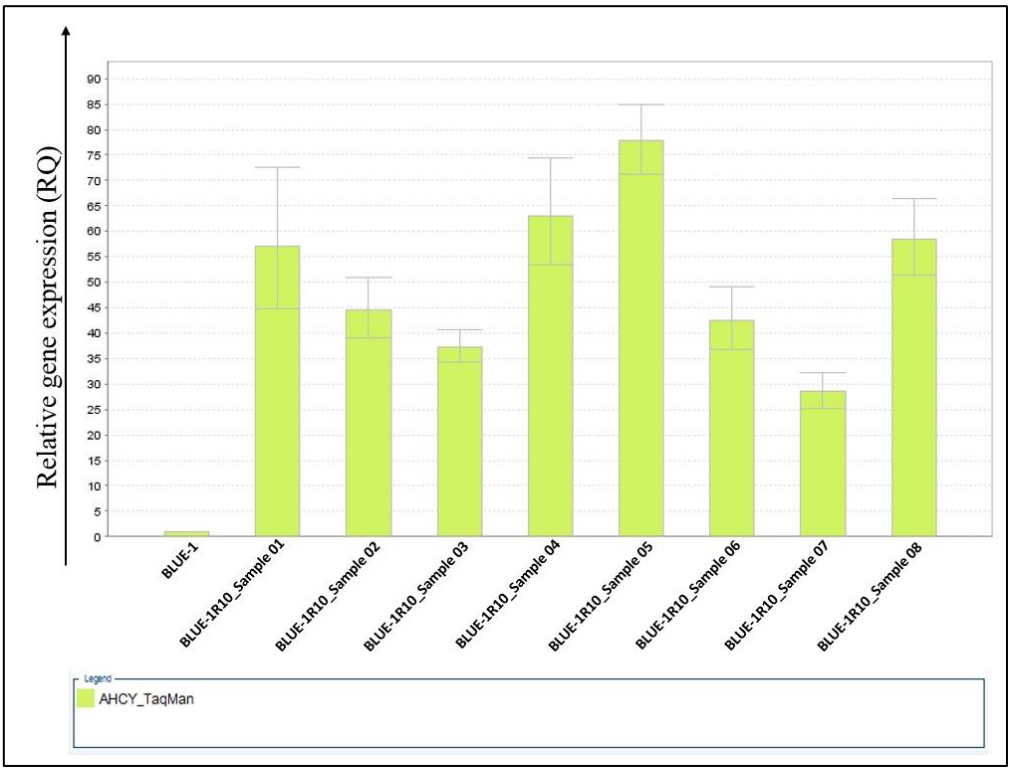

Figure 16F: RNA expression of AHCY in BLUE-1R10 following transfection with 200 pmol/µl and 400 pmol/µl AHCY esiRNA. $5x10^6$ cells of BLUE-1R10 were cultured in 6-well plates and electroporated to deliver the respective siRNAs into the cells. Cells were transfected for both 24 and 48 hours after which they were harvested and RNA extracted. The samples (from table 9E) were subjected to real-time RT-PCR quantitation to determine *AHCY* gene expression using the AHCY TaqMan gene expression assay. The y-axis shows the relative *AHCY* gene expression. TaqMan *B2M* gene expression assay served as an endogenous control.

3.14. Functional validation of *AHCY* copy number gain (AHCY overexpression assays)

We worked on overexpressing *AHCY* in BLUE-1K10 as well as in other DZNep-sensitive cell lines. The goal was to investigate whether these AHCY-overexpressed DZNep-sensitive cell lines would become DZNep resistant when treated with the drug. To achieve this, 3 DZNep sensitive lymphoma cell lines, BLUE-1K10, BL-41 and BL-2 as well as the DZNep-sensitive osteosarcoma cell line U-2-OS, were transfected with an AHCY expression plasmid and a

negative control plasmid as described in section 2.15. Transfection of the cell lines was performed using lipofection and confirmation of transfection efficiency was done using Western blot.

The results show poor transfection efficiency of the lymphoma cell lines, as the protein expression of AHCY in the AHCY plasmid-transfected cells was similar in relation to the negative control and the untransfected cell lines (left of figure 17A). Transfection of the U-2-OS cell line was however successful, with AHCY overexpressed relative to the negative control (right of figure 17A).

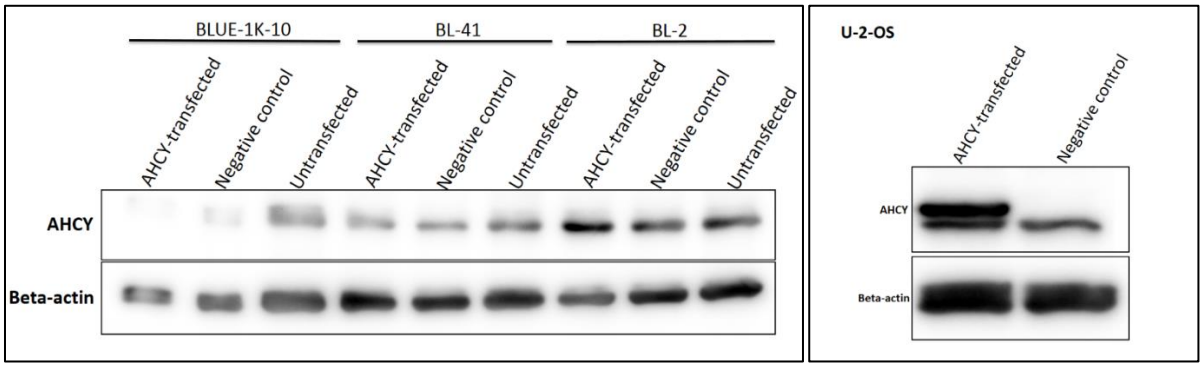

Figure 17A. Western blot showing the transfection efficiency of DZNep-sensitive lymphoma cell lines (left) and an Osteosarcoma cell line (right), transfected with AHCY expression plasmid and negative control plasmid. Whole cell protein lysate from the transfected cells were used for Western blot. Beta-actin was used as a loading control. AHCY overexpression was performed in collaboration with the research group of Prof. Claus Scheidereit.

Since AHCY overexpression was successful in U-2-OS, we performed down-stream assays with this cell line. The AHCY-overexpressed U-2-OS cells, the negative control-transfected U-2-OS cells, as well as the untransfected U-2-OS cells were either untreated or treated with 5 µM DZNep for 72 hours. The percentage of both vital and apoptotic cells was determined afterwards by flow cytometry. Data from the negative control-transfected cells was unavailable due to death of both the DZNep-treated and untreated cells in culture. Results of the untransfected U-2-OS cells showed a high percentage of apoptotic cells following DZNep treatment in comparison to the untreated control (a difference of about 40%) (left of figure 17B). The AHCY-overexpressed U-2-OS cells treated with DZNep however, displayed a reduced percentage of apoptotic cells relative to its untreated control (a difference of about 15%). Confirmation of AHCY overexpression and apoptosis induction by DZNep at the protein level was demonstrated using Western blot. The Western blot picture illustrates that in the untransfected cells, apoptosis was higher following DZNep treatment (as indicated by an increased expression of cleaved PARP), while in the AHCY-overexpressed cells, apoptosis was obviously lower when treated with DZNep (right figure 17B).

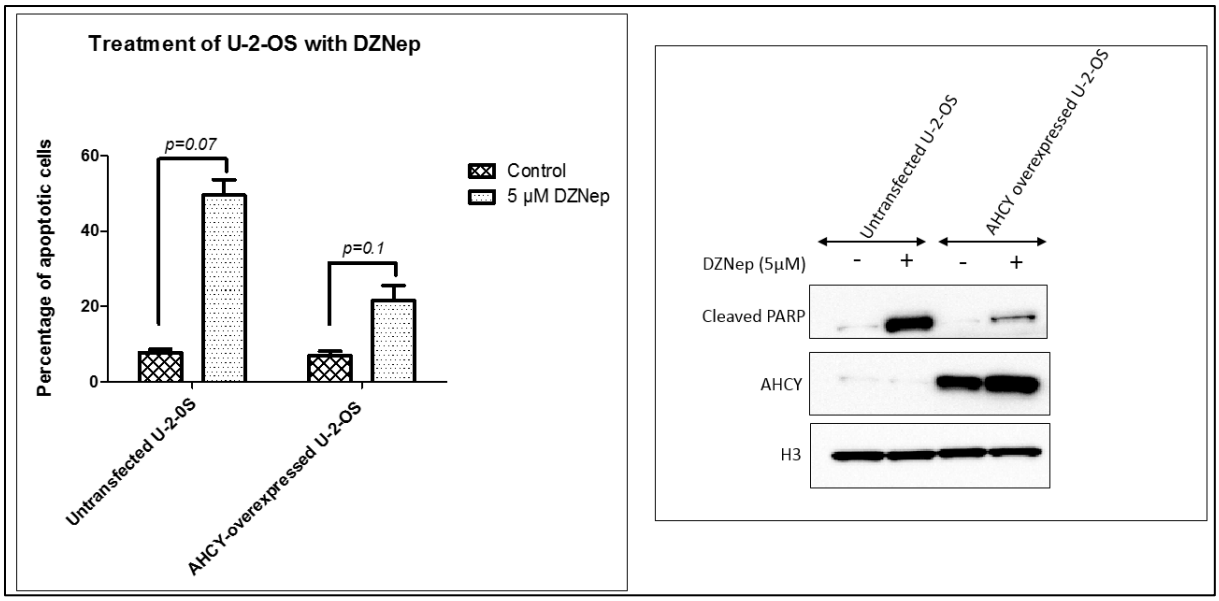

Figure 17B. AHCY-overexpressed U-2-OS cell line tends to be resistant to apoptosis upon DZNep treatment. Left: The adherent U-2-OS cell lines were cultured at a seeding density of $1x10^5$ cells/ml for 24 hours without DZNep treatment to allow attachment of the cells to the surface of the culture vessel. Subsequently, 5 µM DZNep was administered to the cells treated with DZNep. The controls were left untreated. After a duration of 72 hours, the cells were trypsinized to release them from the surface of the culture plate. The resulting cells were counted, and the percentage of apoptotic cells determined with flow cytometry. **Right**: Samples from figure 17B (left) were used for the preparation of protein lysate with which Western blot was performed to show AHCY and cleaved PARP expression. Histone 3 (H3) served as a loading control.

3.15. *AHCY* alterations in other DZNep-resistant cell lines

From an available cell line whole exome sequencing (WES) data source (203), we screened the three DZNep-resistant cell lines (HT, CA-46 and DG-75) to check for alterations in *AHCY*. We identified in one of the cell lines HT, a missense point mutation in *AHCY* resulting in the base exchange A>G (table 10). Other DZNep-resistant cell lines CA-46 and DG-75 lacked this mutation.

Table 10. Heterozygous mutation of the *AHCY* gene in HT cell line, and the predicted consequence.

Cell line	Genotype	Consequence	Amino acid class change (VEP Ensembl)	Protein (VEP Ensembl)	VEP (PolyPhen prediction / SIFT prediction)
HT	0/1	Missense variant	From hydrophobic, polar, small to hydrophobic, small, tiny	ENSP00000217426.2:p.Thr84Ala	Probably damaging / Deleterious (low confidence)

VEP: Variant effect predictor; polymorphism phenotyping (PolyPhen) and sorting intolerant from tolerant (SIFT): Databases predicting effects of nonsynonymous / missense variants.

Observing that the mutation is of a heterozygous genotype, we examined which allele was expressed in the cell. To achieve this, we designed forward and reverse primers spanning the region of the identified mutation Thr84 (see primer sequence in table 3). Using cDNA synthesized from the RNA of this cell line, we amplified this region in a PCR assay. After confirmation of PCR product amplification, the resultant PCR products were cleaned-up and Sanger sequenced to identify the expressed *AHCY* allele. The results of Sanger sequencing

showed that both the mutated as well as the normal *AHCY* allele are expressed in this cell line (figure 18).

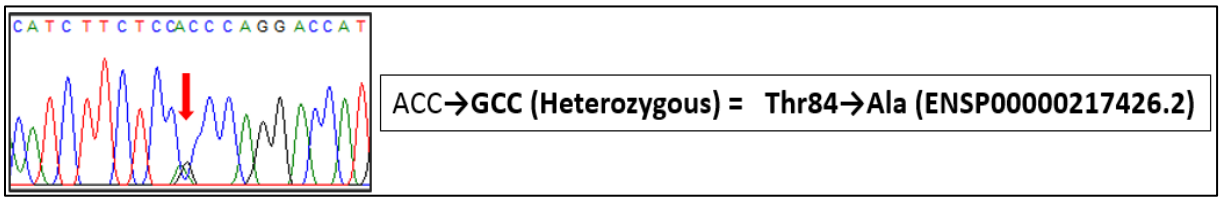

Figure 18. The mutated and wild-type *AHCY* alleles are expressed in HT. Red arrow shows single nucleotide substitution at position 84A>G on exon 3 (reference genome GRCh38.p13). ACC codes for Threonine (Thr), GCC codes for alanine (Ala).

3.16. Analysis of publicly available genomic data sets for alterations of *AHCY*

We also performed mutation analysis and copy number variation analysis of genomic data derived from 5 studies comprising 1295 DLBCL primary samples uploaded onto the cBio Portal for Cancer Genomics (204, 205), however, no *AHCY* alterations were identified.

CHAPTER FOUR

DISCUSSION

Blockage of cell proliferation is thought to be overarching concept of cancer therapy. This can be achieved by a systemic application of cytotoxic drugs (chemotherapy) which stops cellular division of all types of proliferating cells including cancer cells. In contrast, targeted therapy aims at specific blocking of (altered) driver genes known to promote cell proliferations. Blockage of entire cellular processes associated with tumor growth such as epigenetic mechanisms is a further treatment option intermediate between chemotherapy and targeted therapy. Epigenetic drugs are advantageous in that they induce reversible changes that influences gene expression without changing the nucleotide sequence that could adversely affect gene function. However, like many other chemotherapeutic agents, the non-specificity and cytotoxicity of these drugs is a pertinent limitation to their use (206). In this work, the molecular mechanisms of an epigenetic drug (DZNep) was studied in detail.

4.1 DZNep induces apoptosis and inhibits proliferation in B-cell lymphoma irrespective of the lymphoma type, the *EZH2* mutation state and the presence of *MYC*, *BCL2* and *BCL6* translocations

DZNep is still in the preclinical phase of drug development, and so far, studies focusing on its tumor suppressive capacity has shown successful results in different cancer types (141, 143, 156, 171, 207-210). We examined the anti-tumor effects of DZNep in B-cell lymphoma cells in vitro. Our results showed the strong in vitro capacity of DZNep in inducing apoptosis and inhibiting growth of B-cell lymphoma cell lines. The *EZH2* mutation status and the presence of *MYC*, *BCL2* and *BCL6* translocations in the cells did not seem to matter in this respect.

4.1.1 Many cell lines are sensitive to DZNep while some are resistant

We demonstrated that DZNep has a strong apoptotic capacity in lymphoma cell lines. This is in line with findings from other studies investigating the apoptotic effect of DZNep on leukemia cells (210), cholangiocarcinoma cells (209), chondrosarcoma cells (141) and breast cancer cells (167, 211). Moreover, the concentration and time required for a drug to exert its pharmacological action is very essential for a rational achievement of the envisaged effect of that drug. We revealed that the apoptotic effects triggered by DZNep is dependent on the concentration of DZNep used and the duration of DZNep application (figures 4A and 4B). These results conform with similar concentration- and time-dependence of apoptosis reports in

acute myeloid leukemia (169), mantle cell lymphoma (207), non-small cell lung cancer (212), colon cancer (213), breast and colorectal cancer (167), and acute myeloid leukemia cells (168).

We also showed from our IC_{50} results (figure 4D) that not all lymphoma cell lines are sensitive to DZNep. This was further confirmed by the Western blot results (figure 4E) showing cleaved PARP expression in two representative cell lines taken from the resistant group. The consistent expression of cleaved PARP in the DZNep-resistant cell lines following treatment with increasing DZNep concentrations signifies that these cell lines are indeed resistant to apoptosis.

4.1.2 Sensitivity of B-cell lymphoma cell lines to DZNep does not depend on the *EZH2* mutation status, and *MYC*, *BCL2* and *BCL6* translocations

The prognostic impact of *MYC*, *BCL2* and *BCL6* translocations in B-cell lymphomas has been reported (214-220), enabling patient risk assessment including a more intensive monitoring of the disease. We analyzed 12 B-cell lymphoma cell lines for the presence of the frequently reported *EZH2* driver mutations (Tyr646, Ala682 and Ala692), and the presence of translocations involving *MYC* (8q24), *BCL2* (18q21) and *BCL6* (3q27). This was done to investigate the association between the lymphoma type, the *EZH2* mutation situation, the *MYC*, *BCL2* and *BCL6* translocation profile, and the sensitivity of the lymphoma cell lines to apoptosis following DZNep treatment.

Consistent with previous studies (127, 221), analysis of the lymphoma cell lines studied in this work revealed a higher frequency of occurrence of the *EZH2* Tyr646 mutation in relation to the *EZH2* Ala682 and *EZH2* Ala692 mutation (figure 5A and table 6). Several studies focusing on the impact of EZH2 point mutations and overexpression in cancer have also reported this *EZH2* Tyr646 mutation (30, 31, 127, 129, 221, 222). In line with previous works (31, 129, 223), our data (table 6) showed that the Tyr646 mutation presents mainly in DLBCLs having *BCL2* translocations. In contrast to other direct EZH2 inhibitors (139, 146, 152), we illustrated that sensitivity to DZNep-mediated apoptosis or strength of apoptosis upon DZNep treatment does not depend on the presence of the *EZH2* Tyr 646 mutation (Table 6 and figure 5C). More so, our findings (figure 5B and table 6) indicate a poor correlation between sensitivity to DZNep and the type of B-cell lymphoma, as well as the presence of *MYC*, *BCL2* and *BCL6* translocations.

4.1.3 Impact of mutated and wild-type *EZH2* on H3K27me3 in B-cell lymphoma cell lines

It is known that mutated *EZH2* drives the increased H3K27me3 in B-cell lymphoma (222-224). To determine if this also holds true for the lymphoma cell lines used in this work, we isolated total protein lysates from both *EZH2*-mutated and wild-type *EZH2* cell lines and determined the level of H3K27me3 using Western blot. We demonstrated that cell lines with mutated *EZH2* exhibited increased H3K27me3 levels (figure 6), the aftermath culminating in gene silencing (222-226). We also revealed that apoptosis induction in DZNep-sensitive cell lines following DZNep treatment is associated with downregulation of EZH2 and H3K27me3 (figure 7A). This is also the case with chondrosarcoma cell lines (141) and breast cancer cell lines (167) treated with DZNep, signifying that DZNep influences both EZH2 and H3H27me3. Furthermore, even though there is an increase in H3K27me3 levels created by mutated *EZH2*, this does not limit the capacity of DZNep to lower the expression of this protein and cause the cells involved into undergo apoptosis (figure 7B).

4.1.4 DZNep inhibits proliferation of B-cell lymphoma cell lines

As uncontrolled proliferation remains a primary problem propelling cancer development and progression, we interrogated the effect of DZNep on the proliferation of B-cell lymphoma cells. To achieve this, we applied two methods. One was by checking the expression of genes known to be proliferation markers such as *PCNA* (227, 228) and *CDK2* (229, 230). In the cell lines analyzed, there was a decrease in the expression of these genes following treatment of the cells with DZNep (figure 8A), indicating the anti-proliferative property of DZNep. However, bearing in mind that apoptotic and dead cells may downregulate these genes and that they were not excluded from the cohort of cells used for the gene expression analysis, we analyzed cell proliferation using flow cytometry (figure 8B). Our findings align with related reports on the anti-proliferative effects of DZNep in various cancer cell lines (141, 209, 212, 231) and in mice models (156, 169, 171, 207, 232). It is interesting to note that the anti-proliferative effects of DZNep was observed in all cell lines analyzed and was not dependent on the *EZH2* mutation situation of the cells. Inhibition of proliferation by DZNep was also noted to be time-dependent as was observed in other cells such as erythroleukemia cells (233) and colon cancer cells (213).

4.1.5 DZNep shows a stronger apoptotic effect in B-cell lymphoma cell lines compared to EPZ-6438

Upon comparing the apoptotic capacity of DZNep and EPZ-6438 (a direct EZH2 inhibitor in phase II clinical trials for B-cell NHL patients (234)) in aggressive B-cell lymphoma cell lines,

our results illustrated that DZNep has no tendency to preferentially cause apoptosis based on the *EZH2* mutation status of the cells (figure 9A). Our results also portrayed that DZNep is faster in causing apoptosis in comparison to EPZ-6438. A previous study showed that extended treatment with EPZ-6438 resulted in the selective killing of mutant *EZH2* lymphoma cell lines and xenograft models (139). Based on our results (figure 9B), there was no particular difference in the fraction of apoptotic cells measured in the *EZH2*-mutated and wild-type *EZH2* DZNep-sensitive cell lines following prolonged treatment with the inhibitor. In the case of HT, the DZNep-resistant cell line possessing wild-type *EZH2*, we noticed a marked increase in the percentage of apoptotic cells after the third day of treatment with EPZ-6438. This indicates that EPZ-6438 is capable of inducing apoptosis irrespective of the *EZH2* mutation status of lymphoma cell lines, although a longer time may be required for the apoptotic effects become manifest. We were curious to know whether EPZ-6438 could also invoke a robust apoptotic response in the DZNep-sensitive wild-type *EZH2* cell line (BLUE-1) that was used for the generation of the DZNep-resistant clone subsequently used in this work. We treated the parent BLUE-1 cell line, the DZNep-resistant clone (BLUE-1R10) and its corresponding control (BLUE-1K10) with EPZ-6438 for up to 13 days as done in the previous experiment (figure 9B). In all three cell lines, there was no prominent rise in the percentage of apoptotic cells when treated with 10 μM of the inhibitor. This means that it is possible for a DZNep-sensitive cell line to be EPZ-6438-resistant. Meanwhile, the DZNep-resistant clone, although DZNep-resistant was also EPZ-6438-resistant (figure 9C).

4.2 Alterations of the *AHCY* gene could be linked with the resistance of B-cell lymphoma to DZNep-mediated apoptosis

Evolution of resistance to small molecule inhibitors used in cancer therapy is still a huge problem leading to the failure many - initially successful - targeted therapeutics (235). As different mechanisms contribute to the resistance of cancer cells to therapy (178, 236, 237), we sought to investigate in our case, the mechanism underlying the resistance of B-cell lymphoma cell lines to DZNep.

4.2.1 Characterization of the DZNep-resistant clone possessing acquired resistance to DZNep

Having obtained distinct responses to apoptosis following treatment of the 12 B-cell lymphoma cell lines with DZNep, we focused on the DZNep-resistant group, delving into the reason behind this resistance by generating a DZNep-resistant clone from a DZNep-sensitive lymphoma cell line BLUE-1. This clone was used as a model to study the resistance mechanism

to DZNep, as well as to aid with the detection of biomarkers that would be predictive of the therapeutic benefit of EZH2 inhibition using DZNep. Similar in vitro cell line models have been established and used to study mechanisms of resistance to drugs in different cancer types, for instance in gastric cancer (238), colorectal cancer (239), colon cancer (240) and non-small cell lung cancer (241). Subsequent characterization of the DZNep-resistant clone revealed similarities to the parent cell line in many characteristics but its response to DZNep apoptotic pressure.

The first step in characterizing this clone was to check if it actually derived from the parent cell line. Owing to the fact that we worked with several cell line clones in parallel during the generation of the DZNep-resistant clone, we considered that there could be a possibility for cross-contamination of the clone with other cell lines during the long-term cultivation. Moreover, we are aware that sub-clonal populations could arise in the clone due to long-term drug selection pressure. To confirm that the generated resistant clone represents indeed the same cell line derived from the parent cell line BLUE-1, we investigated the resistant clone BLUE-1R10 (isolated after 7 months in culture). We explored the expression of cell surface markers CD19 and CD20 on the cell line, analyzed its STR profile and determined its clonality by checking the IGH gene rearrangement pattern.

CD19 and CD20 are specific B-cell markers with a quite consistent expression in B-cell lymphomas (242, 243). However, in rare cases, some B-cell lymphoma types are CD19-negative (244, 245) or CD20-negative (246, 247). BLUE-1 is one of the cell lines used in this work, which unlike several others, does not express the cell surface marker CD20 (see DSMZ data sheet with number: ACC-594). As expected, BLUE-1R10 and BLUE-1K10, just as BLUE-1 expressed CD19 but not CD20 (figure 10A), indicating a great likelihood that the cell lines were not mixed up with other cell lines during the cultivation period. In addition, the identical IGH chain gene rearrangement profile for the three cell lines (figure 10B) also confirmed that both BLUE-1K10 and BLUE-1R10 originated from the same parent. Furthermore, STR profiling of the three cell lines confirmed that they are all BLUE-1 cell lines.

Subsequent analysis of BLUE-1R10, BLUE-1K10 and BLUE-1 revealed slight differences in the karyotype (figure 10C). This underscores the point that although they originate from the same cell line, there are some chromosomal differences existing among them.

Contrary to a previous study which reported that acquired drug resistance due to prolonged drug exposure is associated with increased doubling time in colon cancer cell lines (240), BLUE-

1R10 showed a reduced doubling time in comparison to the parent cell line (figure 10D). We cannot conclude that the shorter doubling time observed in BLUE-1R10 is due to the DZNep treatments because, BLUE-1K10 (the corresponding control of BLUE-1R10), which did not receive any DZNep treatment also showed a shorter doubling time. Besides, since evolution of human cancer cell lines could result in a high degree of genetic heterogeneity (248), it could be that certain genetic changes might have occurred in the cells due to prolonged cultivation. Perhaps, by analyzing RNA sequencing data derived from the parent cell line (BLUE-1) in addition to that of the resistant clone and its control, we could be able to identify proliferation targets, identical to the two cell lines (BLUE-1K10 and BLUE-1R10) but different from BLUE-1. Functional validation of these targets could give us a hint on the biological markers responsible for the increased proliferation rate observed in the two long-term-cultured cell lines.

We also compared the apoptotic response of the resistant clone and its corresponding control to DZNep. We observed that treatment of this clone with 5 µM DZNep, a concentration 25 fold greater than that used to initiate treatment (during generation of the clone), the cells remained resistant to DZNep (figure 10E). The corresponding control displayed however, a robust apoptotic response following treatment with the same DZNep concentration. This shows that the resistance of the resistant clone to DZNep is a stable phenomenon persisting even following cultivation of BLUE-1R10 in a medium devoid of DZNep.

4.2.2 Detection of biomarkers determining DZNep resistance

Since we already know that chromosomal disparities exist among the three cell lines, we went further to identify DNA structural variants that cause a loss or gain of chromosomal segments by performing the genome-wide OncoScan copy number variation (CNV) assay. We disclosed 3 aberrations exclusive to BLUE-1R10, 3 anomalies present only in BLUE-1 and 4 aberrations existing only in both BLUE-1 and BLUE-1R10 (table 7). This reflects the level of genomic variation and chromosomal instability that could occur following long-term culture of cell lines in vitro under different conditions.

Although the OncoScan assay is a fast, easy and highly sensitive method for the detection of genome-wide copy number alterations (249), data output can be limited by inadequate number of probes for certain genes/genomic regions (250). Whole exome sequencing (WES) approach provides a better resolution and higher accuracy for the interrogation of cancer-related genes (250), especially for detecting small copy number changes in regions of low probe coverage with the former assay.

For this reason, we subjected the resistant clone BLUE-1R10 and its control BLUE-1K10 to WES. Upon analysis of the sequencing data, we identified copy number alterations in several targets in the resistant clone in relation to its control. These include copy number variations on chromosome 6 (*SNHG5*, *SMIM11P1*, *HTR1E* and *CGA* genes) and on chromosome 20 (*AHCY* gene, extending until the proximal part of the *ITCH* gene) (figure 11B). *SNHG5* codes a long non-coding RNA, and has been shown to play a role in the progression of bladder cancer (251). While *SMIM11P1* is a pseudogene and encodes no protein, *HTR1E* codes the serotonin receptor 1E (252). *CGA* codes the alpha subunit of the four human glycoprotein hormones; luteinizing hormone, chorionic gonadotropin, thyroid-stimulating hormone and follicle stimulating hormone, whereas, the *ITCH* gene encodes a member of the HECT domain E3 ubiquitin ligases that target particular proteins for degradation by the lysosome (252). *AHCY* gene encodes S-adenosylhomocysteine hydrolase, which catalyzes the reversible hydrolysis of SAH to adenosine and homocysteine (161, 162), thereby controlling the concentration of SAH necessary for methylation reactions within the cell (252). From the list of genes with copy number variation, *AHCY* seemed most promising for further investigation as to the reason behind the resistance of the clone to DZNep, as DZNep directly inhibits AHCY.

4.2.3 Validation of *AHCY* copy number variation in the DZNep-resistant clone, other B-cell lymphoma cell lines and primary lymphoma samples

To validate the *AHCY* copy number variation observed in the DZNep-resistant clone, we used a simple, but specific and reproducible method - the TaqMan Copy Number Assay - to detect copy number changes. We analyzed genomic DNA from all 12 (DZNep-sensitive and DZNep-resistant) B-cell lymphoma cell lines, including the resistant clone. We detected a remarkable gain in the *AHCY* copy number in BLUE-1R10, and a further increase in the number in BLUE-1R12 (figure 12A). This progressive gain in the number of copies of *AHCY* was observed from BLUE-1R6, obtained on the fifth month of treatment of BLUE-1 with DZNep (figures 12B and 12C). This implies that the presence of DZNep is not necessary for the gain in *AHCY* copy number in the clone once this gain is established. Other lymphoma cell lines analyzed did not show this profound *AHCY* copy number gain.

From the results of the CNV assay performed using the DNA methylation data from BLUE-1, BLUE-1K10 and BLUE-1R10, we also confirmed the *AHCY* copy number gain in the resistant clone (figure 12D). Furthermore, manually evaluating the OncoScan CNV data, laying emphasis on the *AHCY* locus on chromosome 20, we detected 8 probes with a high log2 ratio

in BLUE-1R10, which was absent from BLUE-1K10 and BLUE-1 (figure 12E). This was filtered out due to the stringent criteria for calling an event a CNA (see section 2.13).

Using chromosome 20-specific DNA probes for *AHCY*, we also validated the *AHCY* copy number gain in the resistant clone at the chromosomal level. This was performed using FISH, a powerful technique used for the detection of chromosomal anomalies in tissues (253, 254). Our FISH results confirmed this *AHCY* copy number gain (figure 12F) observed in cells of the resistant clone (BLUE-1R10 and BLUE-1R12) when compared with their corresponding controls (BLUE-1K10 and BLUE-1K12) respectively. This further affirms that the *AHCY* gain in the clone is a continuous process.

In cases where the target of a drug is an enzyme, modifications such as changes in the expression levels of the drug target can lead to resistance to the drug (178, 255). We therefore, investigated the expression of AHCY at both the transcriptional and protein level. We showed that AHCY is overexpressed in BLUE-1R10 and BLUE-1R12. Other B-cell lymphoma cell lines examined did not show a comparable increase in the expression of AHCY in relation to the DZNep-resistant clone (figures 12G, 12H and 12I). The absence of overexpressed AHCY in other B-cell lymphoma cell lines is an indicator that this mechanism of resistance is unique to the resistant clone, which possesses an acquired resistance to DZNep. Other DZNep resistant cell lines with an intrinsic resistance to DZNep may have other underlying mechanisms independent of AHCY overexpression.

In comparison with cervical cancer (256), colon cancer (257) and colorectal cancer (258) where copy number gains of *AHCY* has been associated with disease pathogenesis, not much is known about the part gains of *AHCY* play in aggressive B-cell lymphoma progression. If copy number gains of the *AHCY* gene were a frequent occurrence in lymphomas, then the translation of DZNep into clinical application in patients with this alteration might be accompanied with resistance to the drug. We examined the *AHCY* CNV profile for 11 lymphoma patient samples to check if this alteration could be detected. None of the samples analyzed displayed gains of *AHCY* however, one out of the 11 samples showed a deletion of one copy of the *AHCY* gene (figure 12K). We are uncertain about the effects of reduced *AHCY* copy number in lymphoma cells and what functional impact this may create, or if alternative / rescue mechanisms may set in to enable proper functioning of the cells.

4.2.4 DZNep decreases AHCY expression

In addition to the fact that DZNep directly inhibits AHCY (159, 259), we depict that DZNep also decreases the expression of AHCY in B-cell lymphoma cell lines. Even in the DZNep-resistant clone with overexpressed AHCY, there was a mild decrease in the AHCY expression following DZNep treatment. This effect however, was still ineffective in lowering the AHCY levels to that obtainable in other basic B-cell lymphoma cells lines (figure 13). The slight reduction of AHCY expression in the clone could thus, result in little to no effect of DZNep in potentiating the downstream effects of EZH2 inhibition and apoptosis induction in this cell line. One may argue that the AHCY downregulation observed may be due to dead or apoptotic cells precipitated by DZNep treatment. However, we also noticed that in the DZNep-resistant cell lines BLUE-1R10 and HT, just like in the DZNep-sensitive cell lines BL-41, BLUE-1 and BLUE-1K10, there was also a decrease in AHCY expression following DZNep treatment.

4.2.5 DZNep influences the methylation process by mediating effects on intermediates of methionine

The importance of metabolomics in studying disease mechanisms and in biomarker identification in cannot be overemphasized (260-263). To this end, we studied the dynamics of select intermediates of methionine metabolism including SAH, adenine and adenosine in the resistant clone (BLUE-1R10 and BLUE-1R12), their controls (BLUE-1K10 and BLUE-1K12 respectively) and the parent cell line (BLUE-1). The comparable pattern in which the mentioned intermediates were distributed in BLUE-1, BLUE-1K10 and BLUE-1K12 (figure 14) indicates that even after long-term cultivation of the cell lines, the manner in which the respective intermediates disseminated within the cell was not considerably altered. Upon treatment of the resistant clone (BLUE-1R10) with DZNep however, we clearly observed an increase in the quantity of SAH. This signifies that DZNep really inhibits AHCY resulting in the buildup of SAH levels (159), with EZH2 inhibition being one consequence of this SAH elevation (159, 167, 210). Nevertheless, this AHCY inhibition is not sufficient to make the resistant clone sensitive to the apoptotic effects of DZNep. In the resistant clone without DZNep pressure however (BLUE-1R12), there was a clear rise in both adenine and adenosine levels in comparison with its control BLUE-1K12. This surge could be because, due to the increased AHCY expression in this clone, there is an increased AHCY-mediated hydrolysis of SAH, favoring the forward reaction that results in adenosine production.

4.2.6 Differentially methylated targets involved in DZNep-mediated apoptosis

DNA methylation patterns can provide important information concerning the prognosis of a disease and response to drugs (264, 265). We analyzed the global DNA methylation profile of the resistant clone and its control with and without DZNep pressure, as well as that of the parent BLUE-1 cell line. We observed that the ELISA-based method we initially used for the colorimetric determination of the global DNA methylation level in the cell lines was not reproducible (figure 15A). We therefore used the MethylationEPIC BeadChip microarray, which provides high reproducibility across replicate samples (266). The hierarchical clustering and PCA created using the methylation data of the cell lines showed high similarity between replicates (figures 15B and 15C respectively). This gave more assurance that samples were not mixed-up, and further confirmed the reproducibility of this adopted method. Even with the identical clustering of replicate samples, the parent cell line and the control for the resistant clone clustered more together. In the presence of DZNep however, the control for the resistant clone clustered more with the resistant clone. This shows that in presence of DZNep, there is a tendency for the methylation pattern to progress towards the direction of the DZNep-resistant phenotype. That notwithstanding, even with the intra-group differences, the cell lines clustered more with the inclusion of the primary tumor methylation data. This shows that although there are differences in the methylation pattern of the resistant clone as well as its control, the parent cell line and DZNep treated cells, these changes are rather subtle. Upon comparison of the cell line methylation data with methylation data from primary lymphoma and plasmacytoma samples, we observed from the clustering, more similarity between the primary tumor samples irrespective of the type of primary samples (figure 15B). This suggests that irrespective of the type of primary tumor type, DNA methylation patterns of primary tumor samples are somewhat distinct from that of cell lines.

Further analysis of differentially methylated genes yielded several targets whose methylation patterns differed between the various cell lines analyzed (BLUE-1K10 versus BLUE-1R10, DZNep-sensitive versus DZNep-resistant, and BLUE-1K10 versus BLUE-1K10 plus DZNep) (figures 15D and 15E). Of particular interest, we find no differentially methylated target genes between the resistant clone in presence and absence of DZNep based on the used criteria for defining differentially methylated probes (figure 15E). This is an indicator that the resistant clone is indeed resistant to DZNep. Differently methylated genes were however, detected in the clone's control BLUE-1K10 when comparing DZNep-treated and -untreated conditions. The differentially methylated genes involved in the apoptosis signaling pathway were explored

between groups 1 (BLUE-1K10 versus BLUE-1R10), 2 (DZNep-resistant versus DZNep-sensitive cell lines) and 3 (BLUE-1K10 in presence versus absence of DZNep pressure). The resulting gene list (table 8) highlights the group of differentially methylated target genes whose methylation states may likely affect these cell lines' response to apoptosis by DZNep. Already, particular methylation states of several of these targets have been associated with different types of cancers, for example in hepatocellular carcinoma and papillary renal cell carcinoma, hypermethylation of the *PRKCH* gene has been reported, while in prostate carcinoma, hypomethylation of *AKT3* has been recorded (267). The effect of the different DNA methylation states on the cell lines' response to apoptosis would depend on the type and location of the methylation mark on these genes.

4.2.7 Validation of the functional role of *AHCY* copy number gain

To annotate the functional impact of AHCY overexpression, we worked on knocking down AHCY in the resistant clone BLUE-1R10. This was performed to check if this clone would regain sensitivity to DZNep. Upon several trials (explained in section 3.13), we discovered that due to the overexpressed AHCY in the resistant clone, we were unable to achieve an efficient AHCY knockdown (at the protein level) to levels lower than that obtainable in a basic BLUE-1 cell line. Perhaps, if we had used the resistant clone isolated at an earlier time point during its evolution (for instance, BLUE-1R6), we might have been able to knock down AHCY to much lower levels that would allow for the functional investigation of the effect of *AHCY* copy number gain in the cells.

We also attempted to overexpress AHCY in three DZNep-sensitive B-cell lymphoma cell lines and one DZNep-sensitive osteosarcoma cell line (U-2-OS). After transfecting them using the same method (lipofection), AHCY was overexpressed only in U-2-OS (figure 17A). This is not so surprising because lymphoma cells are one of the known cell types that are difficult to transfect (268-270). Results of downstream analysis of the AHCY-overexpressed U-2-OS cell line and its untransfected control suggests that AHCY overexpression tends to be associated with resistance of the cells to apoptosis mediated by DZNep (figure 17B). This can however not be completely justified since we do not have the data from the negative control-transfected U-2-OS cells. It would also be interesting to test if overexpression of AHCY in the DZNep-sensitive lymphoma cell lines by other gene delivery options such as the use of viral vectors would yield a successful outcome.

4.2.8 *AHCY* alterations are not frequent but can occur in B-cell lymphoma

We checked the WES data of DZNep-resistant cell lines HT, CA-46 and DG-75 (203) for genomic alterations of *AHCY*, and detected an *AHCY* point mutation predicted to have a probably damaging consequence in the cell line HT (table 10). Both the mutated and wild-type alleles were also expressed in this cell line at the mRNA level (figure 18). Since this was the case, it translates that both the mutated and the normal AHCY protein would be present in the cell. We presume that this mutation, although not located in the AHCY binding site, may play a role in the resistance of this cell line to DZNep. The impact of this mutation, which still needs to be verified, would depend on the ratio of the protein amounts translated from the mutated and wild-type AHCY mRNAs, as well as on the effects of post-translational modifications on both proteins.

The lack of *AHCY* alterations in the cases of DLBCL primary samples analyzed from the publicly available database (204, 205) shows that *AHCY* alterations are infrequent in DLBCLs. However, based on the cancer type, *AHCY* mutations and amplifications in solid tumors can be up to 4% and 11% respectively (204, 205).

CONCLUSION

With the increasing need for new and better ways to tackle cancers, there is a high demand for novel drugs with a good therapeutic efficacy and limited side effects. Moreover, resistance to cancer chemotherapeutics could be a problem during drug usage therefore, discerning tumor resistance mechanisms and determining predictive biomarkers that could aid in preventing this issue from emerging beforehand is essential.

In this work, we confirmed the anti-tumor characteristics of DZNep; highlighting its strong apoptotic and anti-proliferative capacity in aggressive B-cell lymphoma cell lines. These tumor-antagonistic effects were mediated independent of the presence of the *EZH2* driver mutation (Tyr646), as well as *MYC*, *BCL2* and *BCL6* translocations. Furthermore, we demonstrated that the presence of *EZH2* gain-of-function mutations did not reduce the capacity of DZNep to promote apoptosis in these B-cell lymphoma cell lines.

We also showed that alterations of the *AHCY* gene are a potential mechanism through which resistance to DZNep-mediated apoptosis could occur in aggressive B-cell lymphomas. These alterations include, but are not limited to copy number variations and mutations of the *AHCY* gene. Furthermore, acquired resistance mechanisms to DZNep-mediated apoptosis in aggressive B-cell lymphomas may differ from mechanisms of intrinsic resistance which themselves, may vary due to the great level of genetic heterogeneity in cells. Despite the rarity of *AHCY* anomalies in primary lymphomas, screening for alterations of *AHCY* or the associated pathway in patients may still be necessary before the use of DZNep. Whether DZNep could be a more powerful epigenetic drug against DZNep-resistant B-cell lymphoma cells when combined with other (epigenetic) drugs still needs to be investigated.

Lastly, despite the challenges involved with in vitro studies, evolution studies with cell lines still present a promising method for studying resistance mechanisms to DZNep. This study provides better understanding on the molecular mechanism of resistance to DZNep and advocates AHCY as a promising prognostic biomarker for EZH2-based therapeutic interventions with DZNep.

REFERENCES

1. Smith A, Crouch S, Lax S, Li J, Painter D, Howell D, et al. Lymphoma incidence, survival and prevalence 2004-2014: sub-type analyses from the UK's Haematological Malignancy Research Network. Brit J Cancer. 2015;112(9):1575-84.
2. Swerdlow SH, Campo E, Pileri SA, Harris NL, Stein H, Siebert R, et al. The 2016 revision of the World Health Organization classification of lymphoid neoplasms. Blood. 2016;127(20):2375-90.
3. Quintanilla-Martinez L. The 2016 updated WHO classification of lymphoid neoplasias. Hematol Oncol. 2017;35:37-45.
4. Swerdlow SH, Campo E, Harris NL, Jaffe ES, Pileri SA, Stein H, et al. WHO Classification of Tumours of Haematopoietic and Lymphoid Tissues. Fourth Edition ed: World Health Organization; 2008.
5. Swerdlow SH, Campo E, Harris NL, Jaffe ES, Pileri SA, Stein H, et al. WHO Classification of Tumours of Haematopoietic and Lymphoid Tissues. Revised 4th edition ed: World Health Organization; 2017.
6. Kuppers R, Hansmann ML. The Hodgkin and Reed/Sternberg cell. Int J Biochem Cell B. 2005;37(3):511-7.
7. Shanbhag S, Ambinder RF. Hodgkin Lymphoma: A Review and Update on Recent Progress. Ca-Cancer J Clin. 2018;68(2):116-32.
8. Reed DM. On the pathological changes in Hodgkin’s disease, with special reference to its relation to tuberculosis: Johns Hopkins Hosp Rep. ; 1902; (10):133-196.
9. Kuppers R, Rajewsky K, Zhao M, Simons G, Laumann R, Fischer R, et al. Hodgkin Disease - Hodgkin and Reed-Sternberg Cells Picked from Histological Sections Show Clonal Immunoglobulin Gene Rearrangements and Appear to Be Derived from B-Cells at Various Stages of Development. P Natl Acad Sci USA. 1994;91(23):10962-6.
10. Inghirami G, Macri L, Rosati S, Zhu BY, Yee HT, Knowles DM. The Reed-Sternberg Cells of Hodgkin Disease Are Clonal. P Natl Acad Sci USA. 1994;91(21):9842-6.
11. Hummel M, Marafioti T, Stein H. Clonality of Reed-Sternberg cells in Hodgkin's disease. New Engl J Med. 1999;340(5):394-5.
12. Fisher SG, Fisher RI. The epidemiology of non-Hodgkin's lymphoma. Oncogene. 2004;23(38):6524-34.
13. Trask PC, Mehta J, Abbe A, RuizSoto R. Epidemiology Projection Trends for Non-Hodgkin Lymphoma (NHL) and Its Subtypes in the United States (US) and Europe (EU). Blood. 2012;120(21).
14. Miles RR, Arnold S, Cairo MS. Risk factors and treatment of childhood and adolescent Burkitt lymphoma/leukaemia. Brit J Haematol. 2012;156(6):730-43.
15. Said JW. Aggressive B-cell lymphomas: how many categories do we need? Modern Pathol. 2013;26:S42-S56.
16. Blum KA, Lozanski G, Byrd JC. Adult Burkitt leukemia and lymphoma. Blood. 2004;104(10):3009-20.
17. Thomas DA, O'Brien S, Faderl S, Manning JT, Romaguera J, Fayad L, et al. Burkitt Lymphoma and Atypical Burkitt or Burkitt-like Lymphoma: Should These be Treated as Different Diseases? Curr Hematol Malig R. 2011;6(1):58-66.
18. Gong JZ, Stenzel TT, Bennett ER, Lagoo AS, Dunphy CH, Moore JO, et al. Burkitt lymphoma arising in organ transplant recipients - A clinicopathologic study of five cases. Am J Surg Pathol. 2003;27(6):818-27.
19. Xicoy B, Ribera JM, Esteve J, Brunet S, Sanz MA, Fernandez-Abellan P, et al. Post-transplant Burkitt's leukemia or lymphoma. Study of five cases treated with specific intensive therapy (PETHEMA ALL-3/97 trial). Leukemia Lymphoma. 2003;44(9):1541-3.

20. Jacobson C, LaCasce A. How I treat Burkitt lymphoma in adults. Blood. 2014;124(19):2913-20.
21. Ott G. Aggressive B-cell lymphomas in the update of the 4th edition of the World Health Organization classification of haematopoietic and lymphatic tissues: refinements of the classification, new entities and genetic findings. Brit J Haematol. 2017;178(6):871-87.
22. Savage KJ, Johnson NA, Ben-Neriah S, Connors JM, Sehn LH, Farinha P, et al. MYC gene rearrangements are associated with a poor prognosis in diffuse large B-cell lymphoma patients treated with R-CHOP chemotherapy. Blood. 2009;114(17):3533-7.
23. Klapper W, Stoecklein H, Zeynalova S, Ott G, Kosari F, Rosenwald A, et al. Structural aberrations affecting the MYC locus indicate a poor prognosis independent of clinical risk factors in diffuse large B-cell lymphomas treated within randomized trials of the German High-Grade Non-Hodgkin's Lymphoma Study Group (DSHNHL). Leukemia. 2008;22(12):2226-9.
24. Li SY, Young KH, Medeiros LJ. Diffuse large B-cell lymphoma. Pathology. 2018;50(1):74-87.
25. Alizadeh AA, Eisen MB, Davis RE, Ma C, Lossos IS, Rosenwald A, et al. Distinct types of diffuse large B-cell lymphoma identified by gene expression profiling. Nature. 2000;403(6769):503-11.
26. Savage KJ, Monti S, Kutok JL, Cattoretti G, Neuberg D, de Leval L, et al. The molecular signature of mediastinal large B-cell lymphoma differs from that of other diffuse large B-cell lymphomas and shares features with classical Hodgkin lymphoma. Blood. 2003;102(12):3871-9.
27. Rosenwald A, Wright G, Chan WC, Connors JM, Campo E, Fisher RI, et al. The use of molecular profiling to predict survival after chemotherapy for diffuse large-B-cell lymphoma. New Engl J Med. 2002;346(25):1937-47.
28. Rosenwald A, Wright G, Leroy K, Yu X, Gaulard P, Gascoyne RD, et al. Molecular diagnosis of primary mediastinal B cell lymphoma identifies a clinically favorable subgroup of diffuse large B cell lymphoma related to Hodgkin lymphoma. J Exp Med. 2003;198(6):851-62.
29. Lawrence MS, Stojanov P, Polak P, Kryukov GV, Cibulskis K, Sivachenko A, et al. Mutational heterogeneity in cancer and the search for new cancer-associated genes. Nature. 2013;499(7457):214-8.
30. Lohr JG, Stojanov P, Lawrence MS, Auclair D, Chapuy B, Sougnez C, et al. Discovery and prioritization of somatic mutations in diffuse large B-cell lymphoma (DLBCL) by whole-exome sequencing. P Natl Acad Sci USA. 2012;109(10):3879-84.
31. Morin RD, Mendez-Lago M, Mungall AJ, Goya R, Mungall KL, Corbett RD, et al. Frequent mutation of histone-modifying genes in non-Hodgkin lymphoma. Nature. 2011;476(7360):298-303.
32. Pasqualucci L, Trifonov V, Fabbri G, Ma J, Rossi D, Chiarenza A, et al. Analysis of the coding genome of diffuse large B-cell lymphoma. Nat Genet. 2011;43(9):830-U33.
33. Nogai H, Dorken B, Lenz G. Pathogenesis of Non-Hodgkin's Lymphoma. J Clin Oncol. 2011;29(14):1803-11.
34. Barrans SL, Evans PAS, O'Connor SJM, Kendall SJ, Owen RG, Haynes AP, et al. The t(14;18) is associated with germinal center-derived diffuse large B-cell lymphoma and is a strong predictor of outcome. Clinical Cancer Research. 2003;9(6):2133-9.
35. Iqbal J, Sanger WG, Horsman DE, Rosenwald A, Pickering DL, Dave B, et al. BCL2 translocation defines a unique tumor subset within the germinal center B-cell-like diffuse large B-cell lymphoma. Am J Pathol. 2004;165(1):159-66.
36. Bakhshi A, Jensen JP, Goldman P, Wright JJ, Mcbride OW, Epstein AL, et al. Cloning the Chromosomal Breakpoint of T(14-18) Human Lymphomas - Clustering around Jh on Chromosome-14 and near a Transcriptional Unit on 18. Cell. 1985;41(3):899-906.

37. Bavi P, Uddin S, Bu R, Ahmed M, Abubaker J, Balde V, et al. The biological and clinical impact of inhibition of NF-kappa B-initiated apoptosis in diffuse large B cell lymphoma (DLBCL). J Pathol. 2011;224(3):355-66.
38. Davis RE, Brown KD, Siebenlist U, Staudt LM. Constitutive nuclear factor kappa B activity is required for survival of activated B cell-like diffuse large B cell lymphoma cells. J Exp Med. 2001;194(12):1861-74.
39. Lenz G, Wright G, Dave SS, Xiao W, Powell J, Zhao H, et al. Stromal Gene Signatures in Large-B-Cell Lymphomas. New Engl J Med. 2008;359(22):2313-23.
40. Coiffier B, Thieblemont C, Van Den Neste E, Lepeu G, Plantier I, Castaigne S, et al. Long-term outcome of patients in the LNH-98.5 trial, the first randomized study comparing rituximab-CHOP to standard CHOP chemotherapy in DLBCL patients: a study by the Groupe d'Etudes des Lymphomes de l'Adulte. Blood. 2010;116(12):2040-5.
41. Coiffier B, Sarkozy C. Diffuse large B-cell lymphoma: R-CHOP failure-what to do? Hematol-Am Soc Hemat. 2016:366-78.
42. Pan H, Jiang YW, Boi M, Tabbo F, Redmond D, Nie K, et al. Epigenomic evolution in diffuse large B-cell lymphomas. Nat Commun. 2015;6.
43. Muntean AG, Hess JL. Epigenetic Dysregulation in Cancer. Am J Pathol. 2009;175(4):1353-61.
44. Shaknovich R, Melnick A. Epigenetics and B-cell lymphoma. Curr Opin Hematol. 2011;18(4):293-9.
45. Berger SL, Kouzarides T, Shiekhattar R, Shilatifard A. An operational definition of epigenetics. Gene Dev. 2009;23(7):781-3.
46. Dupont C, Armant DR, Brenner CA. Epigenetics: Definition, Mechanisms and Clinical Perspective. Semin Reprod Med. 2009;27(5):351-7.
47. Ahuja N, Sharma AR, Baylin SB. Epigenetic Therapeutics: A New Weapon in the War Against Cancer. Annu Rev Med. 2016;67:73-89.
48. Messerschmidt DM, Knowles BB, Solter D. DNA methylation dynamics during epigenetic reprogramming in the germline and preimplantation embryos. Gene Dev. 2014;28(8):812-28.
49. Kelly TK, De Carvalho DD, Jones PA. Epigenetic modifications as therapeutic targets. Nat Biotechnol. 2010;28(10):1069-78.
50. Weinhold B. Epigenetics - The science of change. Environ Health Persp. 2006;114(3):A160-A7.
51. Jang HS, Shin WJ, Lee JE, Do JT. CpG and Non-CpG Methylation in Epigenetic Gene Regulation and Brain Function. Genes-Basel. 2017;8(6).
52. Bhasin M, Reinherz EL, Reche PA. Recognition and classification of histones using support vector machine. J Comput Biol. 2006;13(1):102-12.
53. Luger K, Mader AW, Richmond RK, Sargent DF, Richmond TJ. Crystal structure of the nucleosome core particle at 2.8 angstrom resolution. Nature. 1997;389(6648):251-60.
54. Over RS, Michaels SD. Open and Closed: The Roles of Linker Histones in Plants and Animals. Mol Plant. 2014;7(3):481-91.
55. Fischer JJ, Toedling J, Krueger T, Schueler M, Huber W, Sperling S. Combinatorial effects of four histone modifications in transcription and differentiation. Genomics. 2008;91(1):41-51.
56. de la Cruz X, Lois S, Sanchez-Molina S, Martinez-Balbas MA. Do protein motifs read the histone code? Bioessays. 2005;27(2):164-75.
57. Hebbes TR, Thorne AW, Cranerobinson C. A Direct Link between Core Histone Acetylation and Transcriptionally Active Chromatin. Embo J. 1988;7(5):1395-402.
58. Rea S, Eisenhaber F, O'Carroll N, Strahl BD, Sun ZW, Schmid M, et al. Regulation of chromatin structure by site-specific histone H3 methyltransferases. Nature. 2000;406(6796):593-9.

59. Wu JS, Grunstein M. 25 years after the nucleosome model: chromatin modifications. Trends Biochem Sci. 2000;25(12):619-23.
60. Berger SL. Histone modifications in transcriptional regulation. Curr Opin Genet Dev. 2002;12(2):142-8.
61. Kingston RE, Narlikar GJ. ATP-dependent remodeling and acetylation as regulators of chromatin fluidity. Gene Dev. 1999;13(18):2339-52.
62. Martin C, Zhang Y. The diverse functions of histone lysine methylation. Nat Rev Mol Cell Bio. 2005;6(11):838-49.
63. Zhang Y, Reinberg D. Transcription regulation by histone methylation: interplay between different covalent modifications of the core histone tails. Gene Dev. 2001;15(18):2343-60.
64. Shogren-Knaak M, Ishii H, Sun JM, Pazin MJ, Davie JR, Peterson CL. Histone H4-K16 acetylation controls chromatin structure and protein interactions. Science. 2006;311(5762):844-7.
65. Sims RJ, Nishioka K, Reinberg D. Histone lysine methylation: a signature for chromatin function. Trends Genet. 2003;19(11):629-39.
66. Santos-Rosa H, Caldas C. Chromatin modifier enzymes, the histone code and cancer. Eur J Cancer. 2005;41(16):2381-402.
67. Jain N, Rossi A, Garcia-Manero G. Epigenetic therapy of leukemia: An update. Int J Biochem Cell B. 2009;41(1):72-80.
68. Lue JK, Amengual JE, O'Connor OA. Epigenetics and Lymphoma: Can We Use Epigenetics to Prime or Reset Chemoresistant Lymphoma Programs? Curr Oncol Rep. 2015;17(9).
69. Dawson MA, Kouzarides T. Cancer Epigenetics: From Mechanism to Therapy. Cell. 2012;150(1):12-27.
70. Herman JG, Baylin SB. Mechanisms of disease: Gene silencing in cancer in association with promoter hypermethylation. New Engl J Med. 2003;349(21):2042-54.
71. Seton-Rogers S. LYMPHOMA Epigenetic therapy gains momentum. Nat Rev Cancer. 2012;12(12):799-.
72. Cotto M, Cabanillas F, Tirado M, Garcia MV, Pacheco E. Epigenetic therapy of lymphoma using histone deacetylase inhibitors. Clin Transl Oncol. 2010;12(6):401-9.
73. Ghai V, Sharma K, Abbi KKS, Shimko S, Epner EM. Current Approaches to Epigenetic Therapy for the Treatment of Mantle Cell Lymphoma. Adv Exp Med Biol. 2013;779:257-66.
74. Mann BS, Johnson JR, Cohen MH, Justice R, Pazdur R. FDA approval summary: Vorinostat for treatment of advanced primary cutaneous T-cell lymphoma. Oncologist. 2007;12(10):1247-52.
75. Lee HZ, Kwitkowski VE, Del Valle PL, Ricci MS, Saber H, Habtemariam BA, et al. FDA Approval: Belinostat for the Treatment of Patients with Relapsed or Refractory Peripheral T-cell Lymphoma. Clinical Cancer Research. 2015;21(12):2666-70.
76. Reyes JC, Grossniklaus U. Diverse functions of Polycomb group proteins during plant development. Semin Cell Dev Biol. 2003;14(1):77-84.
77. Klymenko T, Papp B, Fischle W, Kocher T, Schelder M, Fritsch C, et al. A Polycomb group protein complex with sequence-specific DNA-binding and selective methyl-lysine-binding activities. Gene Dev. 2006;20(9):1110-22.
78. Lewis EB. A gene complex controlling segmentation in Drosophila. Nature. 1978;276(5688):565-70.
79. Shao ZH, Raible F, Mollaaghababa R, Guyon JR, Wu CT, Bender W, et al. Stabilization of chromatin structure by PRC1, a polycomb complex. Cell. 1999;98(1):37-46.
80. Simon JA, Tamkun JW. Programming off and on states in chromatin: mechanisms of Polycomb and trithorax group complexes. Curr Opin Genet Dev. 2002;12(2):210-8.

81. Jacobs JJL, van Lohuizen M. Polycomb repression: from cellular memory to cellular proliferation and cancer. Bba-Rev Cancer. 2002;1602(2):151-61.
82. Simon JA, Kingston RE. Mechanisms of Polycomb gene silencing: knowns and unknowns. Nat Rev Mol Cell Bio. 2009;10(10):697-708.
83. Bracken AP, Dietrich N, Pasini D, Hansen KH, Helin K. Genome-wide mapping of Polycomb target genes unravels their roles in cell fate transitions. Gene Dev. 2006;20(9):1123-36.
84. Morey L, Helin K. Polycomb group protein-mediated repression of transcription. Trends Biochem Sci. 2010;35(6):323-32.
85. Surface LE, Thornton SR, Boyer LA. Polycomb Group Proteins Set the Stage for Early Lineage Commitment. Cell Stem Cell. 2010;7(3):288-98.
86. Marchesi I, Bagella L. Targeting Enhancer of Zeste Homolog 2 as a promising strategy for cancer treatment. World J Clin Oncol. 2016;7(2):135-48.
87. Margueron R, Reinberg D. The Polycomb complex PRC2 and its mark in life. Nature. 2011;469(7330):343-9.
88. Pengelly AR, Kalb R, Finkl K, Muller J. Transcriptional repression by PRC1 in the absence of H2A monoubiquitylation. Genes Dev. 2015;29(14):1487-92.
89. Scheuermann JC, Gutierrez L, Muller J. Histone H2A monoubiquitination and Polycomb repression: the missing pieces of the puzzle. Fly (Austin). 2012;6(3):162-8.
90. Cao R, Tsukada Y, Zhang Y. Role of Bmi-1 and Ring1A in H2A ubiquitylation and Hox gene silencing. Mol Cell. 2005;20(6):845-54.
91. Wang HB, Wang LJ, Erdjument-Bromage H, Vidal M, Tempst P, Jones RS, et al. Role of histone H2A ubiquitination in polycomb silencing. Nature. 2004;431(7010):873-8.
92. Eskeland R, Leeb M, Grimes GR, Kress C, Boyle S, Sproul D, et al. Ring1B Compacts Chromatin Structure and Represses Gene Expression Independent of Histone Ubiquitination. Mol Cell. 2010;38(3):452-64.
93. Cao R, Zhang Y. The functions of E(Z)/EZH2-mediated methylation of lysine 27 in histone H3. Curr Opin Genet Dev. 2004;14(2):155-64.
94. Schuettengruber B, Cavalli G. Recruitment of Polycomb group complexes and their role in the dynamic regulation of cell fate choice. Development. 2009;136(21):3531-42.
95. Pasini D, Di Croce L. Emerging roles for Polycomb proteins in cancer. Curr Opin Genet Dev. 2016;36:50-8.
96. Ezponda T, Licht JD. Molecular Pathways: Deregulation of Histone H3 Lysine 27 Methylation in Cancer-Different Paths, Same Destination. Clinical Cancer Research. 2014;20(19):5001-8.
97. Kim KH, Roberts CWM. Targeting EZH2 in cancer. Nat Med. 2016;22(2):128-34.
98. Sarma K, Margueron R, Ivanov A, Pirrotta V, Reinberg D. Ezh2 requires PHF1 to efficiently catalyze H3 lysine 27 trimethylation in vivo. Mol Cell Biol. 2008;28(8):2718-31.
99. Nekrasov M, Klymenko T, Fraterman S, Papp B, Oktaba K, Kocher T, et al. Pcl-PRC2 is needed to generate high levels of H3-K27 trimethylation at Polycomb target genes. Embo J. 2007;26(18):4078-88.
100. Francis NJ, Kingston RE, Woodcock CL. Chromatin compaction by a polycomb group protein complex. Science. 2004;306(5701):1574-7.
101. Zhou W, Zhu P, Wang J, Pascual G, Ohgi KA, Lozach J, et al. Histone H2A monoubiquitination represses transcription by inhibiting RNA polymerase II transcriptional elongation. Mol Cell. 2008;29(1):69-80.
102. Tolhuis B, de Wit E, Muijrers I, Teunissen H, Talhout W, van Steensel B, et al. Genome-wide profiling of PRC1 and PRC2 Polycomb chromatin binding in Drosophila melanogaster. Nat Genet. 2006;38(6):694-9.

103. Kuzmichev A, Nishioka K, Erdjument-Bromage H, Tempst P, Reinberg D. Histone methyltransferase activity associated with a human multiprotein complex containing the Enhancer of Zeste protein. Gene Dev. 2002;16(22):2893-905.
104. Wang L, Brown JL, Cao R, Zhang Y, Kassis JA, Jones RS. Hierarchical recruitment of Polycomb group silencing complexes. Mol Cell. 2004;14(5):637-46.
105. Dorafshan E, Kahn TG, Schwartz YB. Hierarchical recruitment of Polycomb complexes revisited. Nucleus-Phila. 2017;8(5):496-505.
106. Leeb M, Pasini D, Novatchkova M, Jaritz M, Helin K, Wutz A. Polycomb complexes act redundantly to repress genomic repeats and genes. Gene Dev. 2010;24(3):265-76.
107. Ku M, Koche RP, Rheinbay E, Mendenhall EM, Endoh M, Mikkelsen TS, et al. Genomewide Analysis of PRC1 and PRC2 Occupancy Identifies Two Classes of Bivalent Domains. Plos Genet. 2008;4(10).
108. Marchesi I, Giordano A, Bagella L. Roles of enhancer of zeste homolog 2 From skeletal muscle differentiation to rhabdomyosarcoma carcinogenesis. Cell Cycle. 2014;13(4):516-27.
109. Kirmizis A, Bartley SM, Farnham PJ. Identification of the polycomb group protein SU(Z)12 as a potential molecular target for human cancer therapy. Mol Cancer Ther. 2003;2(1):113-21.
110. Huet S, Xerri L, Tesson B, Mareschal S, Taix S, Mescam-Mancini L, et al. EZH2 alterations in follicular lymphoma: biological and clinical correlations. Blood Cancer J. 2017;7.
111. Peker D, Roman-Holba S, Kwon Y, Gordetsky J, Mehta A, Forero A, et al. EZH2 Upregulation Is Associated with Unfavorable Prognosis in Diffuse Large B-Cell Lymphoma through Potential RUNX3 Downregulation. Blood. 2016;128(22).
112. Margueron R, Li GH, Sarma K, Blais A, Zavadil J, Woodcock CL, et al. Ezh1 and Ezh2 Maintain Repressive Chromatin through Different Mechanisms. Mol Cell. 2008;32(4):503-18.
113. Dillon SC, Zhang X, Trievel RC, Cheng XD. The SET-domain protein superfamily: protein lysine methyltransferases. Genome Biol. 2005;6(8).
114. Bracken AP, Pasini D, Capra M, Prosperini E, Colli E, Helin K. EZH2 is downstream of the pRB-E2F pathway, essential for proliferation and amplified in cancer. Embo J. 2003;22(20):5323-35.
115. Dorfman DM, Tian XJ. New insights into the mechanisms of EZH2's promotion of oncogenesis. Transl Cancer Res. 2016;5:S1057-S60.
116. Li CH, Chen YC. Targeting EZH2 for Cancer Therapy: Progress and Perspective. Curr Protein Pept Sc. 2015;16(6):559-70.
117. O'Meara MM, Simon JA. Inner workings and regulatory inputs that control Polycomb repressive complex 2. Chromosoma. 2012;121(3):221-34.
118. Gan L, Yang YN, Li Q, Feng Y, Liu TS, Guo WJ. Epigenetic regulation of cancer progression by EZH2: from biological insights to therapeutic potential. Biomark Res. 2018;6.
119. Yan JL, Ng SB, Tay JLS, Lin BH, Koh TL, Tan J, et al. EZH2 overexpression in natural killer/T-cell lymphoma confers growth advantage independently of histone methyltransferase activity. Blood. 2013;121(22):4512-20.
120. Yamaguchi H, Hung MC. Regulation and Role of EZH2 in Cancer. Cancer Res Treat. 2014;46(3):209-22.
121. Velichutina I, Shaknovich R, Geng HM, Johnson NA, Gascoyne RD, Melnick AM, et al. EZH2-mediated epigenetic silencing in germinal center B cells contributes to proliferation and lymphomagenesis. Blood. 2010;116(24):5247-55.
122. Lee ST, Li ZM, Wu ZL, Aau M, Guan PY, Karuturi RKM, et al. Context-Specific Regulation of NF-kappa B Target Gene Expression by EZH2 in Breast Cancers. Mol Cell. 2011;43(5):798-810.
123. Xu KX, Wu ZJ, Groner AC, He HSHS, Cai CM, Lis RT, et al. EZH2 Oncogenic Activity in Castration-Resistant Prostate Cancer Cells Is Polycomb-Independent. Science. 2012;338(6113):1465-9.

124. Yang YA, Yu JD. EZH2, an epigenetic driver of prostate cancer. Protein Cell. 2013;4(5):331-41.
125. Kleer CG, Cao Q, Varambally S, Shen RL, Ota L, Tomlins SA, et al. EZH2 is a marker of aggressive breast cancer and promotes neoplastic transformation of breast epithelial cells. P Natl Acad Sci USA. 2003;100(20):11606-11.
126. Bachmann IM, Halvorsen OJ, Collett K, Stefansson IM, Straume O, Haukaas SA, et al. EZH2 expression is associated with high proliferation rate and aggressive tumor subgroups in cutaneous melanoma and cancers of the endometrium, prostate, and breast. J Clin Oncol. 2006;24(2):268-73.
127. Bodor C, Grossmann V, Popov N, Okosun J, O'Riain C, Tan K, et al. EZH2 mutations are frequent and represent an early event in follicular lymphoma. Blood. 2013;122(18):3165-8.
128. Liu Y, Yu KJ, Li MY, Zeng KX, Wei J, Li X, et al. EZH2 overexpression in primary gastrointestinal diffuse large B-cell lymphoma and its association with the clinicopathological features. Hum Pathol. 2017;64:213-21.
129. Morin RD, Johnson NA, Severson TM, Mungall AJ, An JH, Goya R, et al. Somatic mutations altering EZH2 (Tyr641) in follicular and diffuse large B-cell lymphomas of germinal-center origin. Nat Genet. 2010;42(2):181-U24.
130. Yamagishi M, Uchimaru K. Targeting EZH2 in cancer therapy. Curr Opin Oncol. 2017;29(5):375-81.
131. Zingg D, Debbache J, Schaefer SM, Tuncer E, Frommel SC, Cheng P, et al. The epigenetic modifier EZH2 controls melanoma growth and metastasis through silencing of distinct tumour suppressors. Nat Commun. 2015;6.
132. Hodis E, Watson IR, Kryukov GV, Arold ST, Imielinski M, Theurillat JP, et al. A Landscape of Driver Mutations in Melanoma. Cell. 2012;150(2):251-63.
133. Varambally S, Dhanasekaran SM, Zhou M, Barrette TR, Kumar-Sinha C, Sanda MG, et al. The polycomb group protein EZH2 is involved in progression of prostate cancer. Nature. 2002;419(6907):624-9.
134. Zhou XZ, Liu N, Zhang JQ, Ji HX, Liu YT, Yang J, et al. Increased expression of EZH2 indicates aggressive potential of urothelial carcinoma of the bladder in a Chinese population. Sci Rep-Uk. 2018;8.
135. Cao W, Feng ZE, Cui ZB, Zhang CP, Sun ZY, Mao L, et al. Up-regulation of enhancer of zeste homolog 2 is associated positively with cyclin D1 overexpression and poor clinical outcome in head and neck squamous cell carcinoma. Cancer-Am Cancer Soc. 2012;118(11):2858-71.
136. Chen ZP, Yang P, Li WL, He F, Wei JC, Zhang T, et al. Expression of EZH2 is associated with poor outcome in colorectal cancer. Oncol Lett. 2018;15(3):2953-61.
137. Knutson SK, Wigle TJ, Warholic NM, Sneeringer CJ, Allain CJ, Klaus CR, et al. A selective inhibitor of EZH2 blocks H3K27 methylation and kills mutant lymphoma cells. Nat Chem Biol. 2012;8(11):890-6.
138. Konze KD, Ma A, Li FL, Barsyte-Lovejoy D, Parton T, MacNevin CJ, et al. An Orally Bioavailable Chemical Probe of the Lysine Methyltransferases EZH2 and EZH1. Acs Chem Biol. 2013;8(6):1324-34.
139. Knutson SK, Kawano S, Minoshima Y, Warholic NM, Huang KC, Xiao YH, et al. Selective Inhibition of EZH2 by EPZ-6438 Leads to Potent Antitumor Activity in EZH2-Mutant Non-Hodgkin Lymphoma. Mol Cancer Ther. 2014;13(4):842-54.
140. Shen L, Cui J, Pang YX, Ma YH, Liu PS. 3-Deazaneplanocin A is a Promising Therapeutic Agent for Ovarian Cancer Cells. Asian Pac J Cancer P. 2013;14(5):2915-8.
141. Girard N, Bazille C, Lhuissier E, Benateau H, Llombart-Bosch A, Boumediene K, et al. 3-Deazaneplanocin A (DZNep), an Inhibitor of the Histone Methyltransferase EZH2, Induces Apoptosis and Reduces Cell Migration in Chondrosarcoma Cells. Plos One. 2014;9(5).

142. Sun F, Lee L, Zhang ZW, Wang XC, Yu Q, Duan XQ, et al. Preclinical pharmacokinetic studies of 3-deazaneplanocin A, a potent epigenetic anticancer agent, and its human pharmacokinetic prediction using GastroPlus (TM). Eur J Pharm Sci. 2015;77:290-302.
143. Chiba T, Suzuki E, Negishi M, Saraya A, Miyagi S, Konuma T, et al. 3-Deazaneplanocin A is a promising therapeutic agent for the eradication of tumor-initiating hepatocellular carcinoma cells. Int J Cancer. 2012;130(11):2557-67.
144. Qi W, Chan HM, Teng L, Li L, Chuai SN, Zhang RP, et al. Selective inhibition of Ezh2 by a small molecule inhibitor blocks tumor cells proliferation. P Natl Acad Sci USA. 2012;109(52):21360-5.
145. Verma SK, Tian XR, LaFrance LV, Duquenne C, Suarez DP, Newlander KA, et al. Identification of Potent, Selective, Cell-Active Inhibitors of the Histone Lysine Methyltransferase EZH2. Acs Med Chem Lett. 2012;3(12):1091-6.
146. McCabe MT, Ott HM, Ganji G, Korenchuk S, Thompson C, Van Aller GS, et al. EZH2 inhibition as a therapeutic strategy for lymphoma with EZH2-activating mutations. Nature. 2012;492(7427):108-+.
147. Knutson SK, Warholic NM, Wigle TJ, Klaus CR, Allain CJ, Raimondi A, et al. Durable tumor regression in genetically altered malignant rhabdoid tumors by inhibition of methyltransferase EZH2. P Natl Acad Sci USA. 2013;110(19):7922-7.
148. Campbell JE, Kuntz KW, Knutson SK, Warholic NM, Keilhack H, Wigle TJ, et al. EPZ011989, A Potent, Orally-Available EZH2 Inhibitor with Robust in Vivo Activity. Acs Med Chem Lett. 2015;6(5):491-5.
149. Taplin ME, Hussain A, Shore ND, Bradley B, Trojer P, Lebedinsky C, et al. A phase 1b/2 study of CPI-1205, a small molecule inhibitor of EZH2, combined with enzalutamide (E) or abiraterone/prednisone (A/P) in patients with metastatic castration resistant prostate cancer (mCRPC). J Clin Oncol. 2018;36(6).
150. Vaswani RG, Gehling VS, Dakin LA, Cook AS, Nasveschuk CG, Duplessis M, et al. Identification of (R)-N-((4-Methoxy-6-methyl-2-oxo-1,2-dihydropyridin-3-yl)methyl)-2-methyl-1-(1-(1-(2,2,2-trifluoroethyl)piperidin-4-yl)ethyl)-1H-indole-3-carboxamide (CPI-1205), a Potent and Selective Inhibitor of Histone Methyltransferase EZH2, Suitable for Phase I Clinical Trials for B-Cell Lymphomas. J Med Chem. 2016;59(21):9928-41.
151. Gehling VS, Vaswani RG, Nasveschuk CG, Duplessis M, Iyer P, Balasubramanian S, et al. Discovery, design, and synthesis of indole-based EZH2 inhibitors. Bioorg Med Chem Lett. 2015;25(17):3644-9.
152. Bradley WD, Arora S, Busby J, Balasubramanian S, Gehling VS, Nasveschuk CG, et al. EZH2 Inhibitor Efficacy in Non-Hodgkin's Lymphoma Does Not Require Suppression of H3K27 Monomethylation. Chem Biol. 2014;21(11):1463-75.
153. Lu B, Shen XD, Zhang L, Liu D, Zhang CH, Cao JS, et al. Discovery of EBI-2511: A Highly Potent and Orally Active EZH2 Inhibitor for the Treatment of Non-Hodgkin's Lymphoma. Acs Med Chem Lett. 2018;9(2):98-102.
154. Song XJ, Gao TT, Wang NY, Feng Q, You XY, Ye TH, et al. Selective inhibition of EZH2 by ZLD1039 blocks H3K27methylation and leads to potent anti-tumor activity in breast cancer (vol 6, 20864, 2016). Sci Rep-Uk. 2016;6.
155. Hayden A, Johnson PWM, Packham G, Crabb SJ. S-adenosylhomocysteine hydrolase inhibition by 3-deazaneplanocin A analogues induces anti-cancer effects in breast cancer cell lines and synergy with both histone deacetylase and HER2 inhibition. Breast Cancer Res Tr. 2011;127(1):109-19.
156. Kemp CD, Rao M, Xi SC, Inchauste S, Mani H, Fetsch P, et al. Polycomb Repressor Complex-2 Is a Novel Target for Mesothelioma Therapy. Clinical Cancer Research. 2012;18(1):77-90.

157. Glazer RI, Knode MC, Tseng CKH, Haines DR, Marquez VE. 3-Deazaneplanocin-a - a New Inhibitor of S-Adenosylhomocysteine Synthesis and Its Effects in Human-Colon Carcinoma-Cells. Biochem Pharmacol. 1986;35(24):4523-7.
158. Glazer RI, Hartman KD, Knode MC, Richard MM, Chiang PK, Tseng CKH, et al. 3-Deazaneplanocin - a New and Potent Inhibitor of S-Adenosylhomocysteine Hydrolase and Its Effects on Human Promyelocytic Leukemia-Cell Line Hl-60. Biochem Bioph Res Co. 1986;135(2):688-94.
159. Miranda TB, Cortez CC, Yoo CB, Liang GN, Abe M, Kelly TK, et al. DZNep is a global histone methylation inhibitor that reactivates developmental genes not silenced by DNA methylation. Mol Cancer Ther. 2009;8(6):1579-88.
160. Mody HR, Hung SW, AlSaggar M, Griffin J, Govindarajan R. Inhibition of S-Adenosylmethionine-Dependent Methyltransferase Attenuates TGF beta 1-Induced EMT and Metastasis in Pancreatic Cancer: Putative Roles of miR-663a and miR-4787-5p. Mol Cancer Res. 2016;14(11):1124-35.
161. Liu S, Wolfe MS, Borchardt RT. Rational Approaches to the Design of Antiviral Agents Based on S-Adenosyl-L-Homocysteine Hydrolase as a Molecular Target. Antivir Res. 1992;19(3):247-65.
162. Chiang PK. Biological effects of inhibitors of S-adenosylhomocysteine hydrolase. Pharmacol Therapeut. 1998;77(2):115-34.
163. Park SJ, Kong HK, Kim YS, Lee YS, Park JH. Inhibition of S-adenosylhomocysteine hydrolase decreases cell mobility and cell proliferation through cell cycle arrest. Am J Cancer Res. 2015;5(7):2127-38.
164. Kim JH, Kim JH, Kim SC, Yi YS, Yang WS, Yang Y, et al. Adenosine dialdehyde suppresses MMP-9-mediated invasion of cancer cells by blocking the Ras/Raf-1/ERK/AP-1 signaling pathway. Biochem Pharmacol. 2013;86(9):1285-300.
165. Beluzic L, Grbesa I, Beluzic R, Park JH, Kong HK, Kopjar N, et al. Knock-down of AHCY and depletion of adenosine induces DNA damage and cell cycle arrest. Sci Rep. 2018;8(1):14012.
166. Li QH, Mao LH, Wang RL, Zhu LQ, Xue LX. Overexpression of S-adenosylhomocysteine hydrolase (SAHH) in esophageal squamous cell carcinoma (ESCC) cell lines: effects on apoptosis, migration and adhesion of cells. Mol Biol Rep. 2014;41(4):2409-17.
167. Tan J, Yang XJ, Zhuang L, Jiang X, Chen W, Lee PL, et al. Pharmacologic disruption of polycomb-repressive complex 2-mediated gene repression selectively induces apoptosis in cancer cells. Gene Dev. 2007;21(9):1050-63.
168. Fiskus W, Wang YC, Sreekumar A, Buckley KM, Shi HD, Jillella A, et al. Combined epigenetic therapy with the histone methyltransferase EZH2 inhibitor 3-deazaneplanocin A and the histone deacetylase inhibitor panobinostat against human AML cells. Blood. 2009;114(13):2733-43.
169. Zhou J, Bi C, Cheong LL, Mahara S, Liu SC, Tay KG, et al. The histone methyltransferase inhibitor, DZNep, up-regulates TXNIP, increases ROS production, and targets leukemia cells in AML. Blood. 2011;118(10):2830-9.
170. Fiskus W, Rao R, Balusu R, Ganguly S, Tao J, Sotomayor E, et al. Superior efficacy of a combined epigenetic therapy against human mantle cell lymphoma cells. Clin Cancer Res. 2012;18(22):6227-38.
171. Crea F, Hurt EM, Mathews LA, Cabarcas SM, Sun L, Marquez VE, et al. Pharmacologic disruption of Polycomb Repressive Complex 2 inhibits tumorigenicity and tumor progression in prostate cancer. Mol Cancer. 2011;10.
172. Wen YP, Cai J, Hou YY, Huang ZJ, Wang ZH. Role of EZH2 in cancer stem cells: from biological insight to a therapeutic target. Oncotarget. 2017;8(23):37974-90.

173. Mochizuki-Kashio M, Aoyama K, Sashida G, Oshima M, Tomioka T, Muto T, et al. Ezh2 loss in hematopoietic stem cells predisposes mice to develop heterogeneous malignancies in an Ezh1-dependent manner. Blood. 2015;126(10):1172-83.
174. Honma D, Kanno O, Watanabe J, Kinoshita J, Hirasawa M, Nosaka E, et al. Novel orally bioavailable EZH1/2 dual inhibitors with greater antitumor efficacy than an EZH2 selective inhibitor. Cancer Sci. 2017;108(10):2069-78.
175. Liu Q, Wang MW. Histone lysine methyltransferases as anti-cancer targets for drug discovery. Acta Pharmacol Sin. 2016;37(10):1273-80.
176. Lu JW, Shen CKJ, Tzeng TY. Epigenetics of cancer: the role of histone methyltransferase, SETDB1, in cancer metastasis. Transl Cancer Res. 2016;5:S139-S41.
177. Albert M, Helin K. Histone methyltransferases in cancer. Semin Cell Dev Biol. 2010;21(2):209-20.
178. Mansoori B, Mohammadi A, Davudian S, Shirjang S, Baradaran B. The Different Mechanisms of Cancer Drug Resistance: A Brief Review. Adv Pharm Bull. 2017;7(3):339-48.
179. Cree IA, Charlton P. Molecular chess? Hallmarks of anti-cancer drug resistance! Bmc Cancer. 2017;17.
180. Akpa CA, Kleo K, Lenze D, Oker E, Dimitrova L, Hummel M. DZNep-mediated apoptosis in B-cell lymphoma is independent of the lymphoma type, EZH2 mutation status and MYC, BCL2 or BCL6 translocations. Plos One. 2019;14(8):e0220681.
181. Quentmeier H, Amini RM, Berglund M, Dirks WG, Ehrentraut S, Geffers R, et al. U-2932: two clones in one cell line, a tool for the study of clonal evolution. Leukemia. 2013;27(5):1155-64.
182. Sun RR, Shen J, Gao Y, Zhou YB, Yu ZJ, Hornicek F, et al. Overexpression of EZH2 is associated with the poor prognosis in osteosarcoma and function analysis indicates a therapeutic potential. Oncotarget. 2016;7(25):38333-46.
183. Joosten M, Seitz V, Zimmermann K, Sommerfeld A, Berg E, Lenze D, et al. Histone acetylation and DNA demethylation of T cells result in an anaplastic large cell lymphoma-like phenotype. Haematologica. 2013;98(2):247-54.
184. Bookout AL, Mangelsdorf DJ. Quantitative real-time PCR protocol for analysis of nuclear receptor signaling pathways. Nucl Recept Signal. 2003;1:e012.
185. Koressaar T, Remm M. Enhancements and modifications of primer design program Primer3. Bioinformatics. 2007;23(10):1289-91.
186. Untergasser A, Nijveen H, Rao X, Bisseling T, Geurts R, Leunissen JAM. Primer3Plus, an enhanced web interface to Primer3. Nucleic Acids Res. 2007;35:W71-W4.
187. van Dongen JJM, Langerak AW, Bruggemann M, Evans PAS, Hummel M, Lavender FL, et al. Design and standardization of PCR primers and protocols for detection of clonal immunoglobulin and T-cell receptor gene recombinations in suspect lymphoproliferations: Report of the BIOMED-2 Concerted Action BMH4-CT98-3936. Leukemia. 2003;17(12):2257-317.
188. Horn H, Ziepert M, Wartenberg M, Staiger AM, Barth TFE, Bernd HW, et al. Different biological risk factors in young poor-prognosis and elderly patients with diffuse large B-cell lymphoma. Leukemia. 2015;29(7):1564-70.
189. Horn H, Ziepert M, Becher C, Barth TFE, Bernd HW, Feller AC, et al. MYC status in concert with BCL2 and BCL6 expression predicts outcome in diffuse large B-cell lymphoma. Blood. 2013;121(12):2253-63.
190. Hovestadt V, Zapatka M. conumee: Enhanced copy-number variation analysis using Illumina DNA methylation arrays. R package.http://bioconductor.org/packages/conumee/.
191. Capper D, Stichel D, Sahm F, Jones DTW, Schrimpf D, Sill M, et al. Practical implementation of DNA methylation and copy-number-based CNS tumor diagnostics: the Heidelberg experience. Acta Neuropathol. 2018;136(2):181-210.

192. Capper D, Jones DTW, Sill M, Hovestadt V, Schrimpf D, Sturm D, et al. DNA methylation-based classification of central nervous system tumours. Nature. 2018;555(7697):469-+.
193. RCoreTeam. R: A language and environment for statistical computing. R Foundation for Statistical Computing, Vienna, Austria. URL https://www.R-project.org/. 2013.
194. Wagener R, Lopez C, Kleinheinz K, Bausinger J, Aukema SM, Nagel I, et al. IG-MYC-positive neoplasms with precursor B-cell phenotype are molecularly distinct from Burkitt lymphomas. Blood. 2018.
195. Schlegelberger B, Zwingers T, Harder L, Nowotny H, Siebert R, Vesely M, et al. Clinicopathogenetic significance of chromosomal abnormalities in patients with blastic peripheral B-cell lymphoma. Kiel-Wien-Lymphoma Study Group. Blood. 1999;94(9):3114-20.
196. Stevens AP, Dettmer K, Kirovski G, Samejima K, Hellerbrand C, Bosserhoff AK, et al. Quantification of intermediates of the methionine and polyamine metabolism by liquid chromatography-tandem mass spectrometry in cultured tumor cells and liver biopsies. J Chromatogr A. 2010;1217(19):3282-8.
197. Kleo K, Dimitrova L, Oker E, Tomaszewski N, Berg E, Taruttis F, et al. Identification of ADGRE5 as discriminating MYC target between Burkitt lymphoma and diffuse large B-cell lymphoma. Bmc Cancer. 2019;19(1):322.
198. Drexler HG, Eberth S, Nagel S, MacLeod RAF. Malignant hematopoietic cell lines: in vitro models for double-hit B-cell lymphomas. Leukemia Lymphoma. 2016;57(5):1015-20.
199. Salaverria I, Martin-Guerrero I, Wagener R, Kreuz M, Kohler CW, Richter J, et al. A recurrent 11q aberration pattern characterizes a subset of MYC-negative high-grade B-cell lymphomas resembling Burkitt lymphoma. Blood. 2014;123(8):1187-98.
200. Moran S, Arribas C, Esteller M. Validation of a DNA methylation microarray for 850,000 CpG sites of the human genome enriched in enhancer sequences. Epigenomics-Uk. 2016;8(3):389-99.
201. Oliveros JC. Venny. An interactive tool for comparing lists with Venn's diagrams. http://bioinfogp.cnb.csic.es/tools/venny/index.html. 2007-2015.
202. Thomas PD, Kejariwal A, Campbell MJ, Mi H, Diemer K, Guo N, et al. PANTHER: a browsable database of gene products organized by biological function, using curated protein family and subfamily classification (vol 31, pg 334, 2003). Nucleic Acids Res. 2003;31(7):2024-.
203. Joosten M, Ginzel S, Blex C, Schmidt D, Gombert M, Chen C, et al. A novel approach to detect resistance mechanisms reveals FGR as a factor mediating HDAC inhibitor SAHA resistance in B-cell lymphoma. Mol Oncol. 2016;10(8):1232-44.
204. Cerami E, Gao JJ, Dogrusoz U, Gross BE, Sumer SO, Aksoy BA, et al. The cBio Cancer Genomics Portal: An Open Platform for Exploring Multidimensional Cancer Genomics Data. Cancer Discov. 2012;2(5):401-4.
205. Gao JJ, Aksoy BA, Dogrusoz U, Dresdner G, Gross B, Sumer SO, et al. Integrative Analysis of Complex Cancer Genomics and Clinical Profiles Using the cBioPortal. Sci Signal. 2013;6(269).
206. Bojang P, Jr., Ramos KS. The promise and failures of epigenetic therapies for cancer treatment. Cancer Treat Rev. 2014;40(1):153-69.
207. Fiskus W, Rao R, Balusu R, Ganguly S, Tao JG, Sotomayor E, et al. Superior Efficacy of a Combined Epigenetic Therapy against Human Mantle Cell Lymphoma Cells. Clinical Cancer Research. 2012;18(22):6227-38.
208. Braun FK, Mathur R, Sehgal L, Wilkie-Grantham R, Chandra J, Berkova Z, et al. Inhibition of Methyltransferases Accelerates Degradation of cFLIP and Sensitizes B-Cell Lymphoma Cells to TRAIL-Induced Apoptosis. Plos One. 2015;10(3).

209. Nakagawa S, Sakamoto Y, Okabe H, Hayashi H, Hashimoto D, Yokoyama N, et al. Epigenetic therapy with the histone methyltransferase EZH2 inhibitor 3-deazaneplanocin A inhibits the growth of cholangiocarcinoma cells. Oncol Rep. 2014;31(2):983-8.
210. Zhou JB, Bi CL, Cheong LL, Mahara S, Liu SC, Tay KG, et al. The histone methyltransferase inhibitor, DZNep, up-regulates TXNIP, increases ROS production, and targets leukemia cells in AML. Blood. 2011;118(10):2830-9.
211. Puppe J, Drost R, Liu XL, Joosse SA, Evers B, Cornelissen-Steijger P, et al. BRCA1-deficient mammary tumor cells are dependent on EZH2 expression and sensitive to Polycomb Repressive Complex 2-inhibitor 3-deazaneplanocin A. Breast Cancer Res. 2009;11(4).
212. Kikuchi J, Takashina T, Kinoshita I, Kikuchi E, Shimizu Y, Sakakibara-Konishi J, et al. Epigenetic therapy with 3-deazaneplanocin A, an inhibitor of the histone methyltransferase EZH2, inhibits growth of non-small cell lung cancer cells. Lung Cancer. 2012;78(2):138-43.
213. Sha M, Mao G, Wang G, Chen Y, Wu X, Wang Z. DZNep inhibits the proliferation of colon cancer HCT116 cells by inducing senescence and apoptosis. Acta Pharm Sin B. 2015;5(3):188-93.
214. Offit K, Lococo F, Louie DC, Parsa NZ, Leung D, Portlock C, et al. Rearrangement of the Bcl-6 Gene as a Prognostic Marker in Diffuse Large-Cell Lymphoma. New Engl J Med. 1994;331(2):74-80.
215. Tzankov A, Xu-Monette ZY, Gerhard M, Visco C, Dirnhofer S, Gisin N, et al. Rearrangements of MYC gene facilitate risk stratification in diffuse large B-cell lymphoma patients treated with rituximab-CHOP. Modern Pathol. 2014;27(7):958-71.
216. Ye Q, Xu-Monette ZY, Tzankov A, Deng LJ, Wang XX, Manyam GC, et al. Prognostic impact of concurrent MYC and BCL6 rearrangements and expression in de novo diffuse large B-cell lymphoma. Oncotarget. 2016;7(3):2401-16.
217. Xu-Monette ZY, Dabaja BS, Wang XX, Tu MF, Manyam GC, Tzankov A, et al. Clinical features, tumor biology, and prognosis associated with MYC rearrangement and Myc overexpression in diffuse large B-cell lymphoma patients treated with rituximab-CHOP. Modern Pathol. 2015;28(12):1555-73.
218. Sun RF, Medeiros LJ, Young KH. Diagnostic and predictive biomarkers for lymphoma diagnosis and treatment in the era of precision medicine. Modern Pathol. 2016;29(10):1118-42.
219. Ye Q, Xu-Monette ZY, Tzankov A, Deng L, Wang X, Manyam GC, et al. Prognostic impact of concurrent MYC and BCL6 rearrangements and expression in de novo diffuse large B-cell lymphoma. Oncotarget. 2016;7(3):2401-16.
220. Li S, Wang Z, Lin LM, Wu ZX, Yu QF, Gao FQ, et al. BCL6 Rearrangement Indicates Poor Prognosis in Diffuse Large B-cell Lymphoma Patients: A Meta-analysis of Cohort Studies. J Cancer. 2019;10(2):530-8.
221. Majer CR, Jin L, Scott MP, Knutson SK, Kuntz KW, Keilhack H, et al. A687V EZH2 is a gain-of-function mutation found in lymphoma patients. Febs Lett. 2012;586(19):3448-51.
222. McCabe MT, Graves AP, Ganji G, Diaz E, Halsey WS, Jiang Y, et al. Mutation of A677 in histone methyltransferase EZH2 in human B-cell lymphoma promotes hypertrimethylation of histone H3 on lysine 27 (H3K27). P Natl Acad Sci USA. 2012;109(8):2989-94.
223. Ryan RJH, Nitta M, Borger D, Zukerberg LR, Ferry JA, Harris NL, et al. EZH2 Codon 641 Mutations are Common in BCL2-Rearranged Germinal Center B Cell Lymphomas. Plos One. 2011;6(12).
224. Yap DB, Chu J, Berg T, Schapira M, Cheng SWG, Moradian A, et al. Somatic mutations at EZH2 Y641 act dominantly through a mechanism of selectively altered PRC2 catalytic activity, to increase H3K27 trimethylation. Blood. 2011;117(8):2451-9.
225. Sneeringer CJ, Scott MP, Kuntz KW, Knutson SK, Pollock RM, Richon VM, et al. Coordinated activities of wild-type plus mutant EZH2 drive tumor-associated hypertrimethylation of lysine 27 on histone H3 (H3K27) in human B-cell lymphomas. P Natl Acad Sci USA. 2010;107(49):20980-5.

226. Shen C, Vakoc CR. Gain-of-function mutation of chromatin regulators as a tumorigenic mechanism and an opportunity for therapeutic intervention. Curr Opin Oncol. 2015;27(1):57-63.
227. Bologna-Molina R, Mosqueda-Taylor A, Molina-Frechero N, Mori-Estevez AD, Sanchez-Acuna G. Comparison of the value of PCNA and Ki-67 as markers of cell proliferation in ameloblastic tumors. Med Oral Patol Oral. 2013;18(2):E174-E9.
228. Wang LX, Kong WX, Liu B, Zhang XQ. Proliferating cell nuclear antigen promotes cell proliferation and tumorigenesis by up-regulating STAT3 in non-small cell lung cancer. Biomed Pharmacother. 2018;104:595-602.
229. Jablonska B, Aguirre A, Vandenbosch R, Belachew S, Berthet C, Kaldis P, et al. Cdk2 is critical for proliferation and self-renewal of neural progenitor cells in the adult subventricular zone. J Cell Biol. 2007;179(6):1231-45.
230. Wang J, Yang T, Xu GF, Liu H, Ren CY, Xie WF, et al. Cyclin-Dependent Kinase 2 Promotes Tumor Proliferation and Induces Radio Resistance in Glioblastoma. Transl Oncol. 2016;9(6):548-56.
231. Chiba T, Suzuki E, Negishi M, Saraya A, Miyagi S, Konuma T, et al. 3-Deazaneplanocin A is a promising therapeutic agent for the eradication of tumor-initiating hepatocellular carcinoma cells. Int J Cancer. 2012;130(11):2557-67.
232. Puppe J, Drost R, Liu X, Joosse SA, Evers B, Cornelissen-Steijger P, et al. BRCA1-deficient mammary tumor cells are dependent on EZH2 expression and sensitive to Polycomb Repressive Complex 2-inhibitor 3-deazaneplanocin A. Breast Cancer Res. 2009;11(4):R63.
233. Fujiwara T, Saitoh H, Inoue A, Kobayashi M, Okitsu Y, Katsuoka Y, et al. 3-Deazaneplanocin A (DZNep), an Inhibitor of S-Adenosylmethionine-dependent Methyltransferase, Promotes Erythroid Differentiation. J Biol Chem. 2014;289(12):8121-34.
234. Morschhauser F, Salles GA, Le Gouill S, Radford JA, Mckay P, Cartron G, et al. Phase 2 multi-center study of tazemetostat (EPZ-6438), an inhibitor of enhancer of zeste-homolog 2 (EZH2), in patients with relapsed or refractory B-cell non-Hodgkin lymphoma (NHL). J Clin Oncol. 2016;34(15).
235. Gottesman MM. Mechanisms of cancer drug resistance. Annu Rev Med. 2002;53:615-27.
236. Pan ST, Li ZL, He ZX, Qiu JX, Zhou SF. Molecular mechanisms for tumour resistance to chemotherapy. Clin Exp Pharmacol P. 2016;43(8):723-37.
237. Iglesias VS, Giuranno L, Dubois LJ, Theys J, Vooijs M. Drug Resistance in Non-Small Cell Lung Cancer: A Potential for NOTCH Targeting? Front Oncol. 2018;8.
238. Nitta A, Chung YS, Nakata B, Yashiro M, Onoda N, Maeda K, et al. Establishment of a cisplatin-resistant gastric carcinoma cell line OCUM-2M/DDP. Cancer Chemoth Pharm. 1997;40(1):94-7.
239. Jensen NF, Stenvang J, Beck MK, Hanakova B, Belling KC, Do KN, et al. Establishment and characterization of models of chemotherapy resistance in colorectal cancer: Towards a predictive signature of chemoresistance. Mol Oncol. 2015;9(6):1169-85.
240. Petitprez A, Poindessous V, Ouaret D, Regairaz M, Bastian G, Guerin E, et al. Acquired irinotecan resistance is accompanied by stable modifications of cell cycle dynamics independent of MSI status. Int J Oncol. 2013;42(5):1644-53.
241. Barr MP, Gray SG, Hoffmann AC, Hilger RA, Thomale J, O'Flaherty JD, et al. Generation and characterisation of cisplatin-resistant non-small cell lung cancer cell lines displaying a stem-like signature. Plos One. 2013;8(1):e54193.
242. Johnson NA, Boyle M, Bashashati A, Leach S, Brooks-Wilson A, Sehn LH, et al. Diffuse large B-cell lymphoma: reduced CD20 expression is associated with an inferior survival. Blood. 2009;113(16):3773-80.

243. Olejniczak SH, Stewart CC, Donohue K, Czuczman MS. A quantitative exploration of surface antigen expression in common B-cell malignancies using flow cytometry. Immunol Invest. 2006;35(1):93-114.
244. Delage L, Manzoni D, Quinquenet C, Fontaine J, Maarek A, Chabane K, et al. Molecular analysis of a CD19-negative diffuse large B-cell lymphoma. Haematologica. 2019;104(3):E114-E6.
245. Kimura M, Yamaguchi M, Ueno S, Ogawa S, Miyazaki K, Oka K, et al. CD19-negative diffuse large B-cell lymphoma shows high serum LDH level and poor prognosis. Blood. 2005;106(11):546a-a.
246. Katchi T, Liu DL. Diagnosis and treatment of CD20 negative B cell lymphomas. Biomark Res. 2017;5.
247. Qunaj L, Castillo JJ, Olszewski AJ. CD20-Negative Large B-Cell Lymphomas: Analysis of the National Cancer Data Base. Blood. 2016;128(22).
248. Ben-David U, Siranosian B, Ha G, Tang H, Oren Y, Hinohara K, et al. Genetic and transcriptional evolution alters cancer cell line drug response. Nature. 2018;560(7718):325-+.
249. Foster JM, Oumie A, Togneri FS, Vasques FR, Hau D, Taylor M, et al. Cross-laboratory validation of the OncoScan (R) FFPE Assay, a multiplex tool for whole genome tumour profiling. Bmc Med Genomics. 2015;8.
250. Xue J, Qian WB, Guo S, Cai J, Li HQ. Detecting copy number variations using WES datasets in patient derived xenografts. Cancer Res. 2017;77.
251. Ma ZP, Xue SY, Zeng B, Qiu DX. lncRNA SNHG5 is associated with poor prognosis of bladder cancer and promotes bladder cancer cell proliferation through targeting p27. Oncol Lett. 2018;15(2):1924-30.
252. Stelzer G, Rosen N, Plaschkes I, Zimmerman S, Twik M, Fishilevich S, et al. The GeneCards Suite: From Gene Data Mining to Disease Genome Sequence Analyses. Curr Protoc Bioinformatics. 2016;54:1 30 1-1 3.
253. Nath J, Johnson KL. A review of fluorescence in situ hybridization (FISH): Current status and future prospects. Biotech Histochem. 2000;75(2):54-78.
254. Bishop R. Applications of fluorescence in situ hybridization (FISH) in detecting genetic aberrations of medical significance. Bioscience Horizons: The International Journal of Student Research. 2010;3(1):85–95.
255. Housman G, Byler S, Heerboth S, Lapinska K, Longacre M, Snyder N, et al. Drug resistance in cancer: an overview. Cancers (Basel). 2014;6(3):1769-92.
256. Scotto L, Narayan G, Nandula S, Arias-Pulido H, Subramaniyam S, Schneider A, et al. Identification of copy number gain and overexpressed genes on chromosome arm 20q by an integrative genomic approach in cervical cancer: Potential role in progression. Gene Chromosome Canc. 2008;47(9):755-65.
257. Loo LWM, Tiirikainen M, Cheng I, Lum-Jones A, Seifried A, Church JM, et al. Integrated analysis of genome-wide copy number alterations and gene expression in microsatellite stable, CpG island methylator phenotype-negative colon cancer. Gene Chromosome Canc. 2013;52(5):450-66.
258. Hassan NZA, Mokhtar NM, Sin TK, Rose IM, Sagap I, Harun R, et al. Integrated Analysis of Copy Number Variation and Genome-Wide Expression Profiling in Colorectal Cancer Tissues. Plos One. 2014;9(4).
259. Uchiyama N, Dougan DR, Lawson JD, Kimura H, Matsumoto SI, Tanaka Y, et al. Identification of AHCY inhibitors using novel high-throughput mass spectrometry. Biochem Bioph Res Co. 2017;491(1):1-7.
260. Zhang AH, Sun H, Yan GL, Wang P, Wang XJ. Metabolomics for Biomarker Discovery: Moving to the Clinic. Biomed Res Int. 2015.
261. Monteiro MS, Carvalho M, Bastos ML, de Pinho PG. Metabolomics Analysis for Biomarker Discovery: Advances and Challenges. Curr Med Chem. 2013;20(2):257-71.

262. Fiehn O, Kim J. Metabolomics Insights Into Pathophysiological Mechanisms of Interstitial Cystitis. Int Neurourol J. 2014;18(3):106-14.
263. Shao YP, Le WD. Recent advances and perspectives of metabolomics-based investigations in Parkinson's disease. Mol Neurodegener. 2019;14.
264. Aparicio A, North B, Barske L, Wang XM, Bollati V, Weisenberger D, et al. LINE-1 methylation in plasma DNA as a biomarker of activity of DNA methylation inhibitors in patients with solid tumors. Epigenetics-Us. 2009;4(3):176-84.
265. Bock C, Halbritter F, Carmona FJ, Tierling S, Datlinger P, Assenov Y, et al. Quantitative comparison of DNA methylation assays for biomarker development and clinical applications. Nat Biotechnol. 2016;34(7):726-+.
266. Pidsley R, Zotenko E, Peters TJ, Lawrence MG, Risbridger GP, Molloy P, et al. Critical evaluation of the Illumina MethylationEPIC BeadChip microarray for whole-genome DNA methylation profiling. Genome Biol. 2016;17.
267. Forbes SA, Beare D, Boutselakis H, Bamford S, Bindal N, Tate J, et al. COSMIC: somatic cancer genetics at high-resolution. Nucleic Acids Res. 2017;45(D1):D777-D83.
268. Schakowski F, Buttgereit P, Mazur M, Marten A, Schottker B, Gorschluter M, et al. Novel non-viral method for transfection of primary leukemia cells and cell lines. Genet Vaccines Ther. 2004;2(1):1.
269. Anastasov N, Klier M, Koch I, Angermeier D, Höfler H, Fend F, et al. Efficient shRNA delivery into B and T lymphoma cells using lentiviral vector-mediated transfer. Journal of Hematopathology. 2009;2(1):9-19.
270. Zhao NX, Qi JJ, Zeng ZH, Parekh P, Chang CC, Tung CH, et al. Transfecting the hard-to-transfect lymphoma/leukemia cells using a simple cationic polymer nanocomplex. J Control Release. 2012;159(1):104-10.

APPENDIX

A. Acknowledgements

My special thanks goes to **Almighty God** for bestowing me with life, health and the fortitude to complete this doctoral thesis. I also thank the **Berlin School of Integrative Oncology (BSIO)** for granting me the opportunity to do my PhD work in the field of Oncology. I am particularly grateful to my thesis Supervisor, **Prof. Dr. Michael Hummel** for believing in me, and his unrelenting support throughout the course of my work. Special thanks also goes to **Dr. Lora Dimitrova, Dr. Karsten Kleo** and **Elisabeth Oker** for their guidance towards the successful achievement of this work. To my extended family members, my beloved husband and daughter, **Nnaemeka Akpa and Olaedo Akpa**, I love and appreciate you all for your untimely love and for moral support, pushing me up during hard and tough times. I extend warm thanks to all members of the research group **'AG Hummel'**, my **collaboration partners, Dr. Elena Mylona** and **Prof. Dr. Claudia Baldus** for their constructive feedback during this research work and during my thesis committee meetings.

B. List of abbreviations

5-mC	5-methylcytocine
6-FAM	6-carboxyfluorescein
ABC	Activated B-cell
AEBP2	Adipocyte enhancer-binding protein 2
AHCY	S-adenosylhomocysteine hydrolase
Ann V	Annexin V
B2M	Beta 2 microglobulin
BCL	B-cell lymphoma
BL	Burkitt lymphoma
CD	Cluster of differentiation
CDK2	Cyclin-dependent kinase 2
cDNA	Complementary DNA
CHOP	Cyclophosphamide, Hydroxydaunorubicin, Oncovin, Prednisone
CNA	Copy number aberration
CNN-LOH	Copy number neutral loss of heterozygosity
CNV	Copy number variation
DLBCL	Diffuse large B-cell lymphoma
DMSO	Dimethyl sulfoxide
DNA	Deoxyribonucleic acid
DSMZ	German collection of microorganisms and cell cultures
DZNep	3-Deazaneplanocin-A
EED	Embryonic ectoderm development
ELISA	Enzyme-linked immunosorbent assay
esiRNA	Endoribonuclease-prepared small interfering RNA
EZH1	Enhancer of zeste homolog 1
EZH2	Enhancer of zeste homolog 2
FFPE	Formalin-fixed paraffin-embedded
FISH	Fluorescence in situ hybridization
FITC	Fluorescein isothiocyanate
FR	Framework
GAPDH	Glyceraldehyde 3-phosphate dehydrogenase
GCB	Germinal center B-cell
GFP	Green fluorescent protein

H3K27me3	Lysine 27 tri-methylation on histone H3
HIV	Human immunodeficiency virus
HL	Hodgkin lymphoma
HRP	Horseradish peroxidase
IC50	Inhibitory concentration 50
IGH	Immunoglobulin heavy chain
IHC	Immunohistochemistry
JARID2	Jumonji and AT-rich interaction domain containing 2
Me	Methyl
NCBI	National Center for Biotechnology Information
NHL	Non-Hodgkin lymphoma
NFkB	Nuclear factor kappa-light-chain-enhancer of activated B cells
NTC	No template control
PARP	Poly (ADP-ribose) polymerase
PCA	Principal component analysis
PCGFs	Polycomb group RING fingers
PCL	Polycomb-like
PCNA	Proliferating cell nuclear antigen
PCR	Polymerase chain reaction
PGPs	Polycomb group proteins
PI	Propidium iodide
PMBL	Primary mediastinal B-cell lymphoma
PolyPhen	Polymorphism phenotyping
PRC1	Polycomb repressive complex 1
PRC2	Polycomb repressive complex 2
R-CHOP	Rituximab, Cyclophosphamide, Hydroxydaunorubicin, Oncovin, Prednisone
RbAp46	Retinoblastoma-binding protein p46
RNA	Ribonucleic acid
RQ	Relative mRNA quantification
RSC	Reed-Sternberg cells
RT-PCR	Reverse transcriptase polymerase chain reaction
SAH	S-adenosyl-L-homocysteine
SAM	S-adenosylmethionine
SD	Standard deviation

SDHA	Succinate dehydrogenase
SET	Suppressor of variegation, Enhancer-of-zeste and Trithorax
SIFT	Sorting intolerant from tolerant
STR	Short tandem repeat
SUZ12	Suppressor of Zeste 12
TCL	T-cell lymphoma
VEP	Variant effect predictor
WES	Whole-exome sequencing
WHO	World health organization

C. Publications, conferences talks and awards

Publications

Chidimma Agatha Akpa, Karsten Kleo, Dido Lenze, Elisabeth Oker, Lora Dimitrova, Michael Hummel. ***DZNep-mediated apoptosis in B-cell lymphoma is independent of the lymphoma type, EZH2 mutation status and MYC, BCL2 or BCL6 translocations.*** PLOS One. 2019 Aug 16; 14(8):e0220681. doi: 10.1371/journal.pone.0220681.

Manuscript in review

- **Chidimma Agatha Akpa,** Karsten Kleo, Elisabeth Oker, Nancy Tomaszewski, Clemens Messerschmidt, Cristina Lopez, Rabea Wagener, Kathrin Oehl-Huber, Katja Dettmer, Anne Schoeler, Dido Lenze, Peter J. Oefner, Dieter Beule, Reiner Siebert, David Capper, Lora Dimitrova, Michael Hummel. ***Acquired resistance to DZNep-mediated apoptosis is associated with copy number gains of AHCY in a B-cell lymphoma model.***

Conference talks

- **Chidimma Agatha Akpa,** Karsten Kleo, Elisabeth Oker, Lora Dimitrova, Michael Hummel. ***Impact of EZH2 mutations for DZNep-mediated apoptosis in B-cell lymphomas.*** 103. Jahrestagung der Deutschen Gesellschaft für Pathologie, Frankfurt am Main, 13-15 June 2019.

Awards

- Berlin School for Integrative Oncology (BSIO) stipend 2015 - 2016.

Declaration of Authorship

I hereby declare that I wrote this dissertation myself and did not make use of any other sources or aids other than those listed. This dissertation was not submitted to any other examinations office.

Chidimma Agatha Akpa
Berlin, 16.03.2020.